공학박사 학위논문

독립형 교류 마이크로그리드에서 정확한 전력분배와 공통연결점의 고조파전압 보상을 위한 임피던스 제어기법

Advanced Impedance Control Schemes for Accurate Power Sharing and PCC Harmonic Voltage Compensation in Islanded AC Microgrid

울산대학교 대학원

전기전자컴퓨터공학과

PHAM MINH DUC

공학박사 학위논문

독립형 교류 마이크로그리드에서 정확한 전력분배와 공통연결점의 고조파전압 보상을 위한 임피던스 제어기법

Advanced Impedance Control Schemes for Accurate Power Sharing and PCC Harmonic Voltage Compensation in Islanded AC Microgrid

지도교수 이홍희

이 논문을 공학박사 학위논문으로 제출함

2021 년 06 월

울산대학교 대학원

전기전자컴퓨터공학과

PHAM MINH DUC

PHAM MINH DUC 의 공학박사위 논문을 인준함

심사위원장	전태원	(인)
심사위원	이홍희	(인)
심사위원	최성진	(인)
심사위원	이동춘	(인)
심사위원	정의헌	(인)

울산대학교 대학원

전기전자컴퓨터공학과

2021 년 6 월

UNIVERSITY OF ULSAN

Advanced Impedance Control Schemes for Accurate Power Sharing and PCC Harmonic Voltage Compensation in Islanded AC Microgrid

by

PHAM MINH DUC

Supervisor: Professor HONG-HEE LEE

A dissertation submitted in partial fulfillment of the requirements for

the degree of Doctor of Philosophy

in the

Department of Electrical, Electronic and Computer Engineering

University of Ulsan

June 2021

This certifies that the doctoral dissertation of PHAM MINH DUC is approved by:

Committee Chair: **Professor Tae-Won Chun**

Signature: Chun Tae Won

Committee Member: **Professor Hong-Hee Lee**

Signature: Hong Hee Lee

Committee Member: **Professor Sung-Jin Choi**

Signature:

Committee Member: **Professor Dong-Choon Lee**

Signature: LeeDongChoon

Committee Member: **Doctor Eui-Heon Jung**

Signature:

Department of Electrical, Electronic and Computer Engineering

University of Ulsan

June 2021

I would like to dedicate this dissertation to my beloved parents, my brother and my lovely girlfriend:

Phạm Minh Đạo

Nguyễn Thị Hà Thanh

Trịnh Thị Lý

Acknowledgements

First of all, I would like to respectfully thank to my supervisor, Professor Hong-Hee Lee for his valuable guidance, encouragement and support during my Ph.D. study at the University of Ulsan. It has been my great happiness to complete my Ph.D study under his guidance.

I would like to express my sincere thanks to my thesis committee members: Professor Tae-Won Chun (University of Ulsan), Professor Sung-Jin Choi (University of Ulsan), Professor Dong-Choon Lee (Yeungnam University), and Dr. Eui-Heon Jung (University of Ulsan) for their valuable time, insightful comments and suggestions on my Ph.D thesis.

I would like to thank all Professors in University of Ulsan for their lectures and supports during my courses.

I express my grateful for the financial supports of Brain Korea 21 Plus (BK21+) and Network-based Automation Research Center (NARC). I would like to express my warm gratitude to my labmates in the Industrial Networks and Power Electronics Laboratory (INPEL) for the useful discussions, encouragement, help, and memorable moments during the course of my study. I would like to thank my beloved parents, my lovely girlfriend, and all my relatives for their encouragement, support, and love.

Last but not least, I would like to thank my senior ***Nguyen Dinh Tuyen*** for his encouragement and support.

Ulsan, June 2021

Pham Minh Duc

Abstract

The need for highly reliable and flexible distribution networks is a critical challenge for industrial application. This issue can be addressed by managing and scheduling microgrids, which is the main core of power distribution system. Microgrid is a small-scale distribution system consisting of distributed generation (DG) units, micro turbines, energy storage system, and transformer [1], [2]. A microgrid is linked to the utility grid at the point of common coupling (PCC) and it can transfer active and reactive power to the load. Compared to the traditional transmission system, the microgrid can operate autonomously in the islanding operation to regulate voltage and frequency at the point of common coupling. The islanded mode, according to the IEEE 1547 standard, can provide numerous benefits, including improved reliability and power quality, cost reduction, and auxiliary services [3].

In the islanding operation, it is important to manage the desired power among DG units, and the droop control algorithm has been widely used to operate DG units independently. However, the conventional control method cannot guarantee the power-sharing accuracy and high PCC voltage quality. Therefore, this thesis presents advanced control strategies to address these inaccurate power sharing and voltage distortion issues in the islanded microgrid system.

Firstly, based on analysis of an islanded microgrid with complex line impedance structure, an effective coordinated virtual impedance control scheme based on centralized approach is developed to accurately share active and reactive power in a microgrid. In the proposed control strategy, both virtual resistance and virtual inductance are simultaneously tuned to compensate for the mismatched line impedance among units. Even if the microgrid configuration and load condition change, the proposed control approaches still provide proper power sharing among DG units. Furthermore, the proposed method can be implemented directly without any knowledge of the detailed microgrid configuration or the required load power measurement, which increases the system reliability and reduces system complexity.

Next, in order to overcome the inaccurate fundamental power sharing and voltage quality issues under nonlinear load conditions, this thesis presents a harmonic compensation control scheme by adaptively regulating resistive-capacitive virtual impedances at the selected harmonic frequencies (3^{rd}, 5^{th}, and 7^{th}). To comply with the practical application, the control

system was developed in both a centralized and distributed network. Regardless of microgrid architecture or load circumstances, the proposed scheme properly distributes the active and reactive power. Additionally, a modification of impedance at harmonic frequency has also been proposed to mitigate the PCC voltage distortion. Because no information regarding the detailed microgrid parameters such as line impedances and nonlinear load current is required, the system complexity and expense are considerably reduced.

Finally, an impedance-based harmonics compensation (IBHC) is presented to provide accurate harmonic power sharing along with voltage harmonic compensation for DG units. The proposed IBHC is developed based on simple proportional integral controllers without using a load current sensor. To confirm the proposed control stability and reliability, the microgrid system is theoretically evaluated using a small-signal state-space model.

All control approaches are validated using PLECS simulations and experiments using scaled-down laboratory microgrid prototypes. The results show that the proposed control methods are both feasible and effective. The final section of the thesis draws conclusions and suggests future research.

Contents

List of Figures

List of Tables

Abbreviations

AC	Alternating Current
DC	Direct Current
FFT	Fast Fourier Transform
IGBT	Insulated-Gate Bipolar Transistor
LPF	Low-Pass Filter
MOSFET	Metal Oxide Silicon Field Effect Transistor
PI	Proportional Integral
PLL	Phase-Locked Loop
SOGI	Second-Order Generalized Integrator
THD	Total Harmonic Distortion
DER	Distributed Energy Resource
DG	Distributed Generator
DSP	Digital Signal Processor
MGCC	Microgrid Central Controller
PCC	Point of Common Coupling
PWM	Pulse Width Modulation
RC	Resistive-Capacitive

Chapter 1

Introduction

1.1 AC Microgrid Concept

Recent interest in the usage of distributed energy resources (DERs) has grown in response to major concerns such as potential fossil fuel shortages, deregulation of electric utility sectors, and public awareness of traditional electric power generation's environmental effect. Because the DERs output voltages are either DC or uncontrolled AC, power electronics-based converters are often employed to interface DERs with the power system [4]–[6]. As the number of DERs in the electrical grid increases, new power quality and stability challenges emerge, such as inaccurate power sharing, frequency variations, voltage variations, and system protection [7]–[9]. To address the aforementioned challenges, a microgrid concept is presented which considers DERs and related loads as a subsystem [10]. Under emergency or planned situations, microgrid can be isolated from the rest of the power system and operated in the islanded mode, which provides uninterruptible power to local loads. Thus, energy demand issues may be mainly locally resolved, resulting in dependability and improved system performance.

Fig. 1.1 shows the basic architecture of microgrid system. Distributed energy resources such as PV and wind turbines are connected to the point of common coupling through DC-AC converters. A microgrid can operate flexibly in either a grid-connected or an islanded mode to provide a cost-effective operation and a reliable power supply [11]–[14]. When the static switch (STS) is closed, the microgrid operates in the grid-connected mode, and the voltage and frequency are maintained by the main grid [15]. Due to the rotational mass inertia of the big synchronous generators in the power system, the main grid guarantees stiff voltage

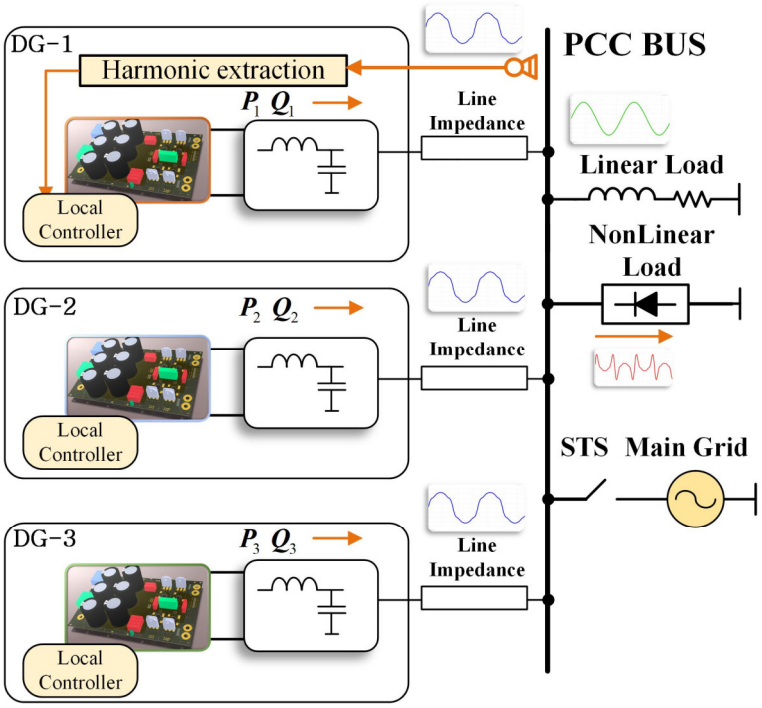

Figure 1.1 Typical AC microgrid architecture.

and frequency regulation [16], [17]. In other words, the main grid is in charge of maintaining the microgrid power balance.

In the islanded mode, controlling the microgrid becomes more difficult because microgrid frequency and voltage regulation, as well as the power balance between DER source and load demand, have to be obtained through coordinated control of DG units [18]. Traditionally, the actual power-frequency ($P-\omega$) and reactive power-voltage magnitude ($Q-V$) droop curves were used to distribute load power demand among DG units in a decentralized control approach [19], [20].

Fig. 1.2 shows the $P-\omega$ and $Q-V$ droop-based control technique for a single DG unit. Each DG units regulates the output active and reactive powers by adjusting the DG angular frequency and voltage magnitude, as follows:

$$\omega_{dri} = \omega_0 - m P_i, \tag{1.1}$$

$$V_{dri} = V_0 - n Q_i, \tag{1.2}$$

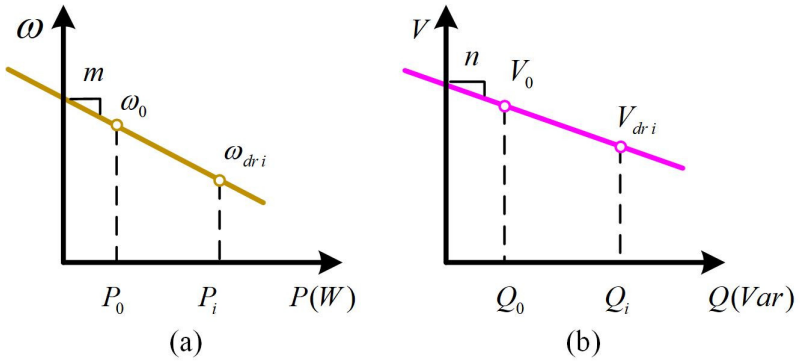

Figure 1.2 Droop-based control scheme for a DG unit.

where an index i denotes the i[th] inverter, m and n are the $P-\omega$ and $Q-V$ coefficients, ω_0 and ω_{dri} are the nominal and angular frequency at the fundamental frequency, and V_0 and V_{dri} are the nominal and inverter output voltages at the fundamental frequency, respectively.

Based on equations (1.1) and (1.2), the $P-\omega$ and $Q-V$ droop curves are illustrated in Fig. 1.2. From Fig. 1.2, the output real and reactive powers can be controlled by using the output frequency and voltage, respectively. From (1.1) and (1.2), the instantaneous voltage reference V_{ref}^{f} is generated as [21]

$$V_{ref}^{f} = V_{dri} \sin\left(\int \omega_{dri}\, dt\right). \tag{1.3}$$

In order to track the voltage reference V_{ref}^{f} in (1.3), the double-loop voltage controller is offend adopted [22], [23]. In the double-loop voltage controller, the outer loop uses a proportional-resonant controller tuned at the fundamental frequency [24]:

$$G_V(s) = K_{P\_V} + \frac{K_{R\_V}^{f}\, s}{s^2 + \omega_f^2}. \tag{1.4}$$

where K_{P_V} is the outer proportional gain, $K_{R\_V}^{f}$ is the resonant gain at the fundamental frequency. The inner loop has a simple proportional control gain K_{P_I} with the filter inductor current feedback, which give sufficient damping to the output LC filter [25]:

$$G_I(s) = K_{P\_I}. \tag{1.5}$$

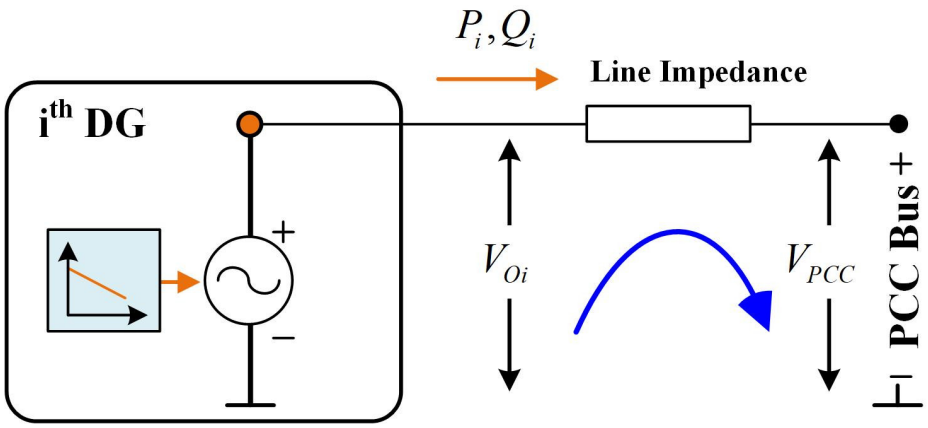

Figure 1.3 Model of a droop-controlled DG unit.

By implementing the double loop voltage controller, the regulated inverter output voltage can track the voltage reference in (1.3) properly, and the load power in the microgrid is shared autonomously among inverters.

1.2 Review of AC Microgrid Developments and Issues

Because only local measurements and no communication link are required, the droop control technique offers numerous advantages, including redundancy, flexibility, and expandability. Nonetheless, its implementation reveals a number of serious issues. The following sections examine issues with the droop controller and other control approaches that have been proposed in the literature.

1.2.1 Inaccurate Reactive Power Sharing among DG Units

Even though the active power demand is properly distributed among DG units with the aid of the conventional droop control method, it is impossible to share reactive power precisely, which reducing the power sharing performance.

Fig. 1.3 shows a simplified DG circuit with droop controller. The DG unit interfaced with the PCC through the feeder line impedance. In Fig. 1.3, the DG unit is represented as a controllable voltage source, V_{Oi} is ith DG output voltage, and V_{PCC} is the PCC voltage. In the microgrid, the impedance of line impedance is mainly inductive because of the output inductance, and the line resistance can be ignored [26]. Then, the impedance between the ith

DG unit and PCC can be described as X_i ($X_i = \omega L_i$). Since the phase angle δ_i difference between V_{Oi} and V_{PCC} is very small, the output reactive power is determined as following

$$Q_i = \frac{V_{dri} V_{PCC} \sin(\delta_i) - V_{PCC}^2}{X_i}. \tag{1.6}$$

where X_i is the output reactance of the DGi unit, V_{dri} and V_{PCC} are the amplitude of inverter output and the PCC voltages, and δ_i is the phase angle between the inverter output voltage and the PCC voltage, respectively. Substituting (1.2) into (1.6), the reactive power of the DG unit becomes

$$Q_i = \frac{V_{PCC}\left(V_{dri} - V_{PCC}\right)}{X_i + n_i V_{PCC}}. \tag{1.7}$$

From (1.7), the reactive power sharing error ΔQ_{ij} between two identical DG units (DGi and DGj) is calculated as

$$\Delta Q_{ij} = Q_i - Q_j = \frac{X_i - X_j}{V_{PCC}\left(V_{dri} - V_{PCC}\right)} Q_i Q_j. \tag{1.8}$$

Accurate reactive power sharing is hard to be achieved ($\Delta Q_{ij} = 0$) because the mismatched line impedances are always existing in the practical system ($\left|X_i - X_j\right| \neq 0$).

In order to address the reactive power sharing issue, many methods have been presented [27], [28]. An online voltage drop estimation was integrated into the DG local controller to reduce the power sharing error [29]. However, the control method requires microgrid to work in grid-connected mode before estimating the voltage drop, which increases the system complexity. The authors in [30] regulated the output reactive power in proportion to the DG output voltage derivative to compensated for the imbalanced voltage drop among DG units. Although the control method can minimize the voltage drop, the reactive power sharing error was not eliminated due to the lack of load voltage information. To ensure accurate power sharing, a robust droop control was proposed that using the load voltage information [31]. However, it is hard to measure the load voltage since the local DG unit and PCC are located far from each other. To remove the load voltage measurement and ensure accurate power sharing, a modified double-loop voltage controller was developed without the droop controller in [32]. However, the control algorithm would stop whenever the

communication fault occurs, so that reliability and feasibility are the main concern with this control scheme.

To simultaneously overcome the power instability and the inaccurate power sharing difficulty, the virtual impedance technique, which modified the output voltage reference by means of a load current feed-forward loop, was introduced [33], [34]. However, reactive power sharing was not distributed correctly because of the mismatches among the line impedances. In [35], the DG equivalent impedance was designed based on prior knowledge of the line impedance parameters, and the power sharing error was eliminated effectively. On the other hand, an estimation of DG equivalent line impedance was developed by using the feeder current and line impedance [36]. Nevertheless, it is not easy to detect all values of line impedance in real microgrid system with a large number of DG units.

To enhance the power sharing accuracy without using the pre-knowledge line impedance, the modified droop control technique was proposed [37], [38]. But, the modified droop coefficient has a substantial impact on microgrid stability [21]. The authors in [39] and [40] resolve this stability issue by developing a tunable virtual impedance to compensate for the voltage mismatches among inverter units. Although each DG units can properly share the reactive power sharing, the active power oscillation issue has not been solved sufficiently. The authors in [41], [42] mitigated the active power oscillation by injecting a real power disturbance at the output of the inverter, but the injected power disturbance reduces the microgrid voltage quality. To improve voltage quality, a virtual negative resistance is introduced to counteract the effect of the line resistance [43], [44]. Although the power sharing performance is enhanced by increasing the inductive component, the system stability is degraded due to the reduced system damping factor. Recently, authors in [45], [46] presented an adaptive virtual impedance based on multi-agent consensus to enhance power sharing performance. However, the consensus control method has a long communication delay, and it shows poor active and reactive power sharing when data drop exists [47]. To overcome this issue, the virtual impedance optimization [48] and voltage-based Thevenin estimation [49] were presented. However, they have a complicated estimation algorithm, and the system performance depends on many control variables. Although many literatures have discussed and solved inaccurate power sharing, there are still some things to be improved. For example,

it is important to compensate the active power oscillation, mitigate the circulating current and accurately share the reactive power regardless of the line impedance variation.

1.2.2 Inaccurate Harmonic Power Sharing among DG Units

When nonlinear loads are considered in the microgrid system, the harmonic load power is autonomously shared among DG units according to the line impedances. Unfortunately, because the line impedance difference is always existing in the practical distribution system, the harmonic load power is unevenly distributed, which potentially triggering current protection or causing DG unit overcurrent. Despite the development of several active and reactive power sharing method, the inaccurate harmonic power sharing issue has remained up to now. To reduce the harmonic power sharing error, a harmonic droop-based technique was introduced by using the microgrid voltage at the point of common coupling [50]. However, because the PCC is generally far from the DG unit, the control method may increase the control complexity, especially when a large number of DG is connected in the microgrid. In [41], the reactive, imbalance, and harmonic power were distributed in microgrid by regulating the virtual impedances at the fundamental and selected dominant harmonic frequencies. However, the power sharing accuracy cannot be ensured if the load condition changes during the tuning virtual impedance. Recently, a distributed virtual impedance control method based consensus algorithm was proposed to achieve both accurate fundamental and harmonic power sharing [51]. Nevertheless, the impedance regulator becomes quite complex as a result of the numerous controller gains.

1.2.3 Highly Distorted PCC Voltage

In addition to the incorrect harmonic power sharing issue, the PCC voltage quality is reduced significantly when nonlinear loads are employed in the microgrid. An individual harmonic droop controller was provided in order to distribute the nonlinear load power and improve the PCC voltage quality [52]. However, the control method does not consider the impact of the feeder impedance. A virtual capacitor was utilized to compensate for the harmonic voltage drop across the line impedance to mitigate the harmonics [53]. Nevertheless, the actual value of system line impedances is needed in the control approach. To avoid this

problem, a hierarchical harmonic control strategy was proposed with the aid of communication links [54]–[56], where an external harmonic regulation loop was added to enhance the PCC voltage quality. Although the voltage quality is improved, the control system is complex because the many control loops and Park/Inverse Park transformation are adopted.

To attenuate the system complexity, a droop based harmonic control loop was developed together with a virtual impedance control loop, and proper harmonic power sharing, as well as voltage harmonic mitigation, are achieved [51]. However, the PCC voltage quality still has a high total harmonic distortion, which does not comply with the IEEE 519-1992 standard (total harmonic distortion (THD) < 5%) [57]. PCC voltage harmonics can be compensated by properly adjusting the DG equivalent impedances [58], [59]. Nevertheless, Transferring the non-dc signal from the MGCC to the DG units through low-bandwidth communication connections is not feasible.

1.3 Objectives of the Thesis

In this thesis, we aim to address the conventional issues in the islanded microgrid system such as inaccurate fundamental power sharing, harmonic power sharing, and voltage distortion at the PCC. Following a state of art in the microgrid, control objectives for properly sharing linear and nonlinear loads across DG units, eliminating harmonic power sharing error, and compensating for PCC voltage harmonics in islanded microgrids are presented. The research methodology will be developed as follows:

- Advanced control techniques to offer accurate active and reactive power sharing in islanded microgrid systems regardless of microgrid configuration and load conditions.
- The control methods can be applied easily to the microgrid without any knowledge of the system line impedances.
- Enhanced control strategies to attenuate PCC voltage harmonics and guarantee a high PCC voltage quality (THD< 5%), which complies with the IEEE 519-1992 standard.
- PCC voltage at the dominant harmonics (3^{rd}, 5^{th}, 7^{th}) is selectively compensated, and the compensation performance is ensured even if the linear and nonlinear loads change.

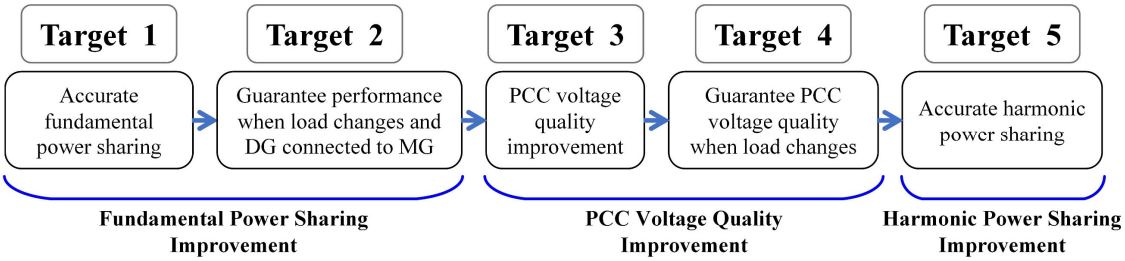

Figure 1.4 The control targets of the thesis.

Fig. 1.4 shows the thesis control targets. In Fig. 1.4, targets 1 and 2 belongs to the fundamental power sharing improvement, targets 3 and 4 focus on improving the PCC voltage quality, and target 5 is to improve the harmonic power sharing among DG units.

1.4 Outline of the Thesis

The thesis is organized into 5 chapters, as follows:

Chapter 1 introduces the concept of microgrid and surveys the past work related to reactive power sharing, harmonic power sharing, and PCC voltage harmonic compensation. Then, the objectives and contributions of the research work are outlined.

Chapter 2 presents an enhanced coordinated virtual impedance control scheme based on centralized approach to eliminate the reactive power sharing error in islanded microgrids regardless of microgrid configuration. The proposed controller is theoretically explored and evaluated via simulation and experiment.

Chapter 3 introduces an enhanced control scheme by adaptively regulating resistive-capacitive virtual impedances to share active and reactive power sharing despite variations of microgrid configuration or load condition. In addition, a modification of impedance at harmonic frequency has also been proposed to improve the PCC voltage quality. To increase the control feasibility, the control method was developed in both centralized approach and distributed approach without requiring the detailed microgrid configuration.

Chapter 4 presents an impedance-based harmonics compensation to compensate for the PCC voltage harmonics and inaccurate harmonic power sharing. Theoretical analysis and experimental results are also provided in detail.

Chapter 5 summarizes the works in this thesis and provides feasible recommendations for future research.

Table 1.1 summarizes the differences in proposed control methods. From the comparison table, it is clear that each control method is suitable for a specific microgrid condition.

Table 1.1 Comparison of different control methods

	Proposed control methods		
	Method in Chapter 2 "Enhanced coordinated virtual impedance control scheme based on centralized approach"	Method in Chapter 3 "Resistive-capacitive virtual impedances for PCC voltage quality improvement"	Method in Chapter 4 "Impedance-based harmonics compensation for accurate harmonic power sharing"
Types of Loads	Linear Load	Linear Load Nonlinear Load	Linear Load Nonlinear Load
Microgrid Centralized Configuration	Applicable	Applicable	Not Applicable
Microgrid Decentralized Configuration	Not Applicable	Applicable	Applicable
Computation	Low (fundamental frequency regulation)	High (fundamental and harmonic frequencies regulation)	High (fundamental and harmonic frequencies regulation)

Chapter 2

Accurate Active and Reactive Power Sharing Strategies

In this chapter, an improved power sharing scheme based on a centralized approach is proposed to share active and reactive power accurately in an islanded microgrid. In the proposed control scheme, an additional virtual impedance is inserted into the output of the inverter to compensate for the mismatched line impedance. By adaptively regulating the virtual impedance, accurate power sharing is ensured among DG units even when the one DG is connected or disconnected from the grid. Furthermore, the proposed control strategy can be implemented directly without any prior knowledge of line impedance parameter and load current measurement, which reduces the total cost and increase the reliability of the system. The proposed control is examined theoretically, and its effectiveness is verified by simulation and experiment.

2.1 Operating Principle of an Islanded Microgrid

2.1.1 Microgrid Operation

In Fig. 2.1 shows the configuration of an islanded microgrid composed of a number of DG units and loads. In Fig. 2.1, a load connected directly to a DG unit is called a local load, and one connected to a system at the PCC bus is called a public load. Based on the operating

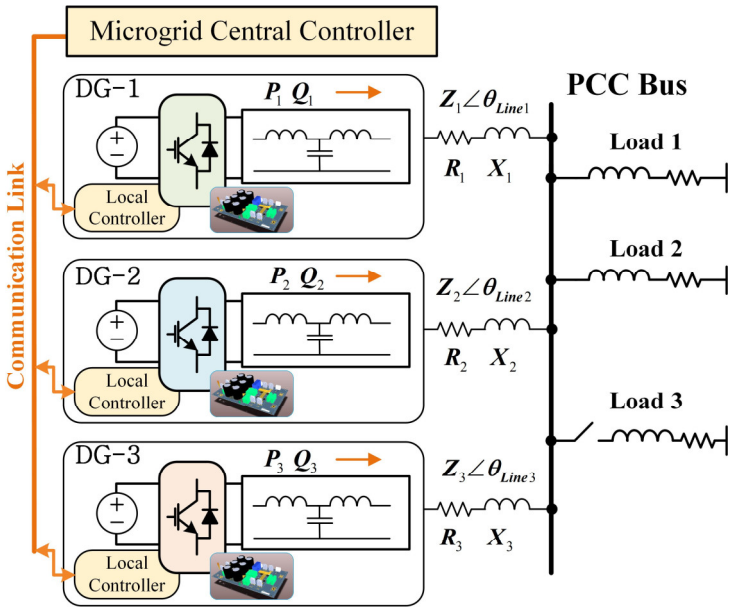

Figure 2.1 Typical islanded microgrid configuration with complex line impedance.

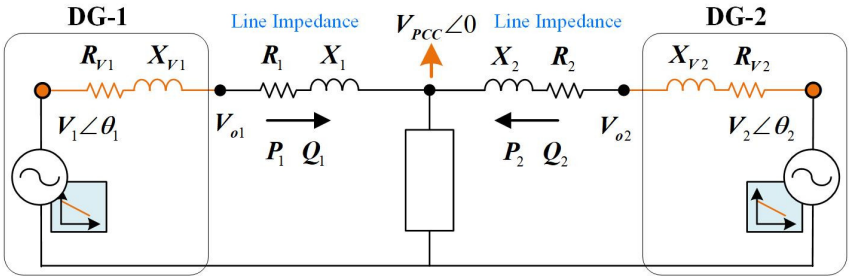

Figure 2.2 Equivalent model of microgrid system with the additional virtual impedance.

information exchanged between the MGCC and DG unit through low-bandwidth communication links, the MGCC can monitor all the DG units for microgrid protection.

During islanded operation, each DG unit is operated via the conventional droop controller, in which the angular frequency and voltage magnitude are given as follows, respectively [60]:

$$\omega_{dri} = \omega_0 - m P_i, \tag{2.1}$$

$$V_{dri} = V_0 - n Q_i, \tag{2.2}$$

where ω_0 and V_0 are the nominal values of the DG angular frequency and DG voltage magnitude, respectively; P_i and Q_i are the measured real and reactive powers after the low-pass filter (LPF), respectively; m and n are the $P-\omega$ and $Q-V$ coefficients, respectively. From (1.1) and (1.2), the instantaneous voltage reference V_{ref}^{f} is given as

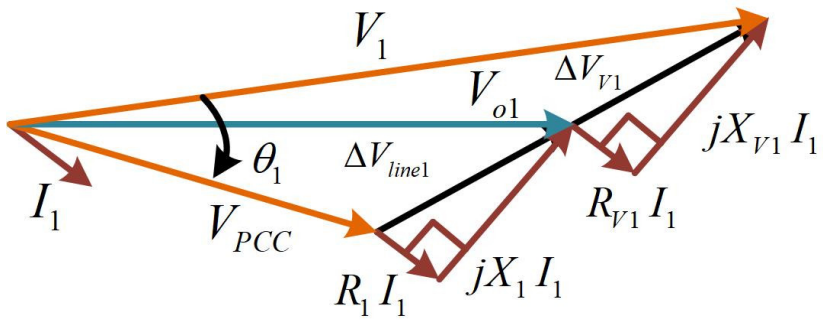

Figure 2.3 DG1 phasor diagram.

$$V_{ref}^{f} = V_{dri}\sin\left(\int \omega_{dri}\,dt\right). \tag{2.3}$$

2.1.2 Reactive Power-Sharing Analysis

For a simple analysis, the equivalent model of microgrid in Fig. 2.1 is established using two DG units with the same power rating, as shown in Fig. 2.2, and their output voltage magnitudes V_{O1} and V_{O2} are given in (2.4) and (2.5), respectively

$$V_{O1} = V_0 - n_1 Q_1, \tag{2.4}$$

$$V_{O2} = V_0 - n_2 Q_2, \tag{2.5}$$

In order to regulate the output voltage without any power losses, the additional virtual resistance and inductance are inserted at the output of the DG, as shown in Fig. 2.2. In Fig. 2.2, R_{V1} and X_{V1} are the virtual resistance and inductance of DG1, and R_{V2} and X_{V2} are the virtual resistance and inductance of DG2.

Based on the equivalent circuit in Fig. 2.2, the DG1 phasor diagram is obtained in Fig. 2.3, and its output voltage (V_{O1}) is derived by using the voltage drop approximation in (2.6):

$$\begin{aligned} V_{O1} &= V_{PCC} + \Delta V_{line1} + \Delta V_{V1} \\ &\approx V_{PCC} + \frac{R_1 P_1 + X_1 Q_1}{V_o} + \frac{R_{V1} P_1 + X_{V1} Q_1}{V_o}, \end{aligned} \tag{2.6}$$

where ΔV_{line1} and ΔV_{V1} are the voltage drop due to the line impedance and the additional virtual impedance.

Similarly, the DG2 output voltage is expressed as follows:

$$V_{O2} \approx V_{PCC} + \frac{R_2 P_2 + X_2 Q_2}{V_o} + \frac{R_{V2} P_2 + X_{V2} Q_2}{V_o}. \tag{2.7}$$

Assuming that DG1 and DG2 have the same power capability ($m_1 = m_2$, $n_1 = n_2 = n$) to simplify analysis. By solving equations (2.4) to (2.7), the reactive power sharing error is obtained as follows:

$$\Delta Q = \frac{Q_1\left(\Delta X_{1,2} + X_{V2} - X_{V1}\right) + P_1\left(\Delta R_{1,2} + R_{V2} - R_{V1}\right)}{G_Q\ V_0}, \tag{2.8}$$

where $\Delta X_{1,2} = X_2 - X_1$, $\Delta R_{1,2} = R_2 - R_1$. In order to eliminate the reactive power sharing error in (2.8), both virtual resistance and inductance ($R_{Vi}, X_{Vi} \mid i = 1,2$) should be simultaneously tuned to compensate for the mismatched line impedance among DG units. As a result, reactive power sharing is accurately achieved, and its dynamic performance is guaranteed even if the load changes. In addition, the circulating current is suppressed due to the balanced voltage drop between the DG and PCC.

2.2 Proposed Coordinated Virtual Impedance Control Scheme

In order to overcome the drawbacks of the traditional reactive power compensation method, the coordinated virtual impedance control strategy is developed based on the complex virtual impedance to achieve accurate power sharing irrespective of the microgrid system parameters.

2.2.1 Microgrid Central Controller

Fig. 2.4 shows the proposed control diagram. In Fig. 2.4, P_i and Q_i are calculated from each local DG, and this data is sent to the microgrid central controller. Then, the microgrid central controller calculates the reference power P_i^* and Q_i^*:

$$P_i^* = \left(1/\left(\left(1/\mathrm{G}_{P1}\right) + \left(1/\mathrm{G}_{P2}\right) + .. + \left(1/\mathrm{G}_{Pn}\right)\right)\right)\left(1/\mathrm{G}_{Pi}\right)\sum_{i=1}^{n} P_i, \tag{2.9}$$

$$Q_i^* = \left(1/\left(\left(1/\mathrm{G}_{Q1}\right) + \left(1/\mathrm{G}_{Q2}\right) + .. + \left(1/\mathrm{G}_{Qn}\right)\right)\right)\left(1/\mathrm{G}_{Qi}\right)\sum_{i=1}^{n} Q_i, \tag{2.10}$$

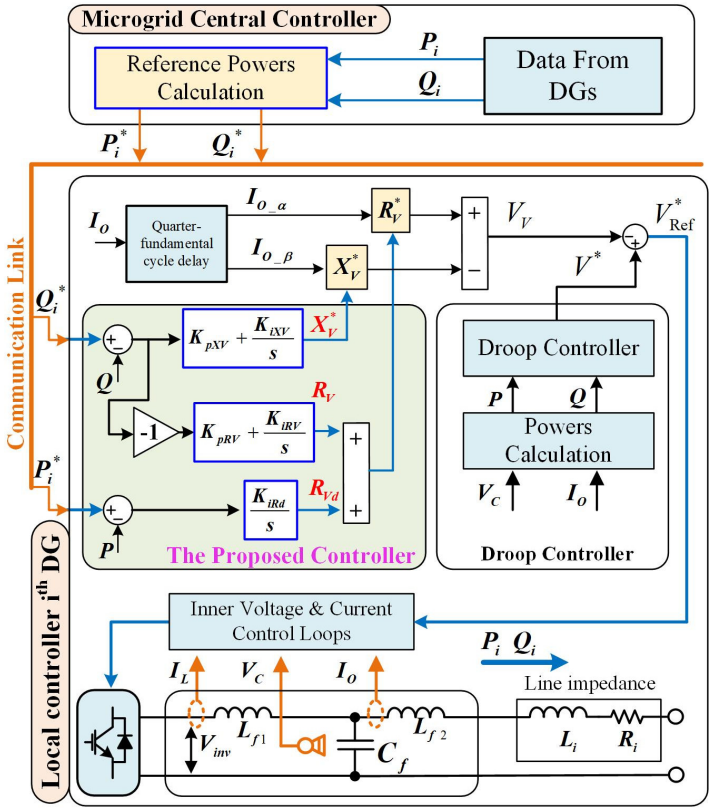

Figure 2.4 Proposed coordinated virtual impedance controller.

where n is the number of DG units in the microgrid. Then, the reference power P_i^* and Q_i^* are sent to the individual DG unit through the low bandwidth communication link.

2.2.2 Local Controller

After receiving the power information from the MGCC, each DG local controller adaptively tunes the virtual inductance X_V^* and virtual resistance R_V with the aid of the secondary controller:

$$X_V^* = \left(Q_i^* - Q_i\right)\left(K_{pXV} + K_{iXV}/s\right), \tag{2.11}$$

$$R_V = (-1)\left(Q_i^* - Q_i\right)\left(K_{pRV} + K_{iRV}/s\right), \tag{2.12}$$

where K_{pXV} and K_{pRV} are proportional gains; K_{iXV} and K_{iRV} are integral gains. In equation (2.12), R_V is oppositely tuned against the reactive power sharing error because of the counter effect between P and Q in the complex impedance.

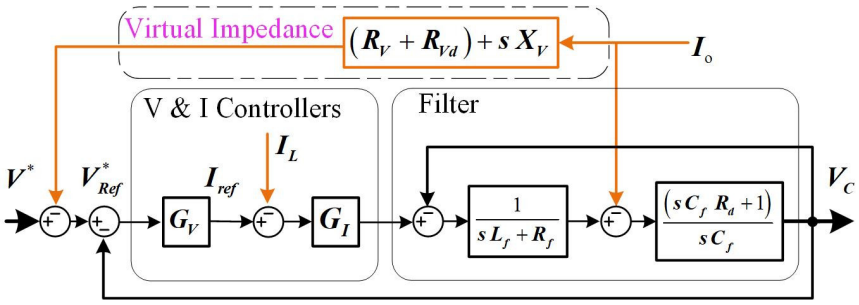

Figure 2.5 Inner loop control with coordinated virtual impedance controller.

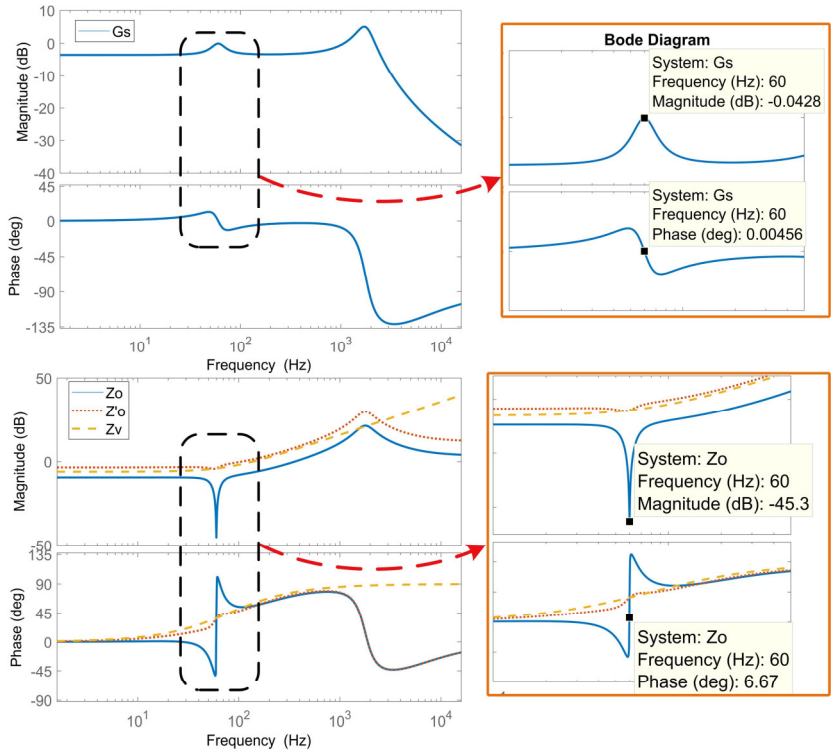

Figure 2.6 Bode diagram of (a) the voltage control transfer function and (b) the output impedance transfer function.

In addition, to compensate for any active power oscillation, the modified virtual resistance is obtained by adding the virtual damping resistance R_{Vd}:

$$R_V^* = R_V + R_{Vd}, \tag{2.13}$$

where R_V^* is the modified virtual resistance, and R_{Vd} is defined as:

$$R_{Vd} = \left(P_i^* - P_i\right)(K_{iRd} / s), \tag{2.14}$$

In equation (2.14), K_{iRd} is the integral gain. The virtual damping resistance (R_{Vd}) ensures accurate active power sharing during the transient and the steady state by damping the resonant frequency caused by the LC/LCL filter and system resonances [61].

Table 2.1 System Parameters

Parameters	Value	Parameters	Value	Parameters	Value
K_{pXV}	1×10^{-3}	ω_0	$2\pi60$ rad/s	L_f	1.2mH
K_{iXV}	5×10^{-3} rad/s	V_O	110V	R_f	0.01Ω
K_{pRV}	1×10^{-3}	G_{Pi}	0.005	C_f	20μF
K_{iRV}	7×10^{-3} rad/s	G_{Qi}	0.012	R_d	1Ω
K_{pV}	0.5	K_{iRd}	1×10^{-4} rad/s	L_O	1.2mH
K_{iV}	180 rad/s	K_{pI}	3	T_{LPF}	0.125s
R_{line_1}	0.3Ω	R_{line_2}	0.45 Ω	R_{line_3}	0.52 Ω
X_{line_1}	0.49Ω	X_{line_2}	0.905Ω	X_{line_3}	1.13Ω
P_{Total} (simulation)	1605W	Q_{Total} (simulation)	1305Var	ω_C	$2\pi8$ rad/s
P_{Total} (Experiment)	1012W	Q_{Total} (Experiment)	835Var	$f_{Switching}$	10KHz
Load 2	15Ω 45mH	Load 3	10Ω 15mH	$f_{Sampling}$	10KHz

As shown in Fig. 2.4, the proposed secondary controller is integrated into DG local controller and it is implemented simultaneously with the primary droop controller to increase the system response and reduce the effect of communication delay. Therefore, the accurate power sharing is achieved with fast convergence, and the performance is immune to communication delay. Moreover, once X_V^* and R_V^* are optimized, accurate power sharing is continuously guaranteed because the voltage drop caused by mismatched line impedance is well compensated irrespective of load changes or interrupted communication.

2.3 Closed-loop Transfer Function

In Fig. 2.5, the closed-loop transfer function is obtained without virtual impedance:

$$V_C = G(s)V_{\text{Ref}}^* - Z_O(s)I_O, \tag{2.15}$$

where $G(s)$ is the voltage gain function, and $Z_O(s)$ represents the output impedance of the inverter:

$$G(s) = \frac{G_V G_I\left(1+sC_fR_d\right)}{s^2L_fC_f + s\left(R_fC_f + G_IC_f\left(R_dG_V+1\right)+R_dC_f\right)+G_VG_I+1}, \tag{2.16}$$

where $G_V = K_{pV} + \dfrac{2K_{iV}\omega_c s}{s^2 + 2\omega_c s + \omega_f{}^2}$; $G_I = K_{pI}$.

$$Z_O(s) = \frac{\left(sL_f + R_f + G_I\right)\left(1 + sC_f R_d\right)}{s^2 L_f C_f + s\left(R_f C_f + G_I C_f \left(R_d G_V + 1\right) + R_d C_f\right) + G_V G_I + 1}. \tag{2.17}$$

The complex virtual impedance $Z_V(s)$ is proposed to control the power sharing by adjusting the voltage reference:

$$V_{\text{Ref}}^* = V^* - I_O Z_V(s) = V^* - I_O\left(R_V + R_{Vd} + sL_V\right). \tag{2.18}$$

By substituting (2.18) into (2.15), a modified equivalent output impedance $Z_O^{/}(s)$ including complex virtual impedance is obtained as follows:

$$Z_O^{/}(s) = Z_O(s) + G(s)\left(R_V + R_{Vd} + sL_V\right). \tag{2.19}$$

In order to investigate the impact of the virtual impedance on the system, Fig. 2.6 shows the frequency-amplitude characteristics plots of $G(s)$, $Z_O(s)$, $Z_O^{/}(s)$ and $Z_V(s)$ with the parameters in Table 2.1. In Fig. 2.6(a), the magnitude and phase of the voltage gain $G(s)$ are approximately 1 and 0, respectively, while the magnitude of $Z_O(s)$ is close to 0 at a fundamental frequency. Hence, the DG output voltage tracks its reference perfectly with a very small phase delay at the fundamental frequency. Therefore, the transfer functions of the LCL filter, voltage, and current control loops are simplified to be unity.

2.4 Stability Analysis

In order to verify the microgrid stability, the eigenvalues of the microgrid small signal model are investigated. The small signal model is derived by linearizing power sharing dynamics, P-ω and Q-V droop controllers, and the proposed virtual impedance control loop.

By linearizing the active and reactive powers, the linearized active and reactive power equations around the equilibrium operating point are obtained:

$$\begin{aligned}\Delta P_i &= \frac{\partial P_i}{\partial V_i}\Delta V_i + \frac{\partial P_i}{\partial \theta_i}\Delta\theta_i + \frac{\partial P_i}{\partial X_{Vi}}\Delta X_{Vi} + \frac{\partial P_i}{\partial R_{Vi}}\Delta R_{Vi} \\ &\triangleq K_{pvi}\Delta V_i + K_{p\theta i}\Delta\theta_i + K_{pXi}\Delta X_{Vi} + K_{pRi}\Delta R_{Vi}\end{aligned}. \tag{2.20}$$

$$\begin{aligned}\Delta Q_i &= \frac{\partial Q_i}{\partial V_i}\Delta V_i + \frac{\partial Q_i}{\partial \theta_i}\Delta\theta_i + \frac{\partial Q_i}{\partial X_{Vi}}\Delta X_{Vi} + \frac{\partial Q_i}{\partial R_{Vi}}\Delta R_{Vi} \\ &\triangleq K_{qvi}\Delta V_i + K_{q\theta i}\Delta\theta_i + K_{qXi}\Delta X_{Vi} + K_{qRi}\Delta R_{Vi}\end{aligned}. \tag{2.21}$$

In our study, the inner voltage and current control loop transfer functions are defined to be unity ($V_i = V_i^*$ and $\omega_i = \omega_i^*$) because they are used to track their reference inputs with a very small phase delay. Therefore, equations (2.1) and (2.2) are rewritten as follows:

$$\omega_i = \omega_o - G_{Pi} P_i, \tag{2.22}$$

$$V_i = V_o - G_{Qi} Q_i, \tag{2.23}$$

where $G_{Pi} = m_i$ and $G_{Qi} = n_i$. By linearizing (2.22) and (2.23), $\Delta\omega_i = n_i$ and ΔV_i around the equilibrium operating point become

$$\Delta\omega_i = -G_{Pi}\,\Delta\overline{P}_i, \tag{2.24}$$

$$\Delta V_i = -G_{Qi}\,\Delta\overline{Q}_i. \tag{2.25}$$

In (2.24) and (2.25), $\Delta\overline{P}_i$ and $\Delta\overline{Q}_i$ are the average active and reactive powers, which are defined as follows:

$$\Delta\overline{P}_i = \Delta P_i\; G_D(s)\;\omega_C/(s+\omega_C), \tag{2.26}$$

$$\Delta\overline{Q}_i = \Delta Q_i\; G_D(s)\;\omega_C/(s+\omega_C). \tag{2.27}$$

where ω_C is the low-pass filter cut-off frequency, $G_D(s)$ is the total delay time including zero-order hold.

Because the effect of time delay and zero-order hold is negligible to detect the average power, the total delay time transfer function is simplified as unity ($G_D(s) \approx 1$) [62]. From equations (2.20) to (2.27), the linearized control equations of the system are given as following:

$$\begin{aligned}\Delta\dot{\overline{P}}_i = &-\omega_C\Delta\overline{P}_i + \omega_C K_{pvi}\left(-G_{Qi}\,\Delta\overline{Q}_i\right) + \omega_C K_{p\theta i}\Delta\theta_i \\ &+ \omega_C K_{pXi}\Delta X_{Vi} + \omega_C K_{pRi}\Delta R_{Vi}\end{aligned}, \tag{2.28}$$

$$\begin{aligned}\Delta\dot{\overline{Q}}_i = &-\omega_C\Delta\overline{Q}_i\left(1 + K_{qvi}G_{Qi}\right) + \omega_C K_{q\theta i}\Delta\theta_i + \omega_C K_{qXi}\Delta X_{Vi} \\ &+ \omega_C K_{qRi}\Delta R_{Vi}\end{aligned}, \tag{2.29}$$

$$\Delta\dot{\theta}_i = -G_{Pi}\,\Delta\overline{P}_i. \tag{2.30}$$

From equations (2.28) to (2.30), the state equation of the i[th] DG is obtained as follows:

$$\begin{bmatrix} \Delta\dot{\theta}_i \\ \Delta\dot{\bar{P}}_i \\ \Delta\dot{\bar{Q}}_i \end{bmatrix} = [A_i] \begin{bmatrix} \Delta\theta_i \\ \Delta\bar{P}_i \\ \Delta\bar{Q}_i \end{bmatrix} + [B_i] \begin{bmatrix} \Delta X_{Vi} \\ \Delta R_{Vi} \end{bmatrix}, \tag{2.31}$$

By linearizing (2.11) to (2.14), the virtual inductance $\Delta\dot{X}_{Vi}$ and virtual resistance $\Delta\dot{R}_{Vi}$ become

$$\Delta\dot{X}_{Vi} = K_{iXV}\left(\Delta\bar{Q}_{ref\,i} - \Delta\bar{Q}_i\right), \tag{2.32}$$

$$\Delta\dot{R}_{Vi} = K_{iRd}\left(\Delta\bar{P}_{ref\,i} - \Delta\bar{P}_i\right) - K_{iRV}\left(\Delta\bar{Q}_{ref\,i} - \Delta\bar{Q}_i\right), \tag{2.33}$$

where $\Delta\bar{P}_{ref\,i}$ and $\Delta\bar{Q}_{ref\,i}$ are the active and reactive power references in (2.9) and (2.10), respectively. For simple analysis, we assume all DG units have the same power capacity and communication delay (τ_D). Then, $\Delta\bar{P}_{ref\,i}$ and $\Delta\bar{Q}_{ref\,i}$ are expressed as follows [63]:

$$\Delta\bar{P}_{ref\,i} = \Delta\bar{P}_{ref} = \frac{1}{\tau_D s + 1}\frac{1}{n}\sum_{i=1}^{n}\Delta\bar{P}_i\,, \tag{2.34}$$

$$\Delta\bar{Q}_{ref\,i} = \Delta\bar{Q}_{ref} = \frac{1}{\tau_D s + 1}\frac{1}{n}\sum_{i=1}^{n}\Delta Q_i\,. \tag{2.35}$$

By linearizing (2.34) and (2.35), $\Delta\dot{\bar{P}}_{ref}$ and $\Delta\dot{\bar{Q}}_{ref}$ are obtained:

$$\Delta\dot{\bar{P}}_{ref} = \frac{-1}{\tau_D}\Delta\bar{P}_{ref} + \frac{1}{\tau_D\, n}\sum_{i=1}^{n}\Delta\bar{P}_i\,, \tag{2.36}$$

$$\Delta\dot{\bar{Q}}_{ref} = \frac{-1}{\tau_D}\Delta\bar{Q}_{ref} + \frac{1}{\tau_D\, n}\sum_{i=1}^{n}\Delta\bar{Q}_i\,. \tag{2.37}$$

Considering equations from (2.28) to (2.37), the small signal model of the microgrid system is derived as following:

$$\Delta\dot{X}_{MG} = A_{MG}\,\Delta X_{MG}\,, \tag{2.38}$$

where

$$\begin{aligned}\Delta X_{MG} = [&\Delta\theta_1 \ldots \Delta\theta_3\ \Delta\bar{P}_1 \ldots \Delta\bar{P}_3\ \Delta\bar{Q}_1 \ldots \Delta\bar{Q}_3\ \Delta X_{V1} \\ &\ldots \Delta X_{V3}\ \Delta R_{V1} \ldots \Delta R_{V3}\ \Delta\bar{P}_{ref}\ \Delta\bar{Q}_{ref}]^T\end{aligned}, \tag{2.39}$$

The eigenvalues of equation (2.39) are solved by using "eigenvalues function" in MATLAB to evaluate the system stability. According to [64], A_{MG} is singular matrix and it has zero eigenvalues, so only the nonzero eigenvalues of A_{MG} (λ_1 to λ_{12}) are used for analyzing

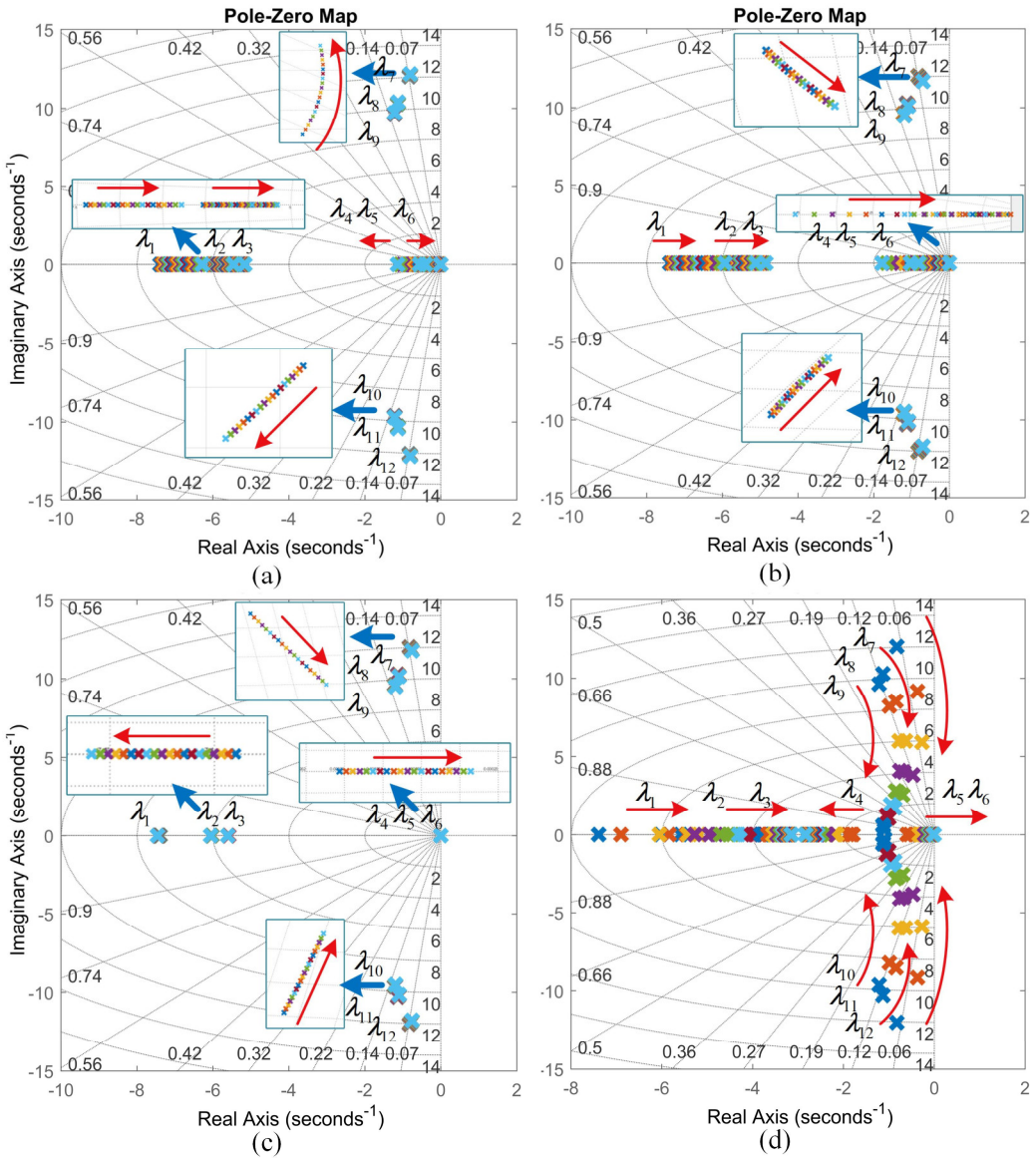

Figure 2.7 Root locus diagram: a) $K_{iRV}=0.005; 10^{-5}\le K_{iXV}\le 200$. (b) $K_{iRd}=0;\ K_{iXV}=0.005;$ $10^{-5}\le K_{iRV}\le 200$. (c) $K_{iRV}=K_{iXV}=0.005;\ 10^{-5}\le K_{iRd}\le 200$. (d) Line resistance variation $10^{-5}\le R_{\ln}\le 10$.

microgrid stability. In order to achieve a good system performance, small proportional gains (K_{pRV}, K_{pXV}) are used as shown in Table 2.1.

Fig. 2.7 shows the root locus for different control parameters. From Fig. 2.7 (a), the system damping is reduced when increasing K_{iXV} because $\lambda_{7\text{-}12}$ move toward the image axis. In Fig. 2.7(b), the system becomes unstable when K_{iRV} is higher than its stable value

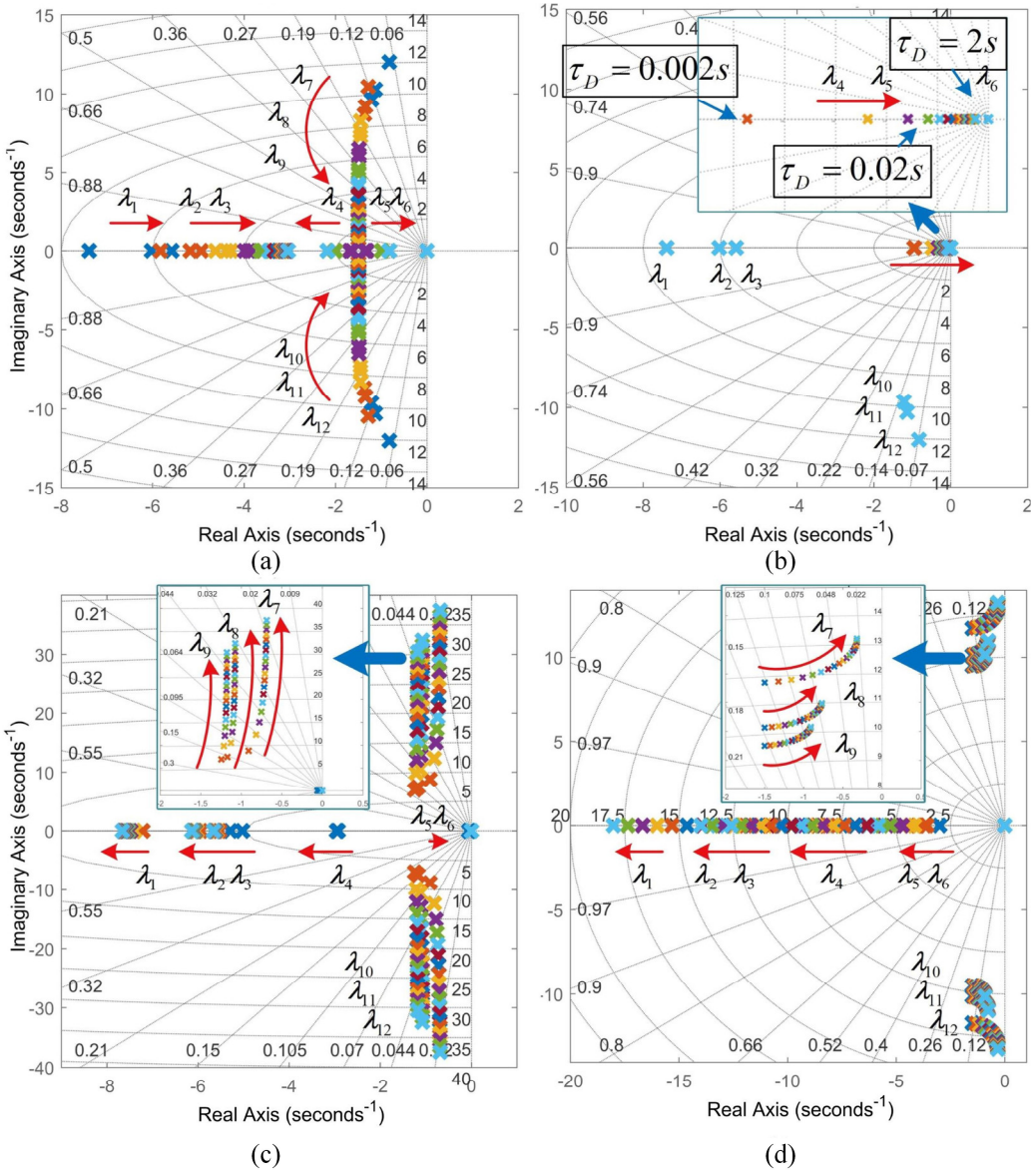

Figure 2.8 Root locus diagram: (a) Line inductance variation $10^{-5} \le X_{\ln} \le 10$. (b) Communication delay variation $0.002s \le \tau_D \le 20s$. (c) $10^{-5} \le G_{Pi} \le 0.05$. (d) $10^{-5} \le G_{Qi} \le 0.05$.

($K_{iRV} > 20$) because λ5 and λ6 are real numbers. As K_{iRd} increases in Fig. 2.7(c), λ4 and λ5 move toward the real axis, which reduces the system stability.

The effect of different line impedances is evaluated by adding additional resistance $R_{\ln}$ and inductance $X_{\ln}$ to DG line impedance, and its root locus diagram is shown in Fig. 2.7(d). When $R_{\ln}$ increases, the dominant eigenvalues move closer to the imaginary axis, and system stability is decreased, as shown in Fig. 2.7(d). Meanwhile, the system becomes more stable when increasing $X_{\ln}$ because the dominant eigenvalues move from the right to the left,

as shown in Fig. 2.8(a). Fig. 2.8(b) shows the effect of the communication delay on the system. As τ_D increases, $\lambda_{4\text{-}6}$ move to the right half-plane, and the system stability is reduced. Figs. 2.8(c) and (d) show the system root locus diagram when the droop coefficients have some variation. As shown in Figs. 2.8(c) and (d), when G_{Pi} and G_{Qi} increase, the system damping is reduced and the system stability is decreased, respectively. By balancing between damping and transient responses, the controller parameters are determined to effectively regulate the virtual resistance and inductance for accurate power sharing. The design parameters are given in Table 2.1.

2.5 Simulation Results

The microgrid with three DG units in Fig. 2.1 is simulated using PLECS to verify the effectiveness and feasibility of the proposed control strategy. An enhanced adaptive virtual impedance control strategy [39], which improves the power sharing by adaptively tuning the virtual impedance variable $\tilde{K}_V$, is compared to evaluate the proposed control strategy. For reasonable comparison, both controller parameters are chosen to have the same steady-state performance and reactive power settling time (τ_Q). Each state used in the simulation is defined as follows:

State 1: The compensation controller starts to compensate the power sharing error.

State 2: Load 2 is connected to the microgrid to examine the performance of the proposed control scheme.

State 3: The communication is interrupted, and load 3 is connected to evaluate the system dynamic performance and system stability.

To evaluate the performance of the proposed system, percentage reactive power error $\Delta Q_{err}(\%)$ is defined as following:

$$\Delta Q_{err}(\%) = \frac{1}{n}\sum_{i=1}^{n}\left|Q_i - Q_i^*\right| / Q_i^* \times 100\% . \tag{2.40}$$

Figs. 2.9(a) and (b) show the power sharing performance of the conventional and the proposed controllers in three states. When the compensation starts at 2.5s, the reactive power sharing is accurately achieved after some transient intervals regardless of the controller.

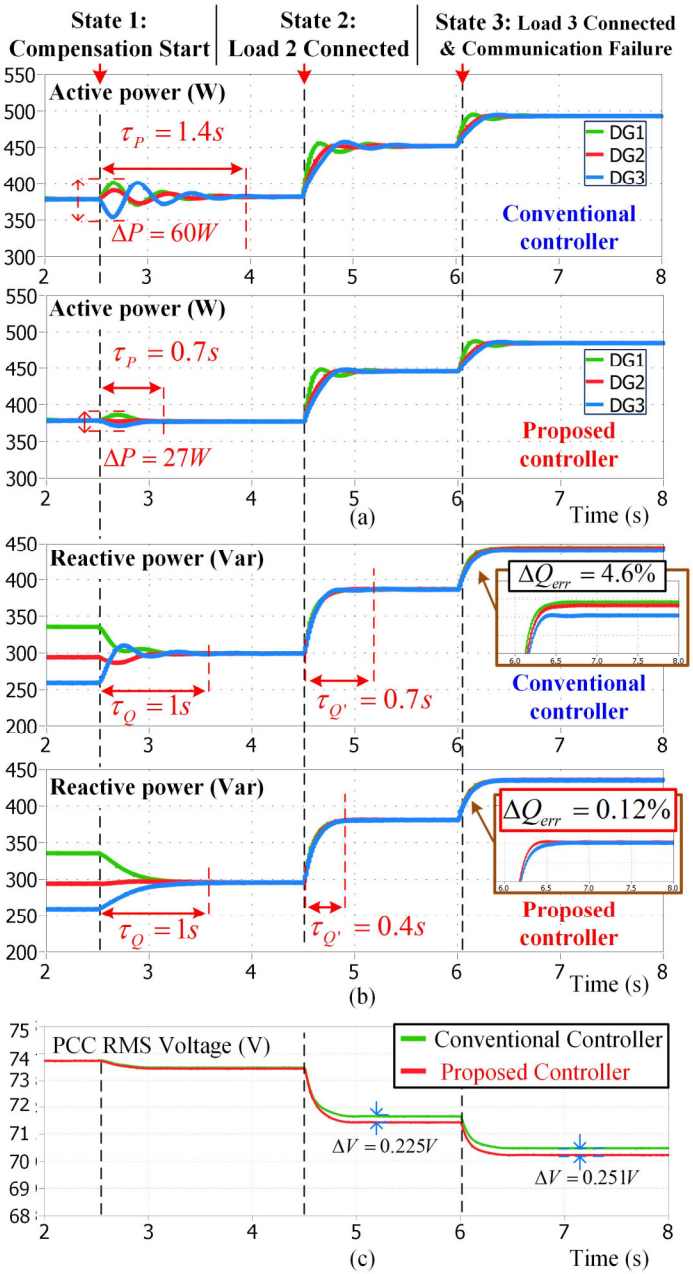

Figure 2.9 Simulation results of the conventional and proposed controller (a) active power sharing. (b) reactive power sharing. (c) PCC voltage.

However, the conventional controller shows more oscillation and its transient performance is not smooth as shown in Figs. 2.9(a) and (b). On the other hand, the proposed controller shows a good dynamic response with a remarkable reduction of $\tau_{Q'}$ from 0.7s to 0.4s when load 2 is connected at 4.5s. To evaluate the system dynamic performance, load 3 is connected at 6s during interrupted communication link. As we can see, the reactive power sharing error of the

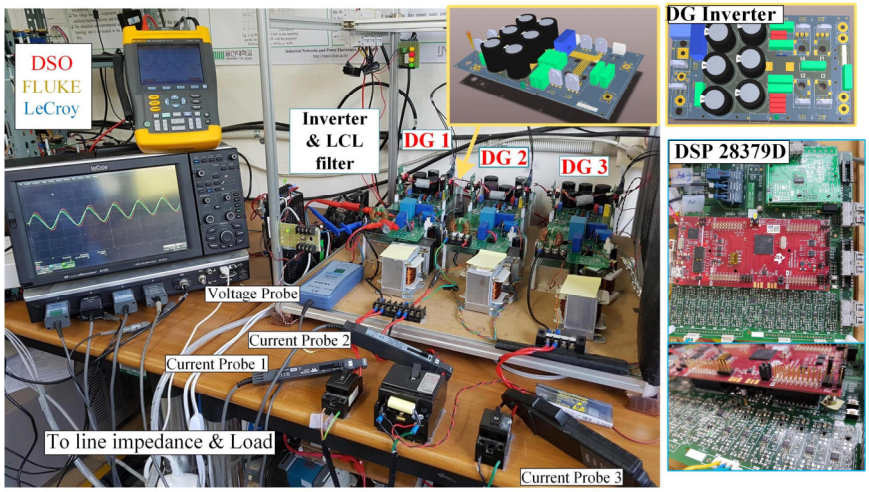

Figure 2.10 Laboratory islanded microgrid system.

proposed controller ($\Delta Q_{err}(\%) = 0.12\%$) becomes much smaller than that of the conventional controller ($\Delta Q_{err}(\%) = 4.6\%$).

During the reactive power compensation, the proposed controller also reduces the active power oscillation ΔP , and settling time τ_P significantly from 60W to 27W and 1.4s to 0.7s, respectively by using the virtual damping resistor. From Fig. 2.9(c), the further voltage drop (ΔV) in state 3 between our proposed and the conventional methods is acceptable with only 0.35% difference. This small voltage drop is caused by higher total virtual impedance in the proposed control method. While the conventional controller only uses the virtual impedance variable ($\tilde{K}_V$), the proposed controller considers virtual resistance, inductance and damping resistance to improve the power sharing performance and damp the active power oscillation.

2.6 Experimental Results

For experimental verification, the AC microgrid in Fig. 2.1 is set up with three DG units with the parameters in Table 2.1. DG units are controlled using a Texas Instruments TMS320F28379D microcontroller, and 20ms communication delay caused by the low-bandwidth communication is emulated by using zero-order hold [35]. Fig. 2.10 shows the laboratory islanded microgrid system with 3 DG units. The active and reactive powers are

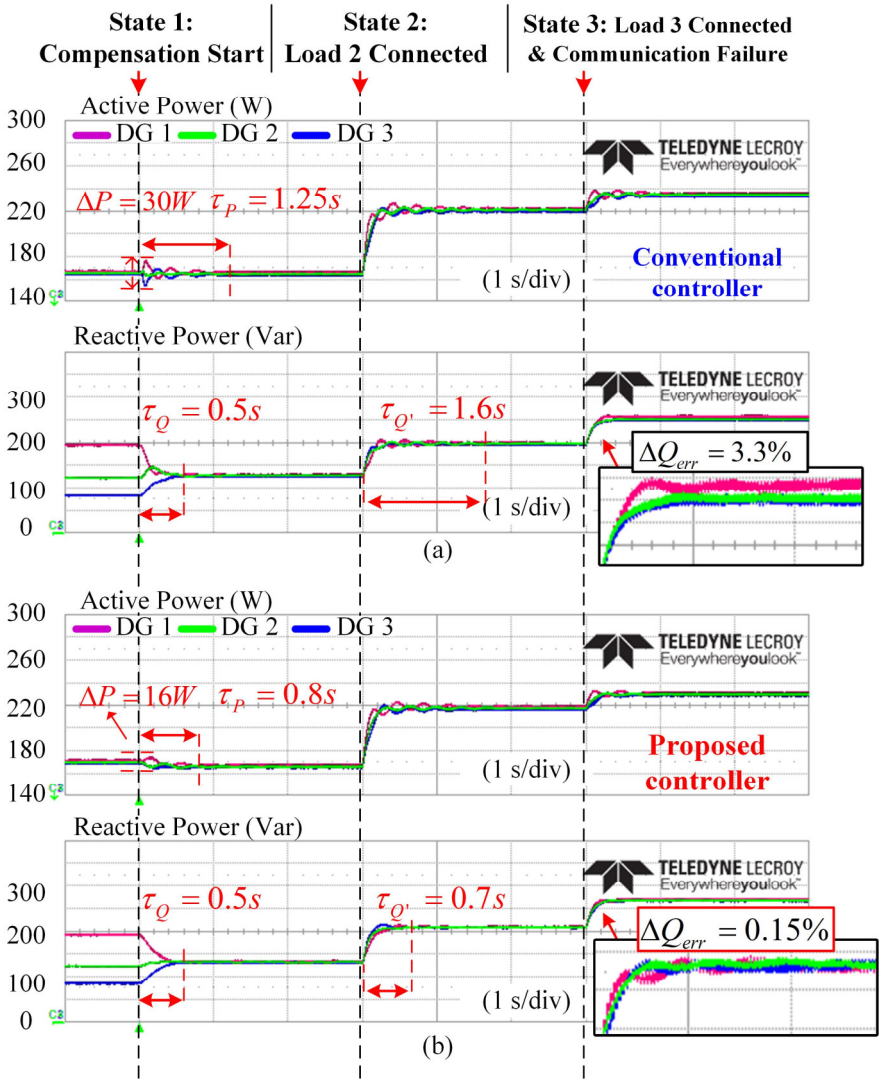

Figure 2.11 Experiment results of power sharing performance for (a) conventional controller and (b) proposed controller.

calculated by the digital signal processor and exported to digital to analog converter module (Analog AD5325BRMZ) to fully monitor the power in real time.

To investigate the performance of the proposed controller, the three states defined for the simulation are investigated experimentally. Fig. 2.11 shows the power sharing performance comparison between the conventional and proposed controller. For reasonable comparison, both controller parameters are chosen to have the same reactive power settling time ($\tau_Q = 0.5s$) in state 1. From Figs. 2.11(a) and (b), the proposed controller has better performance with a smooth transient response compared to the conventional controller. The smooth transient response is important because any reactive power oscillation directly affects

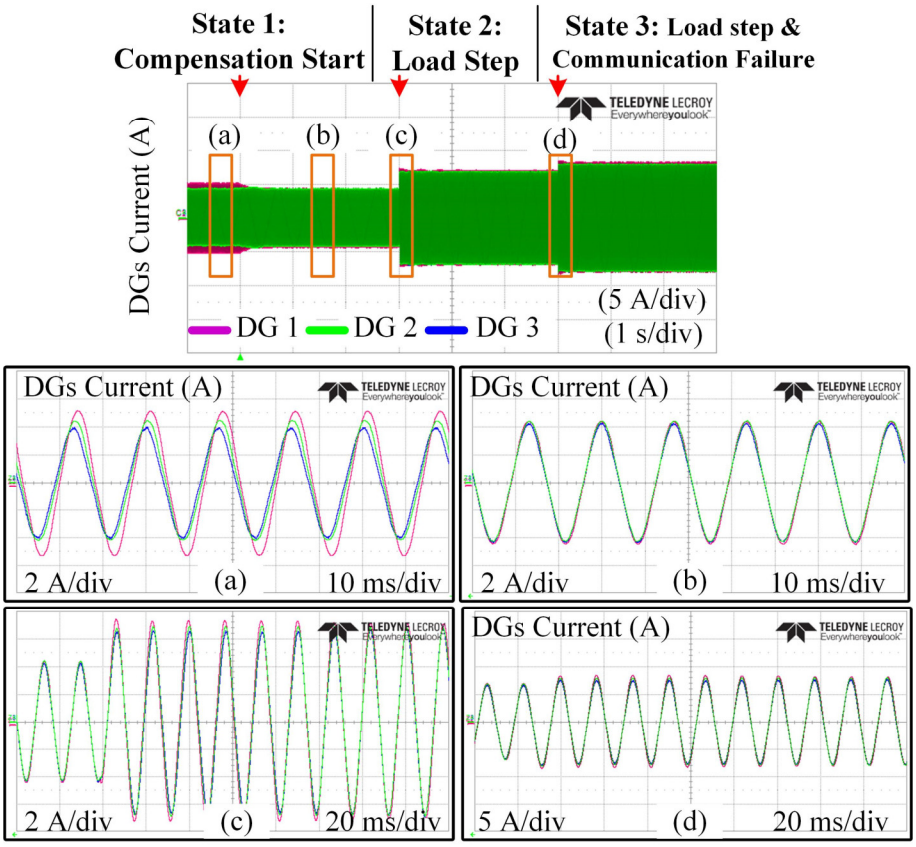

Figure 2.12 The performance of DG current in 3 difference states: (a) State 1: Before the compensation starts (b) After the compensation starts. (c) State 2: Load 2 is connected. (d) State 3: Load 3 is connected at communication failure.

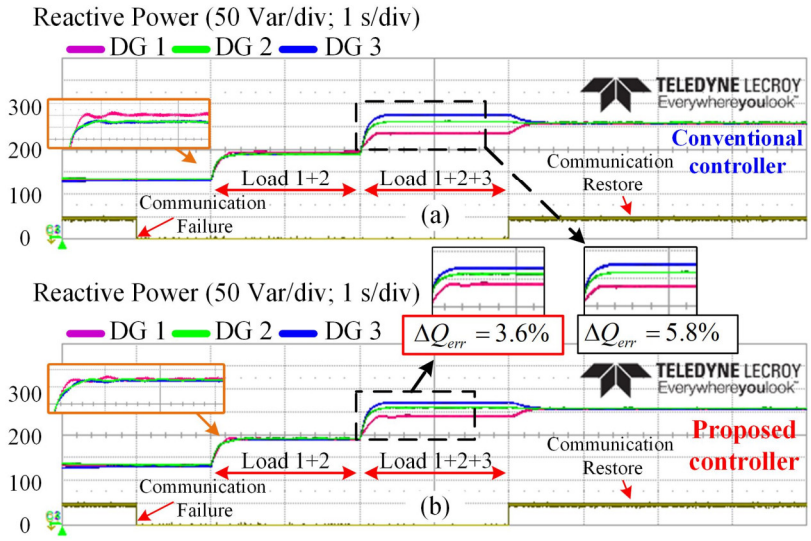

Figure 2.13 Reactive power sharing performance when load change during communication interruption. (a) The conventional controller. (b) The proposed controller.

the output voltage and causes the fluctuation of the circulating currents among DG units. In

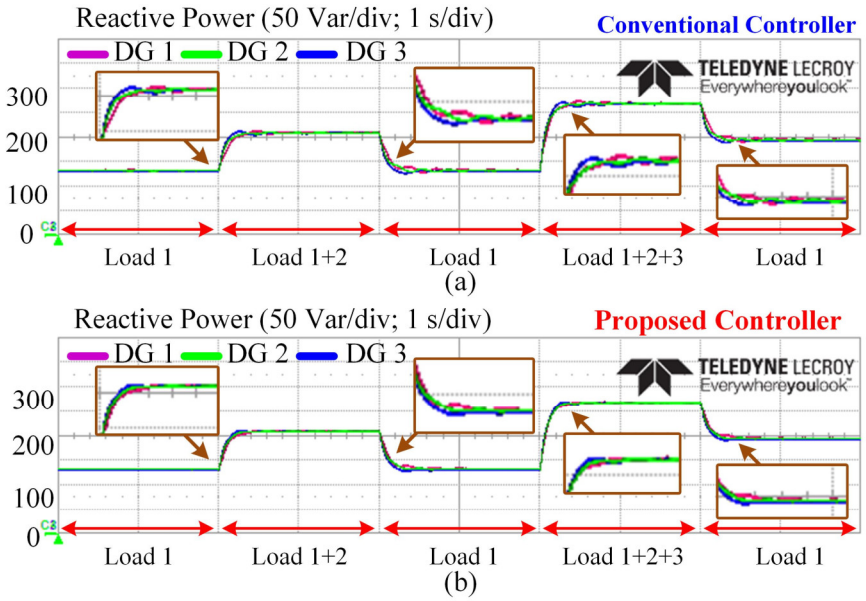

Figure 2.14 Reactive power sharing performance when loads are connected sequentially. (a) The conventional controller. (b) The proposed controller.

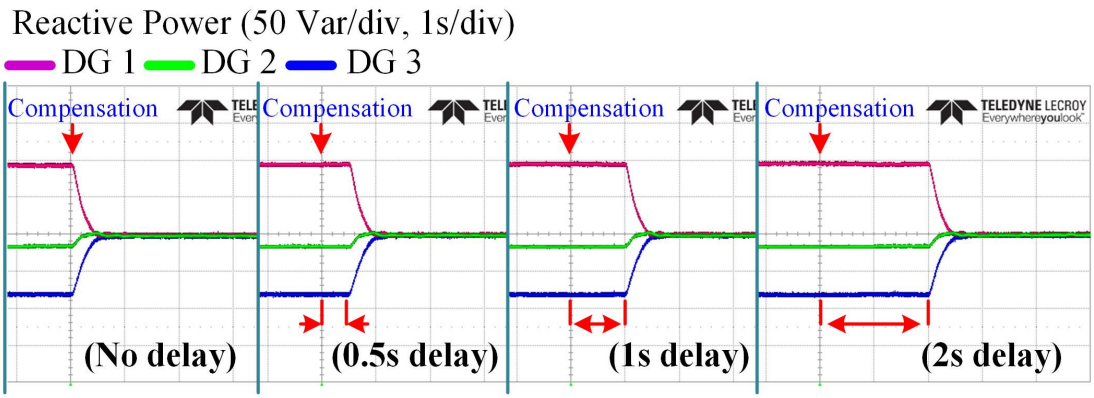

Figure 2.15 Reactive power sharing performance with various communication delay times.

addition, when load 2 is connected to the microgrid, the dynamic performance of the proposed controller is also superior with a remarkable reduction of $\tau_{Q'}$ from 1.6s to 0.7s. So, we can say that the proposed controller effectively controls the complex virtual impedance.

When load 3 is connected to the grid at the communication failure, the conventional controller shows remarkable reactive power sharing error ($\Delta Q_{err}(\%) = 3.3\%$), while the error becomes much smaller with the proposed controller ($\Delta Q_{err}(\%) = 0.15\%$), as shown in Figs. 2.11(a) and (b). As we can see from Figs. 2.11(a) and (b), the active power oscillation ΔP is

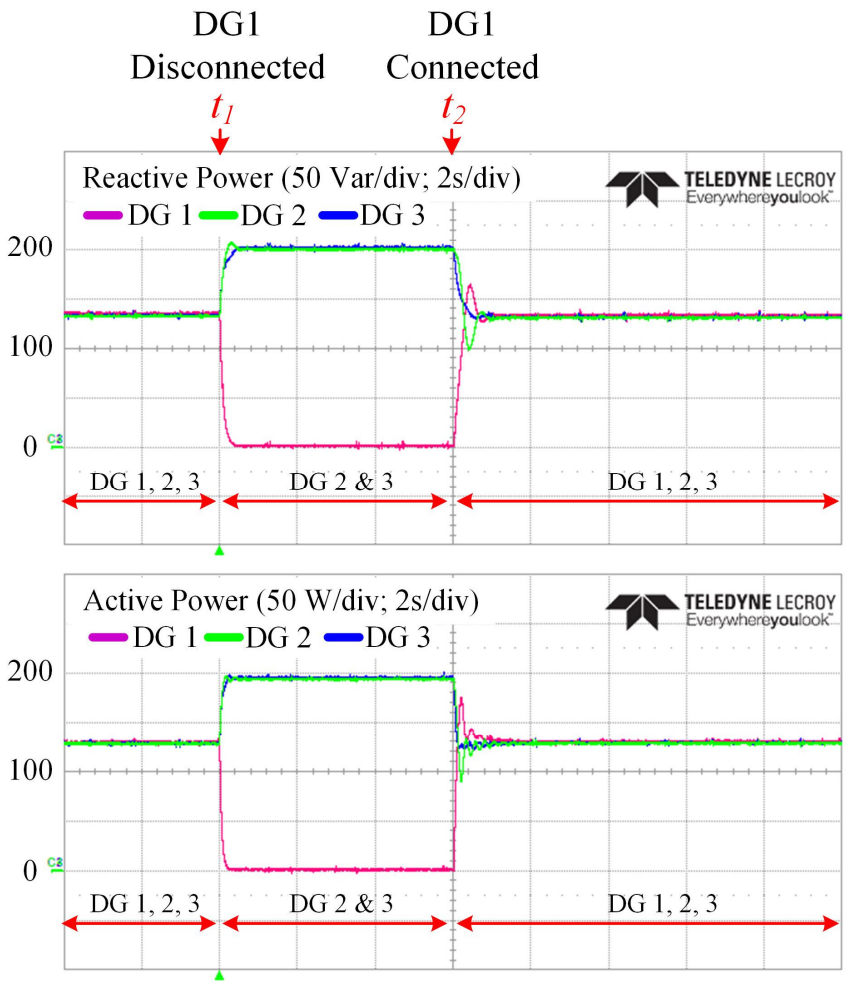

Figure 2.16 The power sharing performance when DG1 is disconnected from and connected to the microgrid.

well damped during the reactive power compensation with a half reduction ($\Delta P = 16\text{W}<30\text{W}$). Also, the active power settling time τ_P is considerably reduced from 1.25s to 0.8s.

In order to show the feasibility of the proposed controller, the DG current is directly measured using current probes to avoid measurement error. In Figs. 2.12, we can see that the current-sharing accuracy is significantly improved with a fast response. So, we can say that the circulating current among the DG units is reduced irrespective of the load power change.

Fig. 2.13 shows the power sharing performance when the communication link is shortly interrupted in a period. From Fig. 2.13, the reactive power sharing error of the proposed controller ($\Delta Q_{err}(\%) = 3.6\%$) is much smaller than that of the conventional controller ($\Delta Q_{err}(\%) = 5.8\%$) even though the load is doubly increased. When

communication is restored, the proposed controller smoothly recovers its power sharing accuracy.

The reliability of the proposed controller is verified in Fig. 2.14 when loads are sequentially connected to the microgrid with 2s intervals. From Fig. 2.14, it is obvious that the proposed controller shows excellent dynamic performance with fast steady-state response compared to the conventional controller.

Fig. 2.15 shows the power sharing performance with various communication delay times. As we can see in Fig. 2.15, the power sharing error is not affected even though the communication delay is changed from 0 to 2s thanks to the proposed secondary controller. Therefore, the dynamic response and stability of the microgrid system are increased.

To investigate the effectiveness of the proposed method during DG connection, DG1 is disconnected and connected at t_1 and t_2, respectively, as shown in Fig. 2.16. From Fig. 2.16, accurate active and reactive powers sharing are guaranteed with a good dynamic response for both disconnected and connected cases thanks to the proposed controller.

From the experiment results, it is clear that the performance of the proposed controller is better than that of the conventional controller with proportional load power sharing among the DG units. Also, the power sharing performance is guaranteed with smaller error even if the load changes during communication interruption, and the power sharing error is unaffected by the communication delay. The experimental results match well with the simulation results.

2.7 Conclusion of the Chapter

This chapter proposes a coordinated virtual impedance control strategy to solve many important issues such as the active power oscillation, inaccurate reactive power sharing among DG units, and the system dynamics. In our control method, both virtual resistance and virtual inductance are adaptively tuned without using the system parameters to effectively compensate the mismatched line impedance among DG units. In addition, a power coupling is considered to effectively mitigate the active power oscillation. As a result, the active power oscillation is mitigated about 50% in transient condition comparing to the conventional control methods, and the system dynamic performance is improved with the reactive power sharing error less than 0.15%. Furthermore, the microgrid system still has good power sharing

performance even if the load changes during the communication interruption. Therefore, our control scheme is very useful for effective operation of DG units in islanded microgrid. This chapter also presents a design procedure and stability analysis for practical applications. The effectiveness and flexibility of the proposed control strategy are verified through simulations and experiments.

Chapter 3

PCC Voltage Harmonic Compensation Strategy

Besides the reactive power sharing issue, the voltage harmonic distortion at the PCC is also a big concern because the droop controller only regulates the fundamental components. When a nonlinear load is connected to the grid, the uncontrolled harmonic currents cause instability in the microgrid and PCC voltage distortion. In previous DG control schemes, it is impossible to satisfy the requirements of PCC voltage quality with only a fundamental virtual impedance controller (VIC). In this chapter, we propose an enhanced virtual impedance control scheme to provide voltage harmonic compensation in islanded microgrids while maintaining accurate power sharing. To increase the control feasibility, the control method was developed in both a centralized approach and distributed approach without requiring the detailed microgrid configuration.

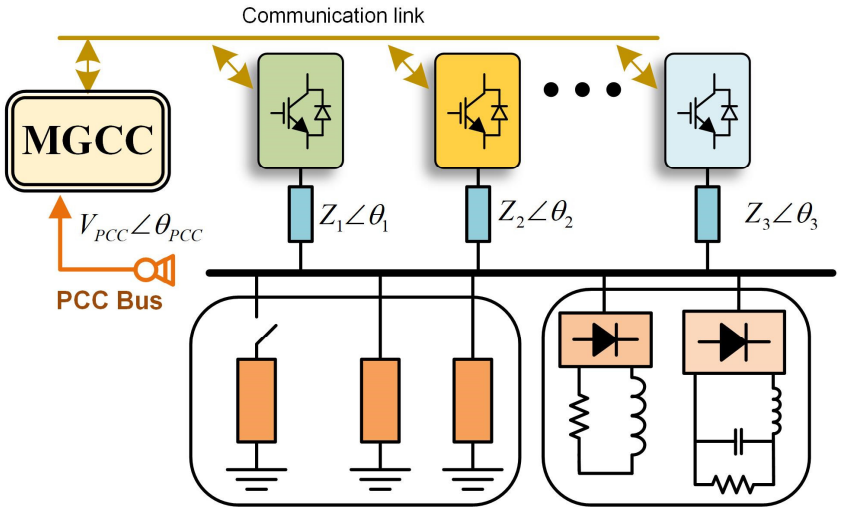

Figure 3.1 The islanded microgrid system with linear and nonlinear load at the PCC bus.

3.1 PCC Voltage Distortion Issue

Although the droop controller can share total load power autonomously in the islanded microgrid, it cannot regulate the harmonic current because the droop control voltage only consists of the fundamental components. When the nonlinear load is connected to the grid, the uncontrolled harmonic currents cause a large harmonic voltage drop on the line impedance, so that the PCC voltage become highly distorted. According to the IEEE 519 standards [57], it is important to maintain a high PCC voltage quality with total harmonic distortion (THD) smaller than 5%.

3.2 Centralized Control Strategy

In the centralized control approach, the MGCC is used to monitor the PCC voltage quality and send the PCC voltage information to each DG unit, as shown in Fig. 3.1. The MGCC collect the information from the DG units and send the control signal to each DG unit. In order to compensate the PCC voltage distortion, the PCC voltage harmonics have to be extracted. To reduce the communication data transmission, the MGCC measures and decompose PCC harmonic components, and these values are sent to all DG units. In this chapter, the harmonic distortion (HD) index is extracted by the MGCC as given below:

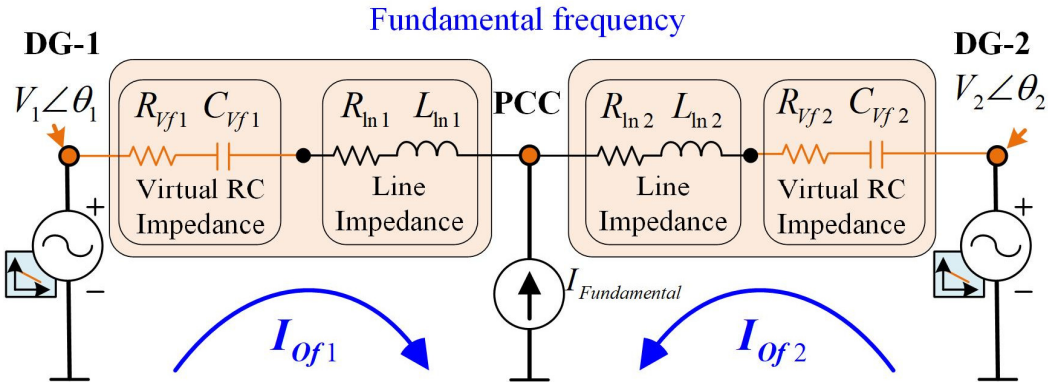

Figure 3.2 Equivalent circuit of 2 DG units for fundamental frequency.

$$HD_h = \left(\frac{V_{PCC}^h}{V_{PCC}^f} \right) 100\%. \tag{3.1}$$

where V_{PCC}^h and V_{PCC}^f are the RMS values of the PCC harmonic and fundamental voltages, respectively.

3.2.1 Power Sharing Scheme under PCC Voltage Distortion

During a nonlinear load connection, active and reactive powers become distorted due to harmonic voltage drop on the line impedance. To obtain a clean active and reactive power measurement, a low-pass filter with smaller cut-off frequency is applied to filter out the distorted the active and reactive powers:

$$G_{LPF}(s) = \frac{\omega_{LPF}}{s + \omega_{LPF}}. \tag{3.2}$$

To realize power sharing and synchronize each DG, the droop control is adopted with the filtered powers:

$$\omega_{dri} = \omega_0 - m P_i, \tag{3.3}$$

$$V_{dri} = V_0 - n Q_i, \tag{3.4}$$

where an index i represents each DG, ω_i and ω_0 are the output and nominal values of the fundamental DG output frequency, V_i and V_0 are the output and nominal values of the fundamental DG output voltage, m and n are the active and reactive droop coefficients, and P_i and Q_i are the filtered output active and reactive powers, respectively.

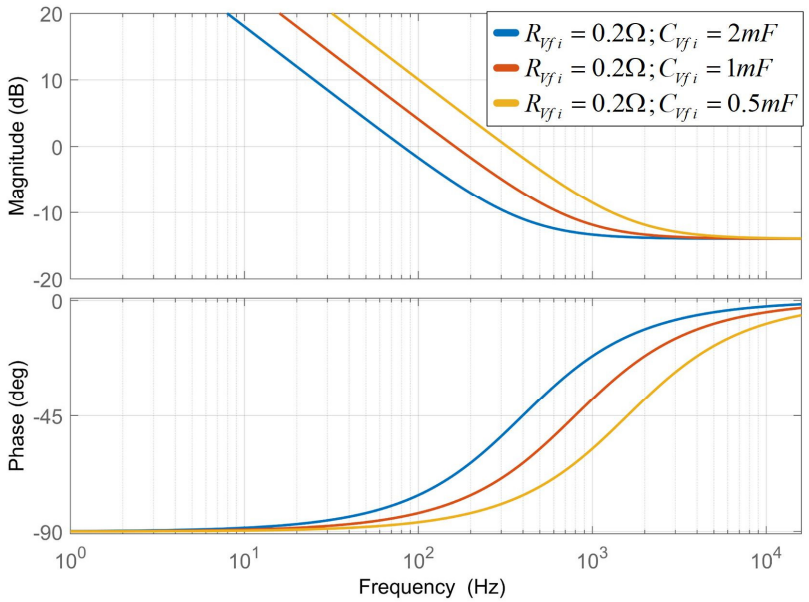

Figure 3.3 Bode diagram of the RC fundamental virtual impedance.

3.2.2 Proposed Fundamental RC Virtual Impedance Control Scheme

In order to achieve the accurate reactive power sharing under distorted microgrid voltage, we propose a virtual capacitance to counteract the effect of the physical line inductance. In addition, a virtual resistance is also considered to compensate the effect of the parasitic line resistance. The equivalent circuit of two paralleled DG units for fundamental frequency with the proposed virtual impedances is shown in Fig. 3.2.

The resistive-capacitive (RC) virtual impedance at the fundamental frequency Z_{Vfi} is obtained as follows:

$$Z_{Vfi} = R_{Vfi} + \frac{1}{sC_{Vfi}} \tag{3.5}$$

The Bode diagram of Z_{Vfi} with some specific values is shown in Fig. 3.3. From Fig. 3.3, it is obvious that the RC virtual impedance in (3.5) combines all characteristics of the resistance and capacitance. Compared to the conventional methods [65], [66], which only regulate the magnitude of the virtual impedance, the proposed control method can flexibly control both the phase and magnitude of the virtual impedance. Thus, the proposed RC virtual

impedance overcomes the phase difference issue in the conventional method, and the line impedance mismatch among DG units is effectively compensated.

The proposed virtual resistor (R_{Vfi}) and capacitor (C_{Vfi}) of i[th] DG in Fig. 3.2 are regulated by using the following external control loops:

$$R_{Vfi} = \left(K_{iP} / s\right)\left(P_i^* - P_i\right), \tag{3.6}$$

$$C_{Vfi} = \left(K_{iQ} / s\right)\left(Q_i^* - Q_i\right), \tag{3.7}$$

where P_i^* and Q_i^* are the reference active and reactive powers, which are calculated from the microgrid central controller:

$$P_i^* = \left(1/\mathrm{G}_{Pi}\right)\left(1/\left(\sum_{i=1}^{n} 1/\mathrm{G}_{Pi}\right)\right)\sum_{i=1}^{n} P_i\,, \tag{3.8}$$

$$Q_i^* = \left(1/\mathrm{G}_{Qi}\right)\left(1/\left(\sum_{i=1}^{n} 1/\mathrm{G}_{Qi}\right)\right)\sum_{i=1}^{n} Q_i\,. \tag{3.9}$$

By emulating the output resistance and capacitance, the reference signal from the droop controller is modified as follows:

$$V_{ref,i}^{f} = V_{dri}\sin\left(\int \omega_{dri}\ dt\right) - \frac{1}{\omega_{dri} C_{Vfi}} I_{odi}^{f} - R_{Vfi}, \tag{3.10}$$

where $V_{ref,i}^{f}$ is the DG fundamental voltage reference for the voltage controller, and I_{odi}^{f} is the conjugated signal of the DG fundamental current I_{oi}^{f}, which is obtained by delaying I_{oi}^{f} for one quarter of the fundamental cycle [67].

3.2.3 Proposed Harmonic RC Virtual Impedance Control Scheme

In order to compensate the PCC harmonic voltage, the proposed resistive-capacitive virtual impedance can be extended for the harmonic frequency to regulate the harmonic current Fig. 3.4 shows the equivalent circuit of the microgrid for harmonic frequency. From Fig. 3.4, the proposed RC virtual impedance is coordinated with the line inductance to form a virtual passive filter. By controlling RC virtual impedance, the passive filter resonance is adaptively regulated to meet the PCC harmonic frequency, and the PCC voltage distortion is compensated.

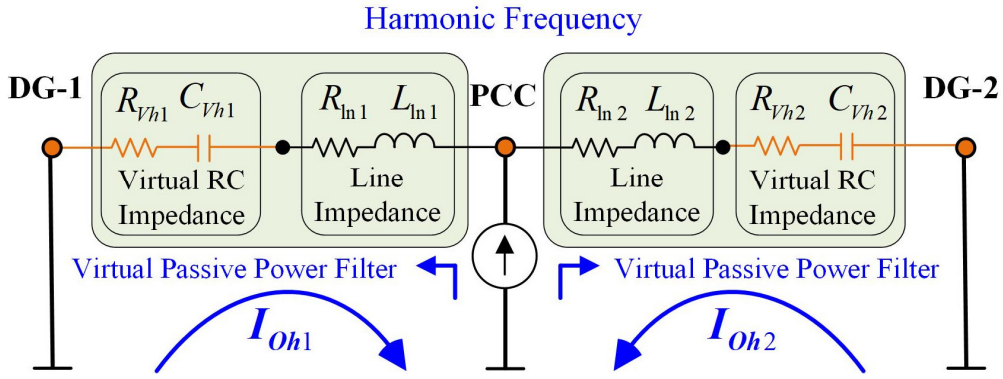

Figure 3.4 Equivalent circuit of 2 DG units for harmonic frequency.

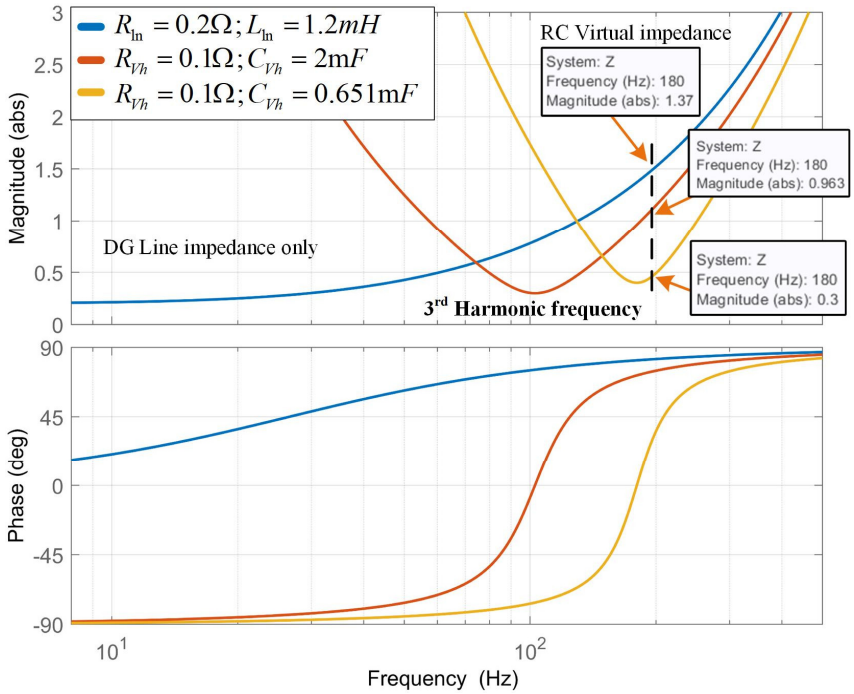

Figure 3.5 Block diagram of the DG equivalent impedance at 3rd harmonic frequency with the RC virtual impedance.

To show the effectiveness of the proposed RC virtual impedance, the Bode diagram of DG equivalent impedance at the 3rd harmonic frequency is plotted in Fig. 3.5. The DG equivalent impedance at the 3rd harmonic frequency is reduced significantly thanks to the RC virtual impedance. Therefore, DG absorbs more load harmonic current, and the 3rd PCC harmonic voltage is compensated.

In the ideal case, the virtual harmonic resistance (R_{Vhi}) is set as zero to compensate PCC voltage with high performance. However, this ideal value of R_{Vhi} reduces the system

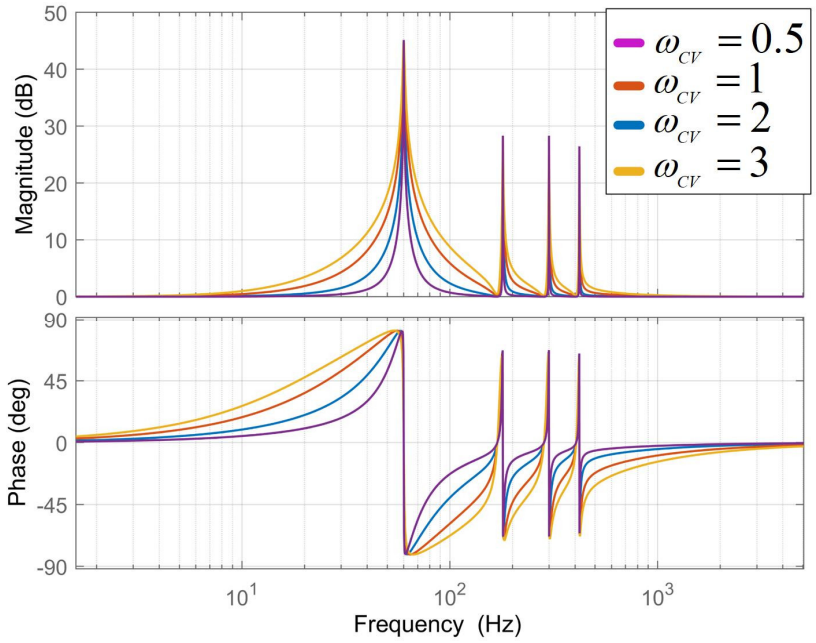

Figure 3.6 Bode diagram of multi non-ideal PR controllers.

stability because of the increased sensitivity to PCC voltage harmonics variation [68]. Therefore, the value of R_{Vhi} should be large enough to enhance the system damping and small enough to maintain harmonic compensating performance. To satisfy these constraints, the virtual harmonic resistance is chosen from 0.1Ω to 3Ω [68], [69]. In this paper, the virtual harmonic resistance (R_{Vhi}) is set as 0.1Ω, while the virtual harmonic capacitance (C_{Vhi}) is continuously adjusted:

$$C_{Vhi} = \left(K_{ih} / s\right)\left(HD_{ref\,h} - HD_h\right) \tag{3.11}$$

where $HD_{ref\,h}$ and HD_h are the reference and present values of the h[th] PCC harmonic distortion, and HD_h is the index received from the MGCC.

3.2.4 Modified Inner Voltage and Current Controller

In order to track the voltage reference effectively, the following multiple non-ideal proportional-resonant (PR) voltage and current controllers are applied to regulate the DG output voltage

$$G_V(s) = K_{PV} + \sum_{h=1,3,5,7} \frac{2K_{IVh}\,\omega_{CV}\,s}{s^2 + 2\,\omega_{CV}\,s + \omega_h^{\,2}}, \tag{3.12}$$

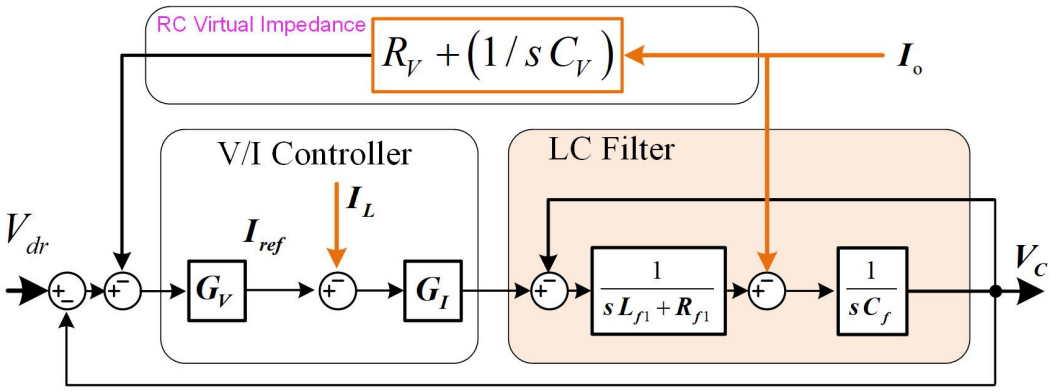

Figure 3.7 Bode diagram of multi non-ideal PR controllers.

$$G_I(s) = K_{PI}, \tag{3.13}$$

where K_{PV} and K_{PI} are the proportional gains, K_{IVh} is the resonant gain of the PR controller, and ω_{CV} and ω_h are the cut-off frequency and resonance frequency of the PR controller, respectively.

Fig. 3.6 shows the Bode diagram of the non-ideal PR controller with different ω_{CV} values. From Fig. 3.6, it is obvious that the PR controller has high gain at both fundamental and harmonic frequencies for enforcing small steady-state error. Because disturbance always exists in the islanded microgrid, the PR controller bandwidth is needed to be optimized for ensuring the system stability. For this purpose, ω_{CV} is chosen as 1 rad/s to minimize the system disturbance and the steady-state error. The block diagram of the inner voltage and current control loops is shown in Fig. 3.7.

3.2.5 Output Impedance Analysis

The closed-loop transfer function of the system without considering the virtual impedance is obtained from Fig. 3.7:

$$V_C = G_{sys}(s)V^* - Z_{Out}(s)I_O, \tag{3.14}$$

In (3.14), $G_{sys}(s)$ and $Z_{Out}(s)$ are the transfer functions of DG voltage gain and output impedance, respectively, which are given below:

$$G_{sys}(s) = \frac{G_V G_I}{s^2 L_f C_f + sR_f C_f + sG_I C_f + G_V G_I + 1}, \tag{3.15}$$

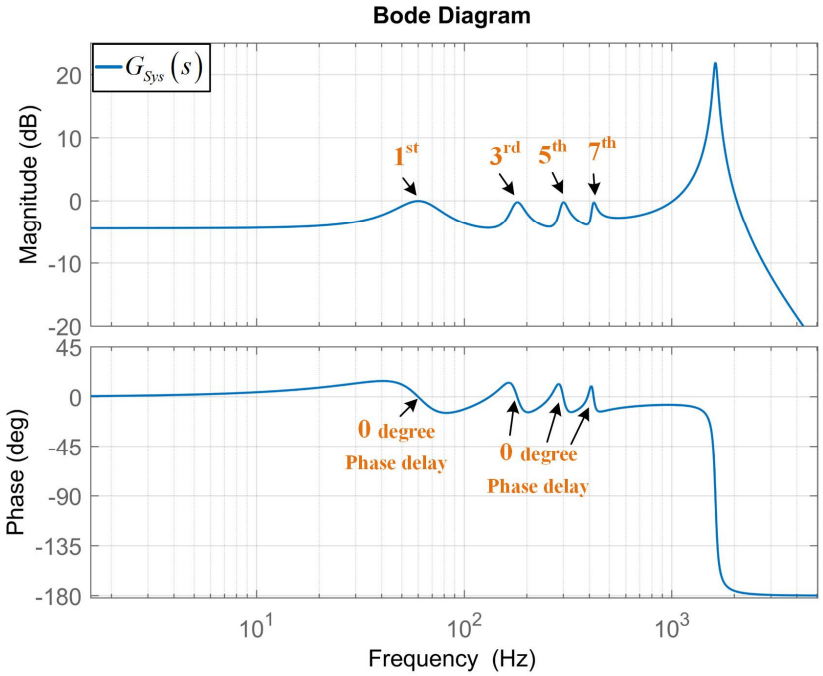

Figure 3.8 Bode diagram of $G_{sys}(s)$.

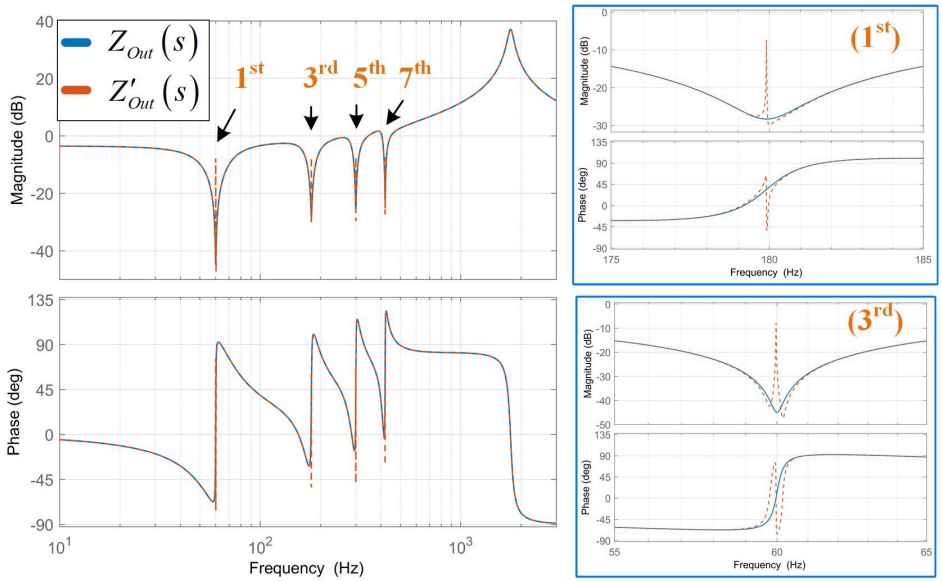

Figure 3.9 Bode diagram of $Z_{Out}(s)$ and $Z'_{Out}(s)$.

$$Z_{Out}(s) = \frac{\left(sL_f + R_f + G_I\right)}{s^2 L_f C_f + sR_f C_f + s\,G_I C_f + G_V G_I + 1}, \tag{3.16}$$

By considering the proposed RC virtual impedance, the DG output impedance $Z_{Out}(s)$ is modified as follows:

Table 3.1 Islanded Microgrid System Parameters

Parameters	Value	Parameters	Value
K_{iP}	0.5×10^{-2} rad/s	L_{f1}	1.2mH
K_{iQ}	5×10^{-2} rad/s	R_{f1}	0.02Ω
K_{ih}	1×10^{-3} rad/s	L_O	1.2mH
K_{PI}	2	C_f	20uF
K_{PV}	1.0	G_{Pi}	0.012
K_{IVh}	20 rad/s	G_{Qi}	0.015
$Z_{\ln1}$	0.1+0.39j Ω	V_0	110V
$Z_{\ln2}$	0.15+0.7j Ω	ω_0	377 rad/s
$Z_{\ln3}$	0.2+1.1j Ω	ω_{CV}	1 rad/s
Load Change	10Ω 45mH	$HD_{ref\,3,5,7}$	1%

$$Z'_{Out}(s) = Z_{Out}(s) + G_{Sys}(s)\, Z_V(s), \tag{3.17}$$

To evaluate the effectiveness of the proposed controller, the frequency-amplitude characteristic of DG voltage gain $G_{sys}(s)$ is plotted in Fig. 3.8. From Fig. 3.8, the magnitudes of $G_{sys}(s)$ are equal to 1 for all of the 1st, 3rd, 5th, and 7th frequencies, and the voltage drop between the voltage reference and DG output voltage becomes zero. In addition, the phase of $G_{sys}(s)$ at both fundamental and harmonic frequencies is close to 0, which shows that the output voltage has zero phase delay. Thus, we can say the inner controllers perfectly track the voltage reference.

Fig. 3.9 shows the Bode diagram of the DG output impedances $Z_{Out}(s)$ and $Z'_{Out}(s)$. From Fig. 3.9, it is clear that the modified output impedance $Z'_{Out}(s)$ has a sufficient gain at both fundamental and harmonic frequencies to compensate the mismatched line impedance as well as PCC voltage harmonics. As a result, reactive power sharing is accurately achieved, and the system dynamic performance is guaranteed even if the load changes. In addition, the PCC voltage harmonics are effectively compensated by means of RC virtual impedance.

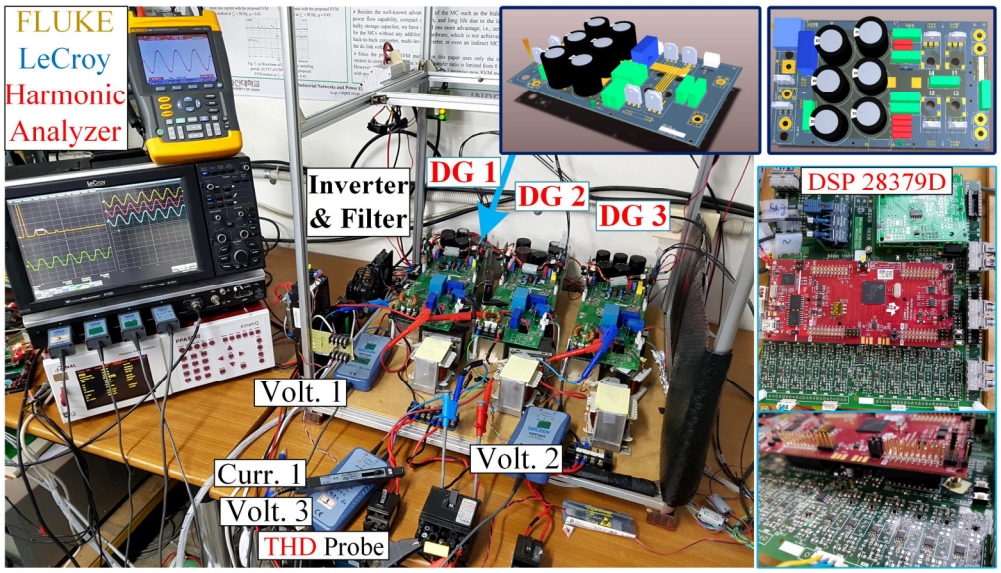

Figure 3.10 Laboratory testbed.

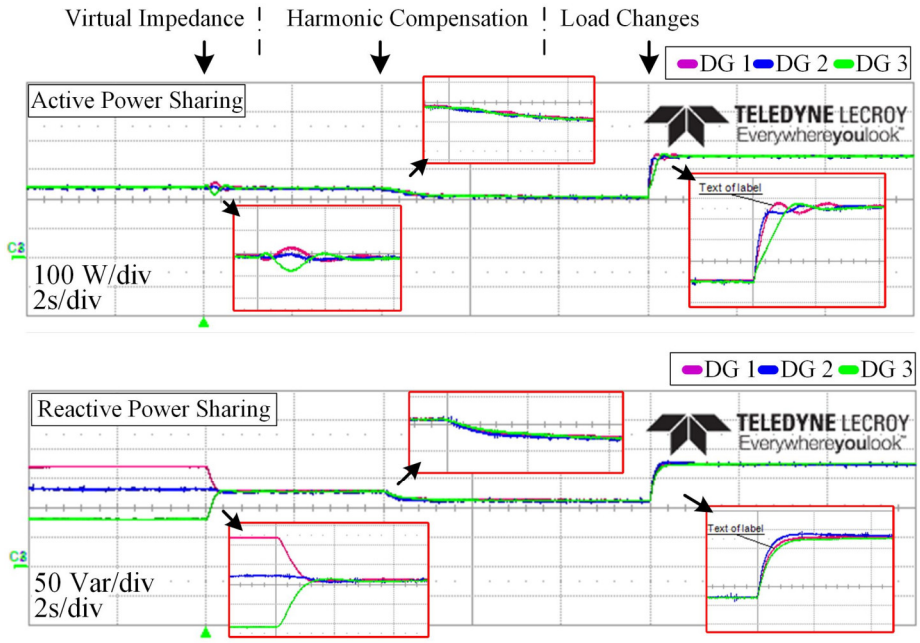

Figure 3.11 Power sharing performance with the proposed controller.

3.2.6 Experimental Results

The effectiveness of the proposed control method is experimentally verified with 3 DG units in Fig. 3.1, and the experimental parameters are given in Table 3.1. DG units are controlled using a Texas Instruments DSP TMS320F28379D microcontroller, and the laboratory islanded microgrid system with 3 DG units is shown in Fig. 3.10.

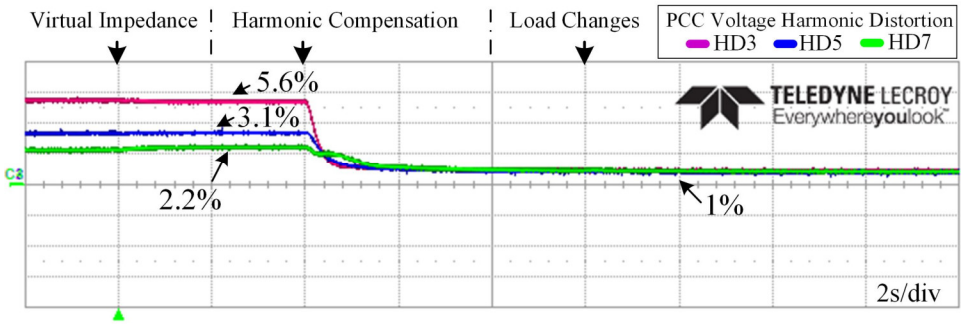

Figure 3.12 Performance of the PCC harmonic voltage compensation.

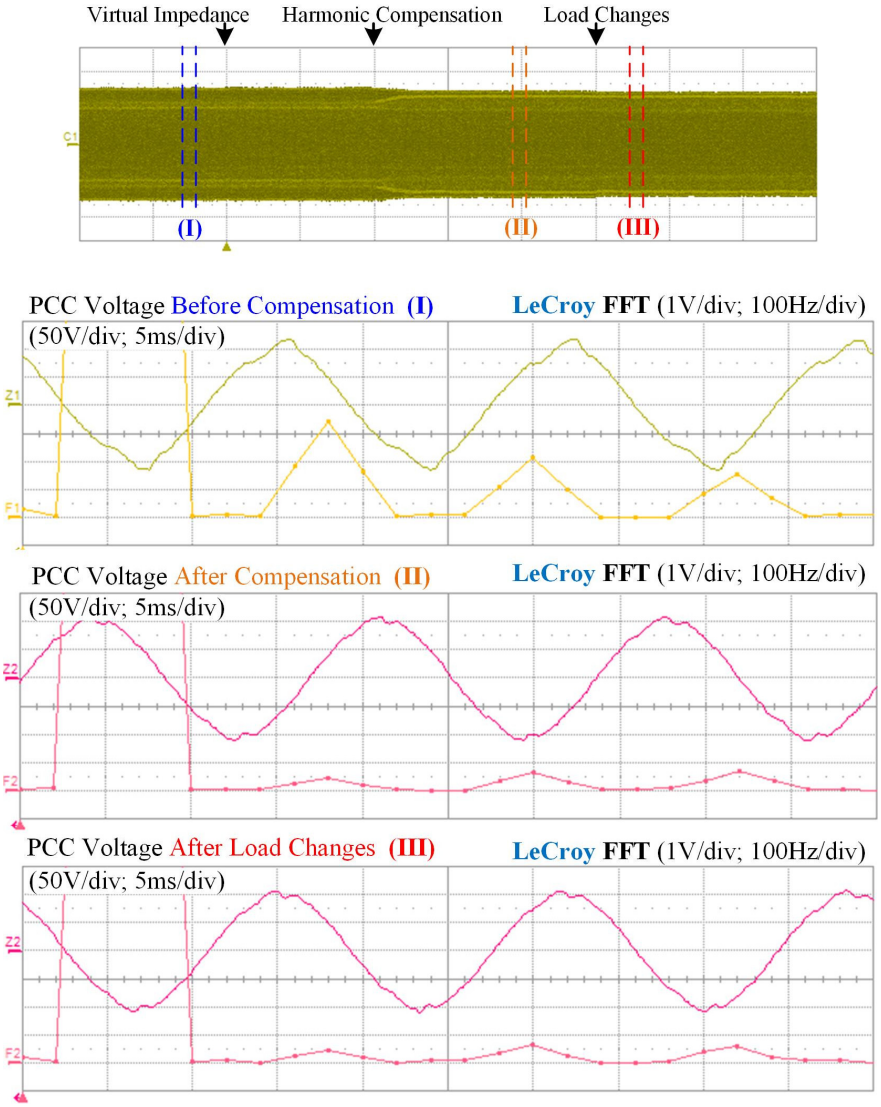

Figure 3.13 PCC harmonic voltage quality with the proposed controller.

Fig. 3.11 shows the power sharing performance of the microgrid with the proposed controller. From Fig. 3.11, the active power is shared equally among DG units with the conventional droop controller, while the reactive power is not accurately shared due to the mismatched line impedance. When the proposed controller is applied, the RC virtual

impedance is inserted to compensate the unequal line impedance, so that the reactive power sharing is accurately achieved after a short transient period as shown in Fig. 3.11. In addition, the accurate active power sharing is still guaranteed during reactive power compensation with a small transient oscillation by means of the proposed virtual resistance. Furthermore, the RC virtual impedance is continuously tuned to keep accurate power sharing even though harmonic compensation and load power changes, as can be seen in Fig. 3.11.

Fig. 3.12 shows the performance of the PCC harmonic voltage compensation. From Fig. 3.12, the HD3, HD5, and HD7 are initially 5.6%, 3.1%, and 2.2%, respectively, and they are all reduced to 1% with a smooth response after compensation. In spite of the load changes, the harmonic compensation shows good dynamic performance. In order to investigate the transient performance of the proposed controller, the PCC voltage is measured in Fig. 3.13. In Fig. 3.13, the PCC voltage harmonics are seamlessly compensated without any oscillations or fluctuations, and the desired harmonic distortions are accurately achieved. From the experimental results, the proposed RC virtual impedance method shows a good performance with a fast and smooth response.

3.3 Distributed Control Strategy

Although the centralized control strategy can improve the power sharing performance and PCC voltage quality, the point-to-point communication link between MGCC and DG units is needed. If one communication link between MGCC and DG units fail, the control algorithm is not updated, and the system stability is reduced. In addition, it is hard to apply the centralized control strategy in the large scale because it required a long-distance communication link among MGCC and DG units.

To improve the system reliability and less complexity, the distributed control strategy is proposed in this section. In the proposed control method, the sparse communication link is considered in the islanded microgrid, and the information is shared among DG units regardless of the MGCC. By distributed controlling the impedance among DG units, the proposed method obtains a same power sharing performance and PCC voltage harmonic compensation compared to the centralized control approach.

Fig. 3.14 shows a typical islanded microgrid configuration with a sparse

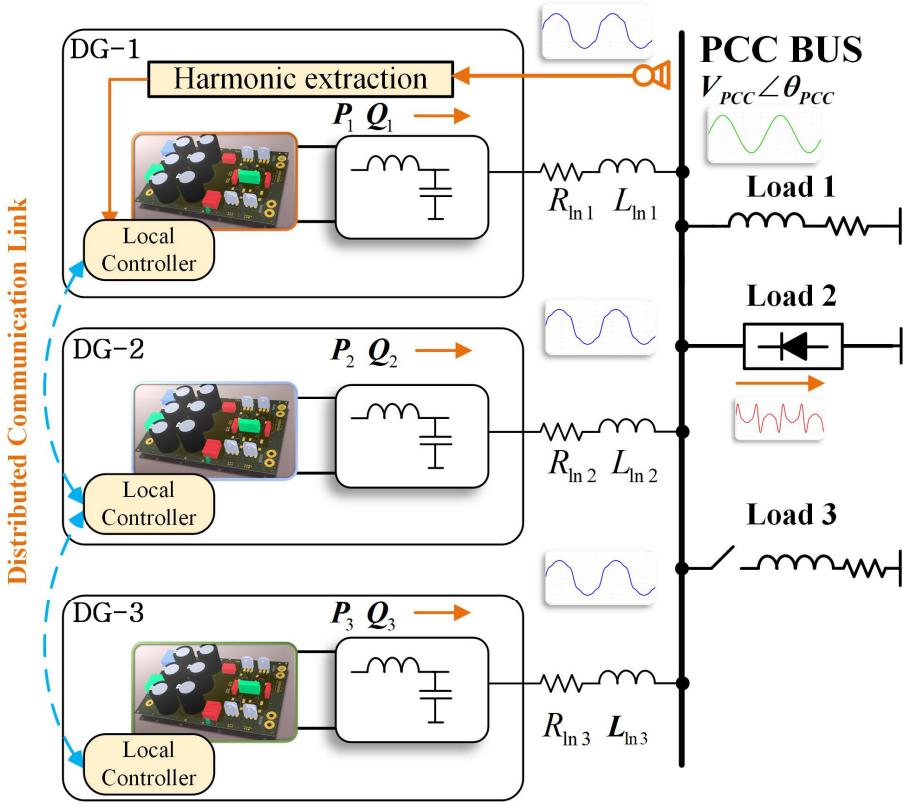

Figure 3.14 Islanded microgrid configuration with a sparse communication link.

communication link, where each DG unit has to work independently and share the load power autonomously. In this configuration, one DG which is nearest the PCC bus will measure the PCC voltage, extracts the harmonic components, and send that information to another DG unit.

3.3.1 Proposed Distributed Control Scheme

In order to address the inaccurate power sharing and PCC voltage distortion issues, this paper proposes the coordinated virtual impedance control scheme that inserts the fundamental virtual resistance and capacitance at the inverter output to balance the equivalent impedance among DG units. In addition, the virtual resistance and capacitance are considered at the harmonic frequency to compensate the PCC voltage harmonics.

Fig. 3.15 shows an equivalent circuit of two DG units with the proposed coordinated virtual impedance control scheme at the fundamental frequency. From Fig. 3.15, the fundamental virtual capacitance is presented to counteract the effect of the physical line inductance. Besides, the fundamental virtual resistance is proposed to compensate the

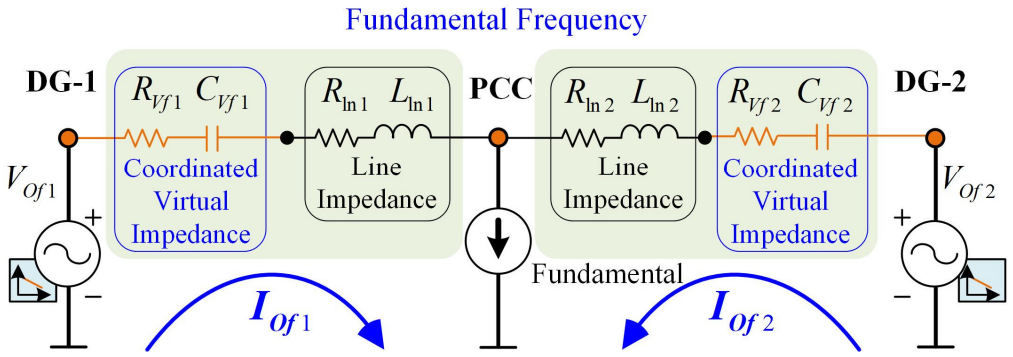

Figure 3.15 Equivalent circuit of two DG units with the coordinated virtual impedance control scheme at fundamental frequency.

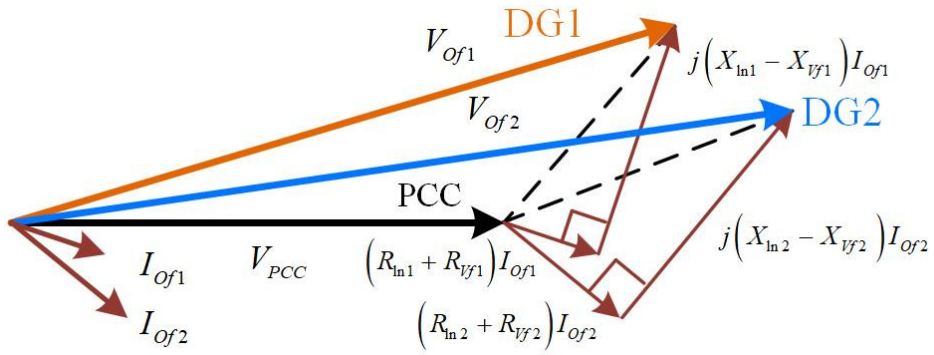

Figure 3.16 Phasor diagram of two DG units at the fundamental frequency.

mismatched line resistance among DG units. Based on the equivalent circuit in Fig. 3.15, the DG phasor diagram is obtained in Fig. 3.16, and their DG output voltages (V_{Of1},V_{Of2}) are derived as follows:

$$\begin{aligned} V_{Of1} &= V_{PCC\_f} + \left(\Delta V_{ln1} + \Delta V_{Vf1}\right) \\ &= V_{PCC\_f} + \frac{\left(R_{ln1}+R_{Vf1}\right)P_1 + \left(X_{ln1}-X_{Vf1}\right)Q_1}{V_o}, \end{aligned} \tag{3.18}$$

$$V_{Of2} = V_{PCC\_f} + \frac{\left(R_{ln2}+R_{Vf2}\right)P_2 + \left(X_{ln2}-X_{Vf2}\right)Q_2}{V_o}, \tag{3.19}$$

where V_{PCC_f} is the PCC fundamental voltage, and R_{Vfi} and X_{Vfi} ($i=1,2$) are the virtual resistance and capacitive reactance at the fundamental frequency, respectively. For simple analysis, we assume that DG1 and DG2 have the same rated power ($G_{P1}=G_{P2}, G_{Q1}=G_{Q2}$). Because the line impedance is highly inductive due to the large grid side output inductance,

the $P-\omega$ droop controller can properly share the active power shared between 2 DG units ($P_1 \approx P_2$) [46]. The reactive power is shared accurately among DG units only if the DG1 and DG2 output voltages are the same ($V_{Of1} = V_{Of2}$), which is given as follows:

$$V_{Of2} - V_{Of1} = \frac{\left(R_{ln2} - R_{ln1} + R_{Vf2} - R_{Vf1}\right)P_1}{V_o} + \frac{\left(X_{ln2} - X_{ln1} + X_{Vf1} - X_{Vf2}\right)Q_2}{V_o} = 0 \quad (3.20)$$

To satisfy equation (3.20), the virtual resistance and capacitive reactance (R_{Vfi}, X_{Vfi} | i=1,2) have to be coordinated controlled to compensate the mismatched line impedance among DG units. The proposed virtual resistance (R_{Vfi}) and capacitive reactance (X_{Vfi}) of ith DG unit are simultaneously tuned by using the following external control loops:

$$R_{Vfi} = \left(K_{iP}/s\right)\left(\delta P_i\right). \quad (3.21)$$

$$X_{Vfi} = 1/\left(\omega_f C_{Vfi}\right). \quad (3.22)$$

$$C_{Vfi} = \left(K_{pQ} + K_{iQ}/s\right)\left(\delta Q_i\right). \quad (3.23)$$

where K_{pQ} is the proportional gain, K_{iP} and K_{iQ} are the integral gains, and δP_i and δQ_i are the active and reactive power mismatch, respectively, which are calculated among the ith DG unit and its neighbors. The active and reactive power mismatches of the ith DG unit are calculated based on the consensus algorithm [51]:

$$\delta P_i = C_P \sum_{j \in N_i} a_{ij}\left(P_j - P_i\right). \quad (3.24)$$

$$\delta Q_i = C_Q \sum_{j \in N_i} a_{ij}\left(Q_j - Q_i\right). \quad (3.25)$$

where a_{ij} represents the connection status between the ith and jth DG units, and C_P and C_Q are consensus coupling gains. To reject the harmonic disturbance in the fundamental complex virtual impedance, a second-order generalized integrator (SOGI) is adopted to decompose the fundamental output current and generate the voltage drop on the fundamental virtual impedance (V_{Vfi}) [70]:

$$V_{Vfi} = Z_{Vfi}\ I_{Ofi} = R_{Vfi} I_{Ofi\_\alpha} + \left(1/\left(\omega_f C_{Vfi}\right)\right) I_{Ofi\_\beta}. \quad (3.26)$$

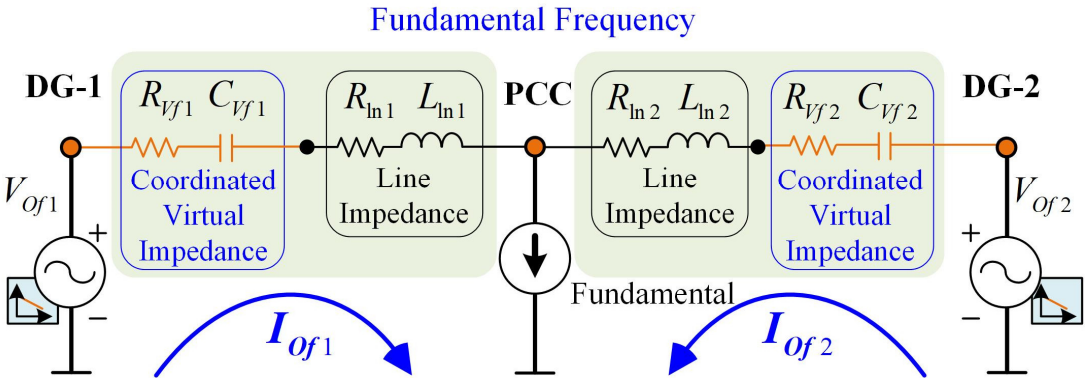

Figure 3.17 Equivalent circuit of two DG units with the coordinated virtual impedance control scheme at fundamental frequency.

where I_{Ofi_α} and I_{Ofi_β} are the SOGI fundamental current and its quadrature fundamental current, respectively.

In addition to the fundamental power sharing improvement, the proposed coordinated virtual impedance control scheme is extended for the harmonic frequency to compensate PCC voltage harmonics. Fig. 3.17 shows an equivalent circuit of two DG units with the proposed control scheme at the harmonic frequency. From Fig. 3.17, the PCC harmonic voltage becomes

$$V_{PCC}^{h} = -I_{Load\_h} / \left(\frac{1}{Z_{eq\,total}^{h}} \right) = -I_{Load\_h} / \left(\frac{1}{Z_{eq1}^{h}} + \frac{1}{Z_{eq2}^{h}} \right), \tag{3.27}$$

where V_{PCC}^{h} is the PCC harmonic voltage, and Z_{eq1}^{h} and Z_{eq2}^{h} are the equivalent impedance of DG1 and DG2 at the harmonic frequency, respectively:

$$Z_{eq1}^{h} = \sqrt{\left(R_{Vh1} + R_{ln1}\right)^2 + \left(X_{lnh1} - X_{Vh1}\right)^2}\,. \tag{3.28}$$

$$Z_{eq2}^{h} = \sqrt{\left(R_{Vh2} + R_{ln2}\right)^2 + \left(X_{lnh2} - X_{Vh2}\right)^2}\,. \tag{3.29}$$

$$X_{Vhi} = 1/\left(\omega_h C_{Vhi}\right);\; X_{lnhi} = \omega_h L_{lnhi}\,. \tag{3.30}$$

In order to improve the PCC voltage quality, V_{PCC}^{h} in (3.27) has to be mitigated by reducing Z_{eq1}^{h} and Z_{eq2}^{h}. Because the line impedance values ($R_{lni,} X_{lnhi}, i = 1,2$) are constant, the proposed harmonic virtual resistance and virtual capacitance ($R_{Vhi,} X_{Vhi}$) are added to Z_{eq1}^{h}

and Z_{eq2}^{h} for emulating a low impedance at the specific harmonic frequency. Thus, harmonic current flows through the virtual impedance, and the PCC voltage quality is improved.

The harmonic virtual resistance (R_{Vhi}) and virtual capacitance (X_{Vhi}) are defined as follows:

$$R_{Vhi} = R_{Vfi} + R_{Vdi}. \tag{3.31}$$

$$X_{Vhi} = 1/\left(h\,\omega_f\, C_{Vhi}\right). \tag{3.32}$$

$$C_{Vhi} = C_{Vfi} + C_{Vcomi}. \tag{3.33}$$

where R_{Vfi} and C_{Vfi} are the virtual impedance values from the fundamental frequency, R_{Vdi} is the virtual damping resistance, and C_{Vcomi} is the virtual compensating capacitance.

The value of R_{Vdi} is selected to be large enough to enhance the system stability by damping any microgrid disturbance, and it is commonly chosen as 0.1 to 2Ω [68], [69]. In this paper, R_{Vdi} is set as 0.2Ω to obtain a minimal voltage drop, and the virtual compensating capacitance (C_{Vcomi}) is adaptively regulated by an external controller:

$$C_{Vcomi} = \left(K_{ph} + K_{ih}/s\right)\left(HD_{refh} - HD_h\right). \tag{3.34}$$

$$HD_h = \left(V_{PCC}^{h}/V_{PCC}^{f}\right)100\%. \tag{3.35}$$

where K_{ph} and K_{ih} are the proportional and integral gains, HD_{refh} and HD_h are the desired and present values of the harmonic distortion at the h[th] harmonic frequency, and V_{PCC}^{f} is the PCC fundamental voltage, respectively. To meet the requirements of IEEE 519 standards [57], HD_{ref} at the 3rd, 5th, and 7th harmonic frequencies is set to be 1.0%.

In order to integrate the harmonic compensation in each DG unit, HD_h is extracted by a single DG unit by using multiple synchronous harmonic dq transformations [71], and the HD_h value is sent to other DG units in the microgrid using a distributed communication link, as shown in Fig. 3.14. Considering the harmonic virtual resistance and virtual capacitance in (3.31) and (3.33), the voltage drop on the harmonic virtual impedance is defined as follows:

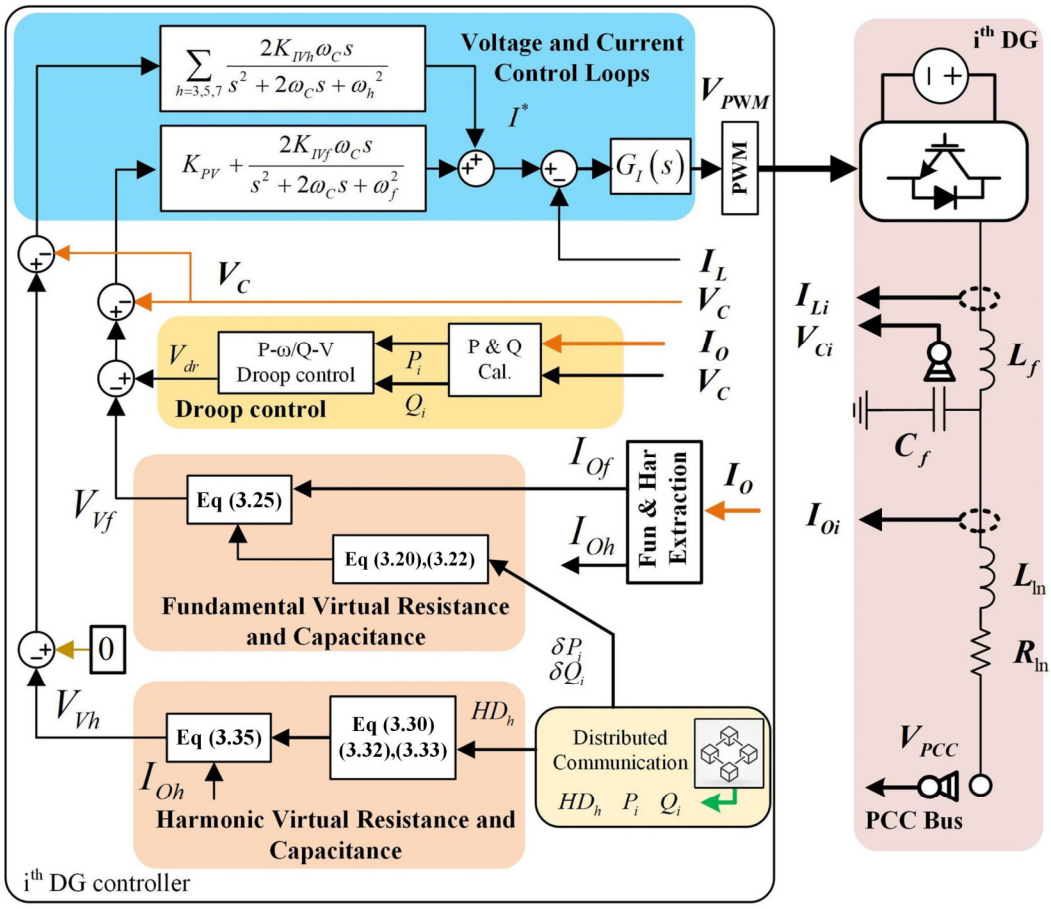

Figure 3.18 Block diagram of the proposed coordinated virtual impedance control scheme.

$$V_{Vhi} = \sum_{h=3,5,7} Z_{Vhi} I_{Ohi} = \sum_{h=3,5,7} R_{Vhi} I_{Ohi\_\alpha} + \left(1/\left(h\omega_h C_{Vhi}\right)\right) I_{Ohi\_\beta} \quad (3.36)$$

where I_{Ohi_α} and I_{Ohi_β} are the SOGI harmonic currents, respectively. By using the voltage drops on the fundamental and harmonic virtual impedance in (3.27) and (3.37), the voltage reference finally becomes

$$\begin{aligned} V_{ref\,i} &= V_{dri} - V_{Vfi} - V_{Vhi} \\ &= V_{dri} - \left(R_{Vfi} I_{Ofi\_\alpha} + \left(1/\left(\omega_f C_{Vfi}\right)\right) I_{Ofi\_\beta}\right) \\ &\quad - \sum_{h=3,5,7} \left(R_{Vhi} I_{Ohi\_\alpha} + \left(1/\left(\omega_h C_{Vhi}\right)\right) I_{Ohi\_\beta}\right) \end{aligned} \quad (3.37)$$

Fig. 3.18 shows a block diagram of the proposed control scheme. In Fig. 3.18, a modified control loop is applied to decouple the fundamental and harmonic frequencies:

$$I^* = \left(K_{PV} + \frac{2K_{IVf}\,\omega_C s}{s^2 + 2\omega_C s + \omega_f^2} \right)\left(V_{dr} - V_{Vf} - V_C \right) + \sum_{h=3,5,7} \left(\frac{2K_{IVh}\,\omega_C s}{s^2 + 2\omega_C s + \omega_h^{\,2}} \right)\left(0 - V_{Vh} - V_C \right) . \tag{3.38}$$

where K_{PV} is the proportional gain, and K_{IVf} and K_{IVh} are the resonant gains, respectively.

3.3.2 Steady-state and Small-Signal Analysis

In order to evaluate the stability of the proposed control scheme, the microgrid is analyzed based on the small signal state-space model [38]. When we assume that the fundamental power is shared proportionally at the steady-state, the system stability mainly depends on the harmonic compensation scheme [72]. To ensure the ripple-free at the PCC, the harmonic distortion in (3.36) is filtered using a low-pass filter:

$$HD_h(\%) = \frac{100\omega_{LPF}}{(s + \omega_{LPF})V_{PCC}^f} V_{PCC}^h \ . \tag{3.39}$$

where ω_{LPF} is the cut-off angular frequency of the filter. By linearizing (3.39), the small signal variation of the harmonic distortion is derived as follows:

$$\Delta HD_h = \frac{100\omega_{LPF}}{(s + \omega_{LPF})V_{PCC}^f} \Delta V_{PCC}^h . \tag{3.40}$$

where the operator Δ represents a small signal disturbance around the microgrid equivalent operating point. The small-signal variation of the harmonic virtual impedance in (3.33) is obtained as

$$\Delta X_{Vhi} = \frac{-\Delta C_{Vhi}}{h\,\omega_f \left(C_{Vhi} \right)^2} = \psi_i \, \Delta C_{Vhi} . \tag{3.41}$$

where $\psi_i = -1 / \left(h\,\omega_f \left(C_{Vhi} \right)^2 \right)$. By substituting the small signal variation of the virtual capacitance ΔC_{Vhi} into (3.41), ΔX_{Vhi} becomes:

$$\Delta X_{Vhi} = \psi_i \left(K_{ph} + K_{ih} / s \right) \Delta HD_h . \tag{3.42}$$

Similarly, the small-signal variation of the equivalent line impedance is obtained from (3.28):

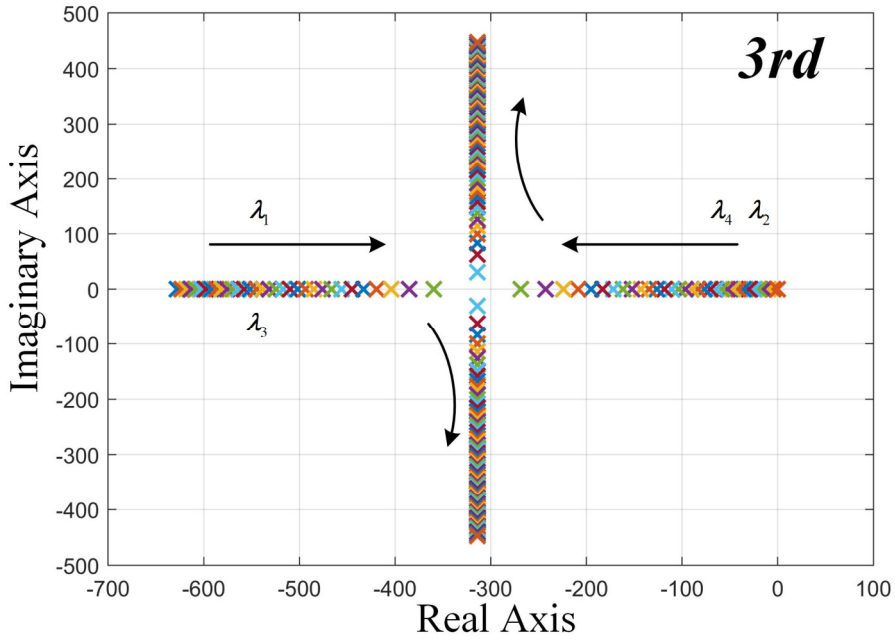

Figure 3.19 Root locus diagram according to control gain $K_{ih}(h=3)$ with $10^{-5} < K_{i3} < 20$.

$$\Delta Z_{eqi}^{h} = \frac{\left(X_{Vhi} - X_{\ln hi}\right)\Delta X_{Vhi}}{\sqrt{R^2 + \left(X_{\ln hi} - X_{Vhi}\right)^2}}. \tag{3.43}$$

where $R = R_{Vhi} + R_{\ln i}$. In case of n DG units, the harmonic voltage in (3.27) becomes:

$$V_{PCC}^{h} = \frac{\left|I_{Load\_h}\right|}{\frac{1}{Z_{eq1}^{h}} + \frac{1}{Z_{eq2}^{h}} + ... + \frac{1}{Z_{eqn}^{h}}}. \tag{3.44}$$

The small-signal variation of V_{PCC}^{h} is obtained by linearizing (3.43):

$$V_{PCC}^{h} = \sum_{i=1}^{n} \alpha_i \Delta Z_{eqi}^{h} = \alpha_1 \Delta Z_{eq1}^{h} + \alpha_2 \Delta Z_{eq2}^{h} + ... + \alpha_n \Delta Z_{eqn}^{h}. \tag{3.45}$$

where $\alpha_i = \partial V_{PCC}^{h} / \partial Z_{eqi}^{h}$ with $i = 1, 2, .., n$. By manipulating equations (3.39) to (3.45), the small-signal state-space model of the proposed control scheme is derived as

$$\dot{X}_{MG} = A_{MG} X_{MG}. \tag{3.46}$$

where $X_{MG} = \left[\Delta X_{Vh1}\ \Delta X_{Vh2} \cdots \Delta X_{Vhn}\ \Delta HD_h\right]$ and A_{MG} is the state matrix. The matrices A_{MG} in (3.46) is expressed as followed

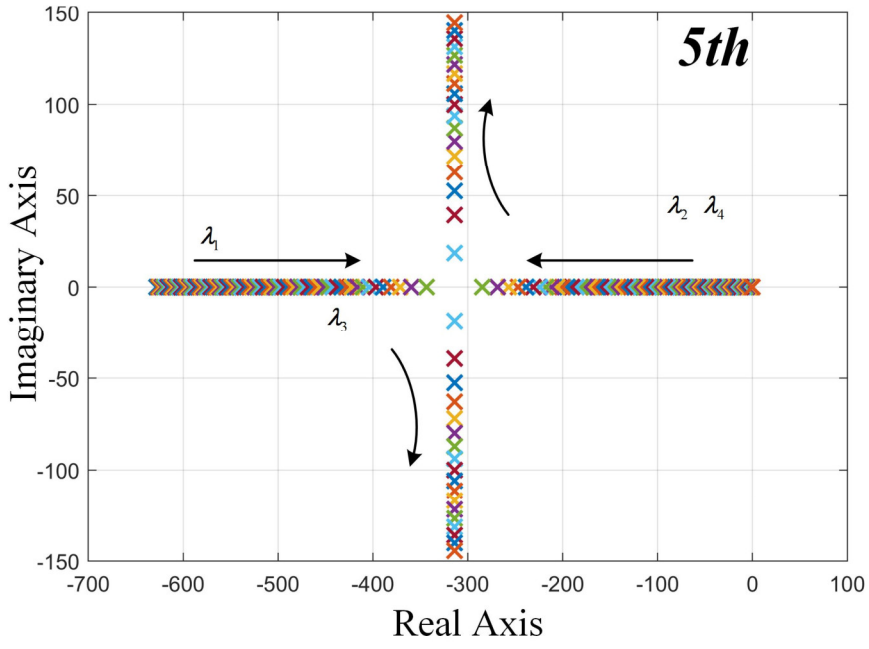

Figure 3.20 Root locus diagram according to control gain $K_{ih}(h=5)$ with $10^{-5} < K_{i5} < 20$.

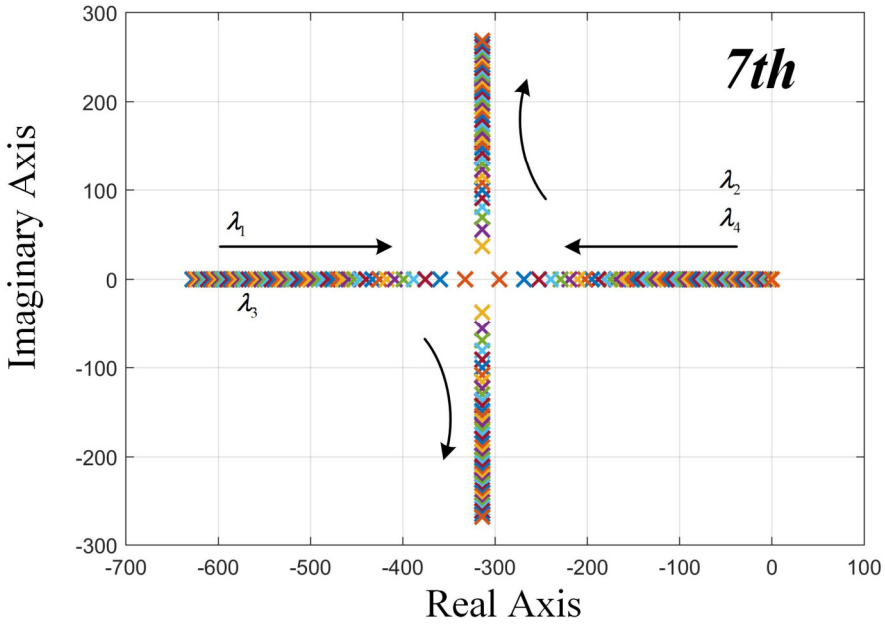

Figure 3.21 Root locus diagram according to control gain $K_{ih}(h=7)$ with $10^{-5} < K_{i7} < 20$.

$$A_{MG} = \begin{bmatrix} O_{nxn} & A_{XHD} \\ A_{HDX} & -\omega_{LPF} \end{bmatrix}. \tag{3.47}$$

where

$$A_{XHD} = \begin{bmatrix} \psi_1 K_{ih} & \psi_2 K_{ih} & \cdots & \psi_n K_{ih} \end{bmatrix}^T,$$

Table 3.2 Microgrid Configuration

Parameters	Value	Parameters	Value
$G_{Pi}\mid_{i=1,2,3}$	0.005	L_f	1.2mH
$G_{Qi}\mid_{i=1,2,3}$	0.002	R_f	0.01Ω
$HD_{ref\,3,5,7}$	1%	C_f	20μF
K_{PV}	1.0	ω_c	1 rad/s
K_{IVf}	180 rad/s	V_O	110V
K_{IVh}	20 rad/s	f_0	60Hz
K_{PI}	1.5	C_P	0.4
K_{iP}	0.45 rad/s	C_Q	0.4
K_{iQ}	0.45 rad/s	$f_{Switching}$	10KHz
K_{pQ}	2×10^{-4}	K_{ph}	2×10^{-4}
K_{ih}	0.98 rad/s	ω_{LPF}	$2\pi100$ rad/s

$$O_{n\times n}=\begin{bmatrix}0 & \cdots & 0\\ \vdots & \ddots & \vdots\\ 0 & \cdots & 0\end{bmatrix}, O_{n\times 1}=\begin{bmatrix}0 & 0 & \cdots & 0\end{bmatrix}^T,$$

$$O_{1\times n}=\begin{bmatrix}0 & 0 & \cdots & 0\end{bmatrix},$$

$$A_{HDX}=\frac{100\omega_{LPF}}{V_{PCC}^{f}}\left[\frac{\alpha_1\left(X_{Vh1}-X_{\ln h1}\right)}{\sqrt{R^2+\left(X_{\ln h1}-X_{Vh1}\right)^2}}\quad\frac{\alpha_2\left(X_{Vh2}-X_{\ln h2}\right)}{\sqrt{R^2+\left(X_{\ln h2}-X_{Vh2}\right)^2}}\quad\cdots\right.$$
$$\left.\cdots\quad\frac{\alpha_n\left(X_{Vhn}-X_{\ln hn}\right)}{\sqrt{R^2+\left(X_{\ln hn}-X_{Vhn}\right)^2}}\right].$$

The eigenvalues of the small-signal state-space model in (3.46) is solved by using "eigenvalues function" in MATLAB to evaluate the system stability. In this paper, we consider the microgrid system with three DG units using the parameters in Table 3.2. The impact of the control gain on the system dynamics is examined using root locus diagrams with different K_{ih} ($h=3,5,7$).

Fig. 3.19 shows the trajectories of all eigenvalues when increasing the gain $K_{ih}(h=3)$. The system becomes more stable as K_{i3} increases because the dominant eigenvalues move from the right to the left half-plane, as shown in Fig. 3.19. Figs. 3.20 and 3.21 show the root locus diagrams for different values of K_{i5} and K_{i7}. When $K_{ih}>10(i=5,7)$, the system damping is reduced because the eigenvalues λ_1 and λ_2 move toward the image axis. From the eigenvalue analysis, the desired system damping, and system dynamics are obtained by selecting the value of 0.98 for each harmonic control gain K_{ih}.

3.3.3 Stability with the Communication Time Delay

In order to investigate the influence of the communication time delay, the small-signal variation of DG equivalent impedance in (3.42) is rewritten as follows:

$$\Delta X_{Vhi\,DL}=\psi_i\left(K_{ph}+K_{ih}/s\right)\Delta HD_{h\_DL}, \tag{3.48}$$

where $\Delta HD_{h\_DL}=\Delta HD_h\left(t-\tau_{DL}\right)$ and τ_{DL} is the delay time among DG units.

With the modified DG equivalent impedance, the proposed control system in (3.46) becomes:

$$\dot{X}_{MG}=B_{MG}X_{MG}+B_{MG\_DL}X_{MG\_DL}. \tag{3.49}$$

where $X_{MG\_DL}=\left[\Delta X_{Vh1\,DL}\ \Delta X_{Vh2\,DL}\ldots\Delta X_{Vhn\,DL}\ \Delta HD_{h\,DL}\right]$.

By considering the communication delay, the characteristic equation of the system in (3.49) is obtained [73]:

$$\det(-sI+B_{MG}+B_{MG\_DL}e^{-\tau_{DL}s})=0. \tag{3.50}$$

where

$$B_{MG}=\begin{bmatrix}O_{n\times n} & O_{n\times 1}\\ A_{HDX} & 0\end{bmatrix},$$

$$B_{MG\_DL}=\begin{bmatrix}O_{n\times n} & A_{XHD}\\ O_{1\times n} & -\omega_{LPF}\end{bmatrix},$$

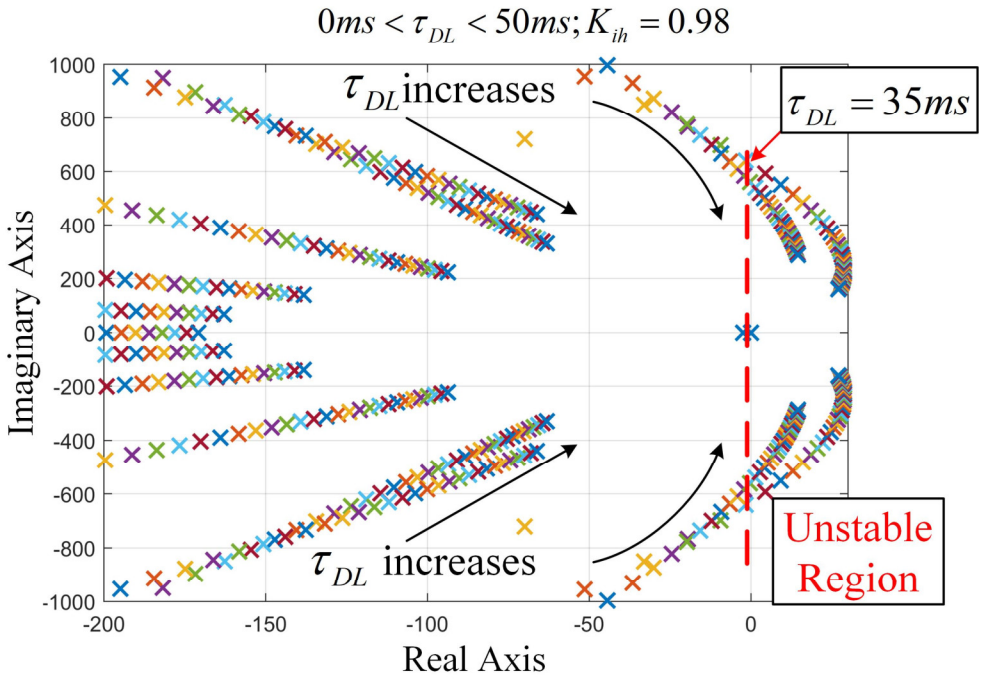

Figure 3.22 Root locus diagram according to communication delay τ_{DL}: $0 < \tau_{DL} < 50ms$.

It is difficult to find all the eigenvalues of the system in (3.50) because the characteristic equation (3.50) has infinite solutions. To find the eigenvalues for a specific communication time delay, we solve the characteristic equation using the numerical approach in [73].

Fig. 3.22 shows the trajectories of all eigenvalues when increasing the communication delay (τ_{DL}) from 0 to 50ms. In Fig. 3.22, all eigenvalues move to the right half-plane when τ_{DL} increases, and the system becomes unstable when $\tau_{DL} > 35ms$. Therefore, the microgrid stability is ensured with the communication delay $\tau_{DL} = 20ms$ which is considered in this study.

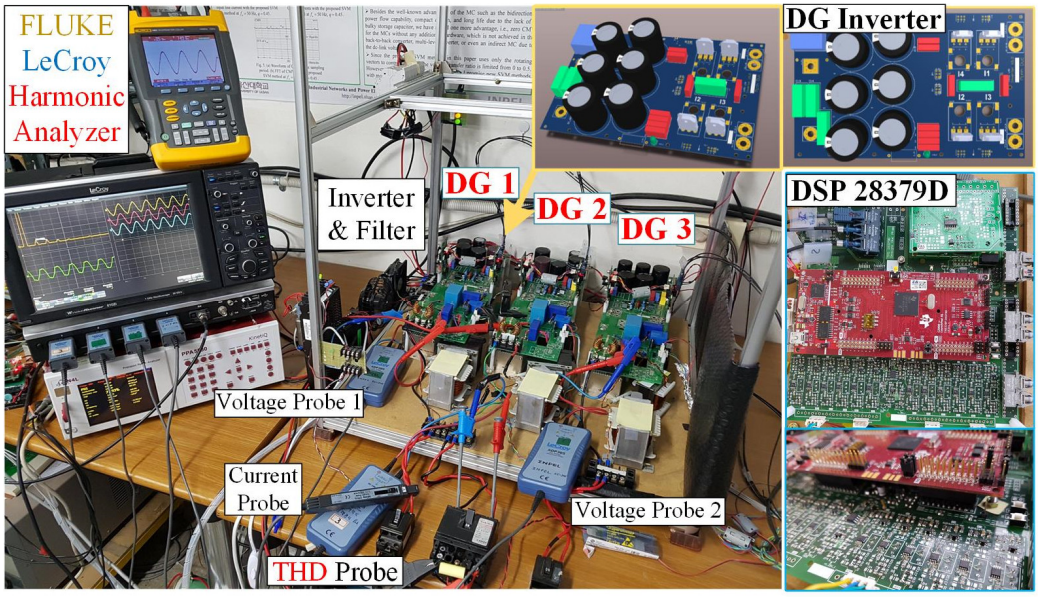

Figure 3.23 Laboratory microgrid system.

3.3.4 Experimental Results

The proposed coordinated virtual impedance control scheme was applied to an islanded microgrid in Fig. 3.14, which is composed of three DG units, linear and nonlinear loads. The microgrid system was built with the parameters in Table 3.2 and Table 3.3, and the test bed is shown in Fig. 3.23. DSP microcontroller TMS320F28379D was used to implement the control algorithm, and both switching frequency and sampling frequency were selected as 10 kHz.

From Figs. 21 to 24, the performance of the proposed coordinated virtual impedance control scheme is experimentally compared with that of a conventional control scheme in [22], and experimental conditions are defined as follows. At $t < t_1$, the conventional droop control scheme is originally adopted. Then, the proposed control scheme is started at $t = t_1$ by inserting the fundamental virtual resistance and capacitance in the DG output impedance for accurate reactive power sharing. At $t = t_2$, the PCC voltage harmonics is compensated by adding the harmonic virtual resistance and capacitance. The compensating performance with the proposed control scheme is then evaluated by connecting load 3 to the microgrid at $t = t_3$.

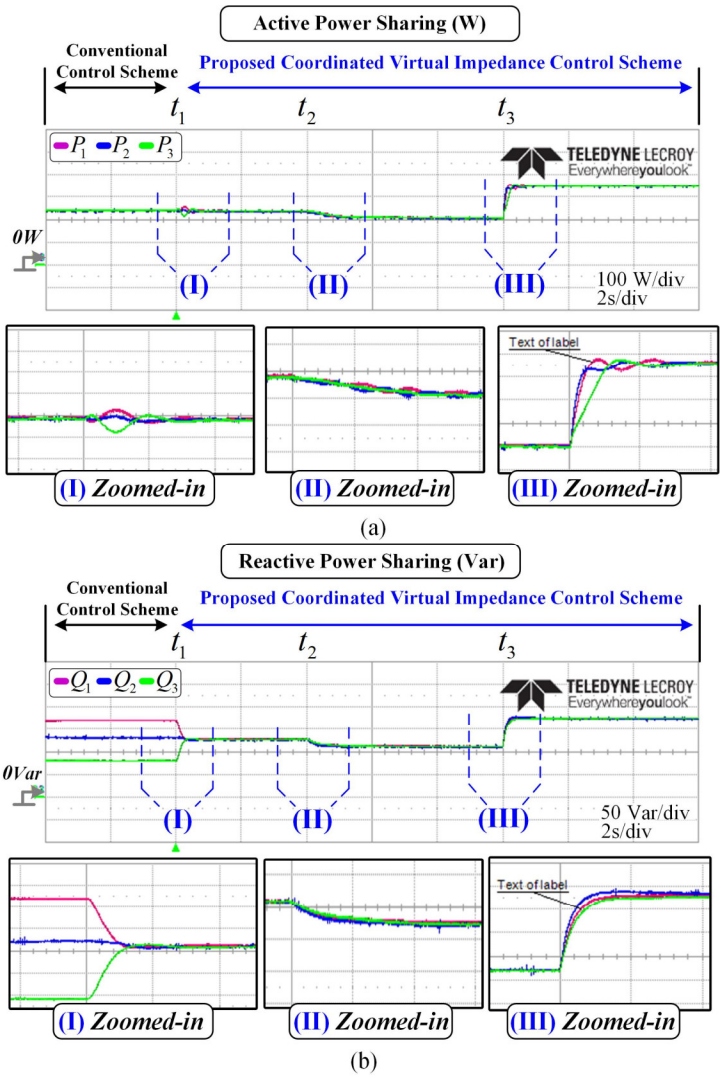

Figure 3.24 (a) Active power sharing. (b) Reactive power sharing.

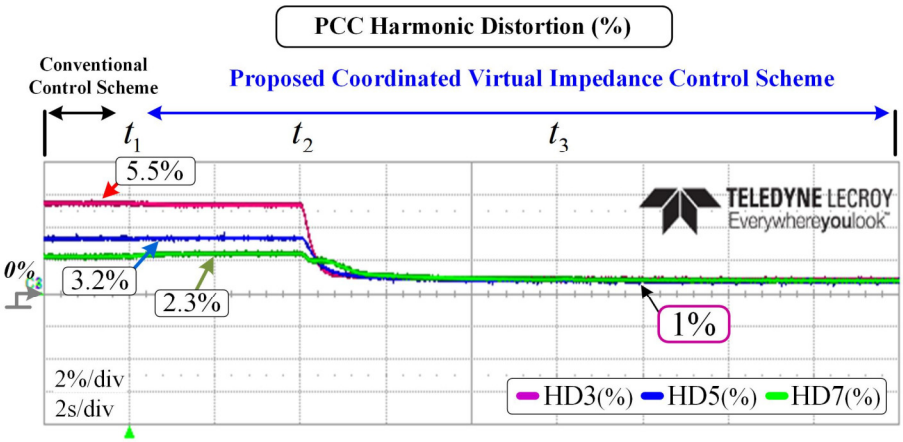

Figure 3.25 PCC harmonic distortion with the proposed control schemes.

Figs. 3.24(a) and (b) show the active and reactive power sharing. At $t < t_1$, in spite of accurate active power sharing in Fig. 3.24(a), the reactive power is not shared correctly with

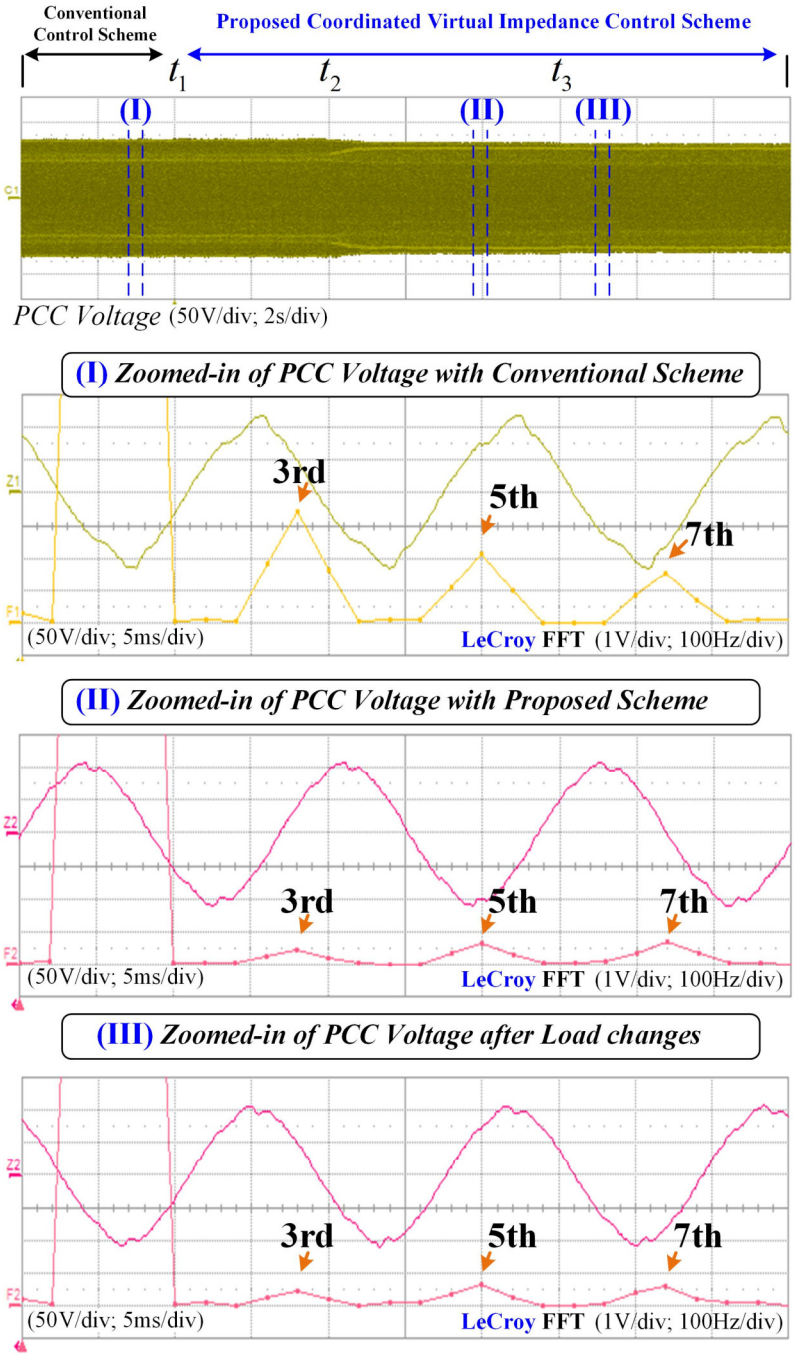

Figure 3.26 PCC voltage and its FFT along with zoomed waveforms.

the conventional control scheme as shown in Fig. 3.24(b). However, when the proposed control scheme is applied at $t = t_1$, the unequal line impedance is compensated by actively controlling the virtual resistance and capacitance at the inverter output, so the reactive power sharing is accurately achieved. Because of the virtual capacitance regulation, the active power has a small oscillation, but it decays to almost zero after 0.8s thanks to the adjustable virtual resistance. In addition, the harmonic virtual impedance does not affect the fundamental power

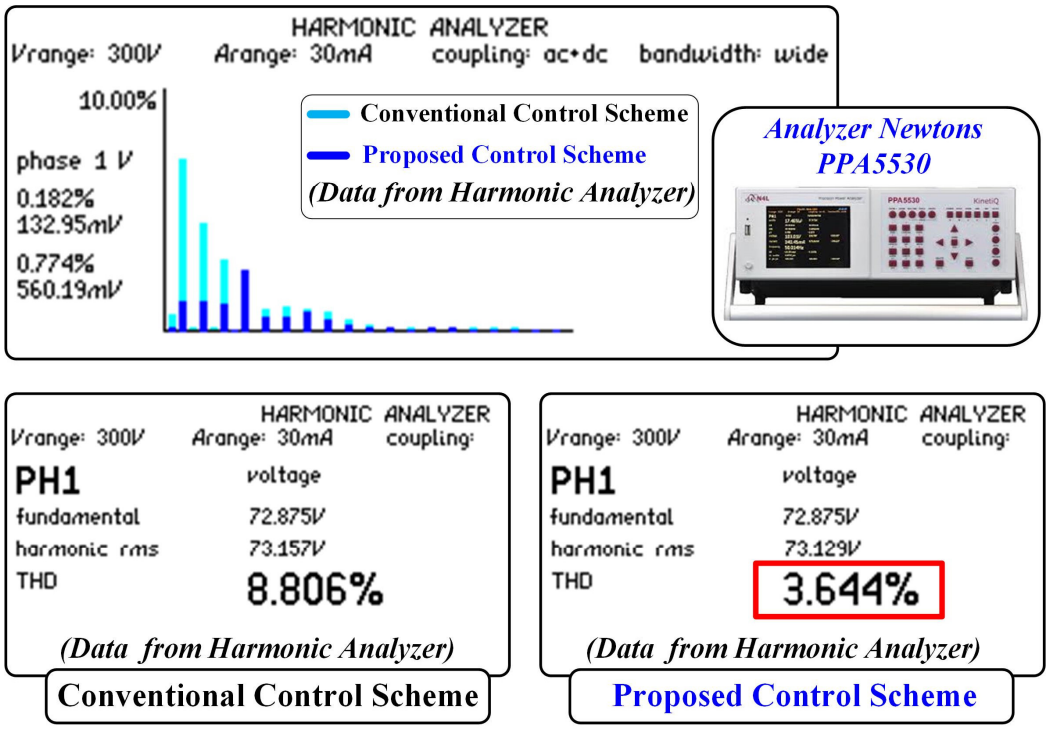

Figure 3.27 Comparison of PCC voltage THD.

sharing in parallel DG system, which shows that the fundamental and harmonic voltage components are fully decoupled by means of the modified voltage control loop. Furthermore, the fundamental virtual resistance and virtual capacitance are continuously regulated to guarantee accurate power sharing even if the load changes at $t = t_3$.

Fig. 3.25 shows the PCC harmonic distortion. During the conventional period ($t < t_1$), HD_3, HD_5, and HD_7 are relatively high at 5.5%, 3.2%, and 2.3%. When the proposed control scheme is applied at $t = t_2$, HD_3, HD_5, and HD_7 are all attenuated to 1% without oscillation and undershoot by means of the harmonic virtual resistance and capacitance. In spite of the load change at $t = t_3$, harmonics are kept without variation. In order to investigate the PCC voltage waveforms according to the coordinated virtual impedance control, the PCC voltages and each sectional zoomed-in waveform are shown in Fig. 3.26 along with the fast Fourier transform (FFT). From Fig. 3.26, when the proposed control scheme is activated, the PCC voltage becomes more sinusoidal because the voltage harmonics are effectively compensated. In addition, the PCC voltage quality is guaranteed even if the load changes, which shows the reliability of the proposed control scheme. Fig. 3.27 shows the total harmonic

Table 3.3 Prototype Hardware Parameters

Parameter	Value
R_{ln1} , X_{ln1}	0.1Ω, 0.52Ω
R_{ln2} , X_{ln2}	0.2Ω, 0.805Ω
R_{ln3} , X_{ln3}	0.3Ω, 1.13Ω
$f_{Sampling}$	10KHz
Microcontroller	TMS320F28379D
Hall current sensor	LA25-NP
Hall voltage sensor	LV25-P
P_{Total}	1050W
Q_{Total}	525Var
Load 2	80Ω; 150uF; 560uH
Load 3	10Ω; 45mH
Communication delay	20ms
Dead time	1.5μs
DC storage capacitor	1000μF/600V

distortion (THD) of the PCC voltage. From Fig. 3.27, it is obvious that the 3rd, 5th, and 7th harmonics are significantly reduced with the proposed control scheme, and THD is reduced from 8.806% to 3.644% after compensation.

3.4 Conclusion of the Chapter

In this paper, a coordinated virtual impedance control scheme was proposed to address the inaccurate power sharing and PCC voltage distortion issues. The proposed control scheme flexibly controls the fundamental virtual resistance and capacitance to compensate for the line impedance mismatch, so the power sharing error is eliminated. In addition, the output impedance at harmonic frequencies is modified by means of the adjustable harmonic virtual impedance to enhance PCC voltage quality. By controlling the harmonic voltage components independently, the harmonic virtual impedances are decoupled in the frequency domain, and

the PCC voltage harmonics are properly compensated to comply with IEEE 519 standards. Furthermore, the values of virtual resistance and capacitance are continuously adjusted to ensure accurate power sharing and desired PCC voltage quality in spite of the load power change. The output impedance characteristics were analyzed by means of a Bode diagram to verify the feasibility of the proposed coordinated virtual impedance control scheme. The experimental results showed the effectiveness and reliability of the proposed control scheme.

Chapter 4

Accurate Harmonic Power Sharing with Enhanced PCC Voltage Quality

This chapter presents an enhanced compensation strategy for distributed generation (DG) systems to simultaneously achieve accurate power sharing and harmonics compensation at the point of common coupling (PCC). In the proposed control strategy, the output impedance is modified at the fundamental and harmonic frequencies to compensate for the line impedance mismatches among DG units, which results in accurate power sharing. In addition, load harmonic currents are effectively adjusted by the DG units to effectively compensate the PCC voltage harmonics. Additionally, the DG equivalent impedance is regulated adaptively to ensure accurate harmonic power sharing even in the presence of sudden load changes. Furthermore, a distributed communication network is adopted instead of a central controller to increase the reliability and stability of the microgrid system. The proposed control strategy is applied to a prototype microgrid system, and its effectiveness and reliability are experimentally validated.

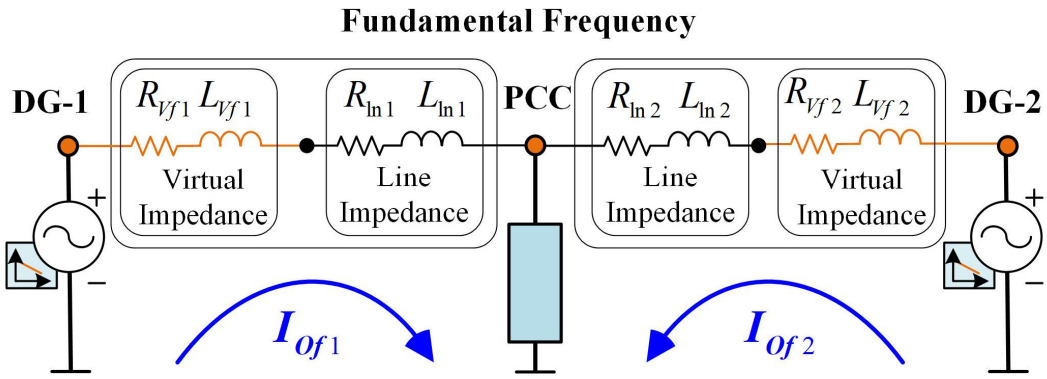

Figure 4.1 Equivalent circuit of two DG units considering the fundamental virtual impedance.

4.1 Virtual Impedance for Accurate Fundamental Power Sharing

To overcome inaccurate reactive power sharing, fundamental virtual resistance (R_{Vfi}) and virtual inductance (L_{Vfi}) are proposed to compensate for the mismatched impedance among DG units. Fig. 4.1 illustrates an equivalent circuit of two DG units considering the fundamental virtual impedance. From Fig. 4.1, it can be seen that the equivalent fundamental impedance ($Z^{f}_{eq\_i}$) of i[th] DG (i=1,2) is derived as follows [74]:

$$Z^{f}_{eq\_i} = Z_{\ln i} + Z_{Vfi} = \left(R_{\ln i} + R_{Vfi}\right) + j\omega_f \left(L_{\ln i} + L_{Vfi}\right), \tag{4.1}$$

where the index i represents the ith DG, ω_f is the fundamental angular frequency, $Z_{\ln i}$ and Z_{Vfi} are the line impedance and virtual impedance, and $R_{\ln i}$ and $L_{\ln i}$ are the line resistance and inductance, respectively. By adaptively controlling R_{Vfi} and L_{Vfi} in (4.1), the equivalent fundamental impedance is regulated to compensate for the mismatched impedance, which results in accurate power sharing. To properly compensate the mismatched line impedance, both R_{Vfi} and L_{Vfi} are continuously adjusted by the external loop controller:

$$R_{Vfi} = K_{pP\_i}\left(\delta P_i\right) + \left(K_{iP\_i}/s\right)\left(\delta P_i\right), \tag{4.2}$$

$$L_{Vfi} = K_{pQ\_i}\left(\delta Q_i\right) + \left(K_{iQ\_i}/s\right)\left(\delta Q_i\right), \tag{4.3}$$

where K_{pP_i} and K_{pQ_i} are the proportional gains, and K_{iP_i} and K_{iQ_i} are the integral gains. In addition, δP_i and δQ_i are the active and reactive power mismatches among the i[th] DG and

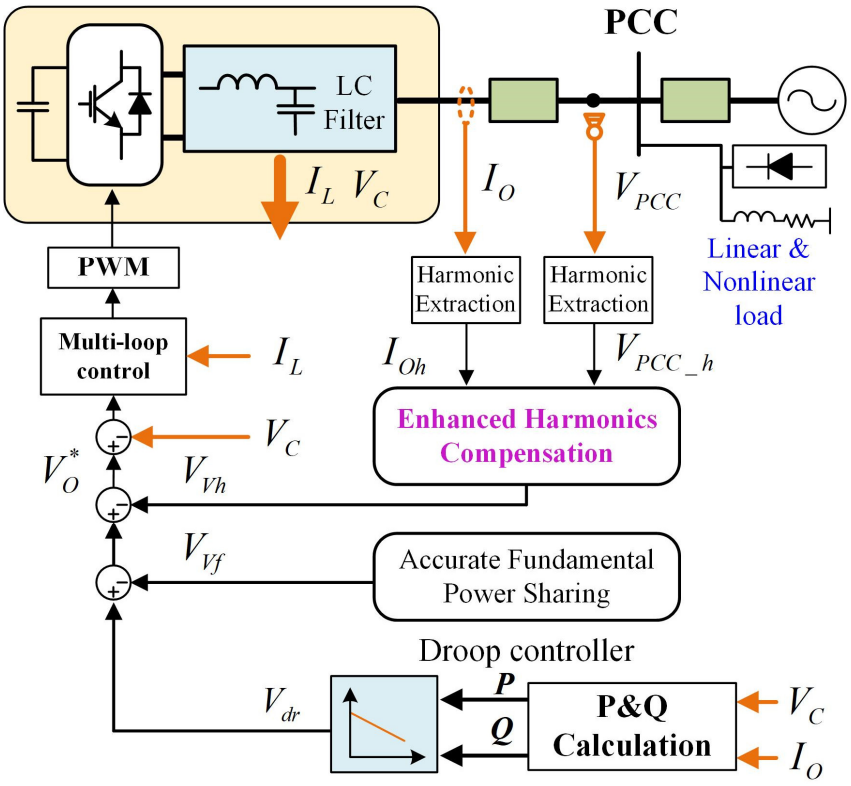

Figure 4.2 Proposed harmonic control scheme.

its neighbors, respectively. To overcome central controller complexity, the consensus algorithm is adopted in the distributed microgrid to calculate the active and reactive power mismatches, and they are determined as follows [46]:

$$\delta P_i = G_P \sum_{j \in N_i} a_{ij} \left(P_j - P_i \right), \tag{4.4}$$

$$\delta Q_i = G_Q \sum_{j \in N_i} a_{ij} \left(Q_j - Q_i \right), \tag{4.5}$$

where G_P and G_Q are the consensus coupling gains, and a_{ij} is the factor that represents the control gain between node i and node j. To reject the harmonic disturbance in the virtual impedance, the second-order generalized integrator (SOGI) currents at the fundamental frequency are adopted to generate the fundamental voltage drop (V_{Vfi}) [70]:

$$V_{Vfi} = Z_{Vfi}\ I_{Ofi} = R_{Vfi} I_{Ofi\_\alpha} - \omega_f L_{Vfi} I_{Ofi\_\beta}, \tag{4.6}$$

where I_{Ofi} is the fundamental output current, and I_{Ofi_α} and I_{Ofi_β} are the fundamental and quadrature currents, respectively.

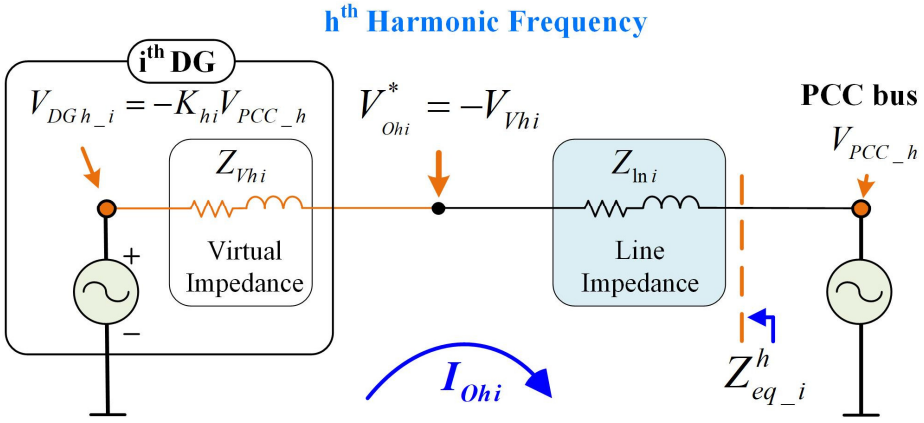

Figure 4.3 Equivalent circuit of the ith DG unit at the hth frequency.

4.2 Proposed Accurate Harmonic Power Sharing Scheme

In order to address the drawbacks of the conventional control scheme such as instability and overmodulation, an enhanced compensation strategy is proposed that directly modify the DG equivalent impedance at harmonic frequencies. Fig. 4.2 shows the proposed harmonic control scheme with an enhanced harmonics compensation module. From Fig. 4.2, the proposed control scheme uses both PCC voltage and output current to build the voltage drop due to harmonic virtual impedance (V_{Vhi}):

$$V_{Vhi} = K_{hi}V_{PCC\_h} + Z_{Vhi}\,I_{Ohi}, \tag{4.7}$$

where I_{Ohi} is the harmonic output current, and K_{hi} is the compensation gain for mitigating the PCC harmonic voltage at the selected hth harmonic frequency (h=3,5,7,9). Z_{Vhi} is the proposed harmonic virtual impedance, which is used for mismatched harmonic impedance compensation, and is defined as follows:

$$Z_{Vhi} = R_{Vfi} + j\,\omega_f\,h\,L_{Vfi}. \tag{4.8}$$

To implement the harmonic virtual impedance, the harmonic voltage reference of the ith DG unit (V^*_{Ohi}) is defined as follows [35]:

$$V^*_{Ohi} = 0 - V_{Vhi}. \tag{4.9}$$

Based on Thevenin theorem, the equivalent harmonic voltage source of a DG unit from (4.6) to (4.9) can be drawn as shown in Fig. 4.3. From Fig. 4.3, it can be seen that the DG model at the hth harmonic frequency is represented by the harmonic voltage source

($V_{DGh\_i} = -K_{hi}V_{PCC\_h}$) in series with the virtual impedance (Z_{Vhi}). To show the effectiveness of the proposed control method, the equivalent harmonic impedance ($Z^h_{eq\_i}$) at the PCC bus is derived from Fig. 4.3 by means of Kirchhoff's theory:

$$Z^h_{eq\_i} = -V_{PCC\_h} / I_{Ohi} = Z_{\ln i} / \left(1 + K_{hi}\right) + Z_{Vhi} / \left(1 + K_{hi}\right). \tag{4.10}$$

When increasing K_{hi}, the equivalent harmonic impedance Z_{Vhi} in (4.10) is decreased so that the i[th] DG absorbs more harmonic current. As a result, the PCC harmonic voltage is compensated, and the voltage quality is improved. In addition, the proposed Z_{Vhi} in (4.10) emulates the harmonic impedance at the DG output to damp the DG harmonic disturbance and the PCC transient perturbance.

To achieve the desired PCC harmonic distortion ($HD_{ref\,h}$), K_{hi} is adaptively adjusted using the external control loop:

$$K_{hi} = \left(K_{ph} + K_{ih} / s\right)\left(HD_{ref\,h} - HD_h\right) \ , \tag{4.11}$$

where K_{pQh} and K_{iQh} are the proportional and integral gains, respectively. HD_h is the current harmonic distortion (HD) at h[th] frequency, which is detected using multiple synchronous harmonic dq transformations [71].

In the conventional harmonics compensation methods in [53], [75], the harmonic virtual impedance was used with fixed values. However, to fully achieve the required harmonic distortion, the proposed control method adaptively regulates the harmonic virtual impedance at the chosen h[th] harmonic frequency. Therefore, the microgrid flexibility and reliability are increased.

In addition to the voltage harmonic compensation, the harmonic power among DG units have to be shared accurately. The harmonic power Q^h_i for the i[th] DG is obtained as follows [76]:

$$Q^h_i = V^f_{DGi} I^h_{DGi} \approx \left(E_0 / \sqrt{2}\right) I^h_{DGi}, \tag{4.12}$$

where V^f_{DGi} and I^h_{DGi} are the RMS values of the fundamental output voltage and harmonic output current, respectively. From (4.12), Q^h_i can be controlled by I^h_{DGi} since V^f_{DGi} is kept almost constant with a small variation due to the droop control characteristics. As shown in Fig. 4.3, the harmonic output current can be directly controlled by regulating the equivalent

harmonic impedance $Z_{eq\_i}^{h}$. To perfectly regulate $Z_{eq\_i}^{h}$, the harmonic voltage in (4.7) is modified by applying the harmonic power sharing variable (C_{hi}):

$$V_{Vhi} = C_{hi}\left(K_{hi}V_{PCC\_h} + Z_{Vhi}\, I_{Ohi}\right), \tag{4.13}$$

In (4.13), C_{hi} is adaptively regulated with the aid of the distributed consensus algorithm:

$$C_{hi} = \left(K_{pQh} + K_{iQh}/s\right)\left(e_{G_{Hi}Q_i^h}\right), \tag{4.14}$$

where K_{pQh} and K_{iQh} are the proportional and integral gains, respectively. $e_{G_{Hi}Q_i^h}$ is the harmonic power sharing error, which is obtained by applying the distributed consensus algorithm:

$$e_{G_{Hi}Q_i^h} = C_H \sum_{j\in N_i} a_{ij}\left(G_{Hj}\,Q_j^h - G_{Hi}\,Q_i^h\right), \tag{4.15}$$

where C_H is the consensus coupling gain, and G_{Hi} is the harmonic power sharing coefficient of the ith DG. G_{Hi} is set to be equal to the $P-\omega$ droop coefficient ($G_{Hi} = m_i$). By using the proposed control method, the equivalent harmonic impedance ($Z_{eq\_i}^{h}$) of the ith DG in (4.10) is modified as follows:

$$Z_{eq\_i}^{h} = \left(Z_{\ln i} + C_{hi}\, Z_{Vhi}\right)\Big/\left(1 + C_{hi}\, K_{hi}\right), \tag{4.16}$$

In (4.15), the equivalent impedance of the ith DG unit at the dominant harmonic frequency is flexibly controlled through K_{hi} and C_{hi}. Here, K_{hi} is continuously adjusted to reduce the DG equivalent impedance for attenuating the PCC voltage harmonics, and C_{hi} is adaptively regulated to compensate the mismatched line impedance compensation for power sharing accuracy. Thus, the proposed control scheme flexibly adjusts the DG equivalent impedance to simultaneously attenuate the PCC voltage harmonics and eliminate harmonic power sharing error. The output voltage reference is generated by combining the fundamental and harmonic virtual impedance:

$$\begin{aligned} V_{Oi}^{*} = V_{dri} - V_{vfi} - \sum_{h=3,5,7,9} V_{Vhi} = V_{dri} - \Big(R_{Vfi}\, I_{Ofi\_\alpha} - \\ \omega_f L_{Vfi}\, I_{Ofi\_\beta}\Big) - \sum_{h=3,5,7,9} C_{hi}\left(K_{hi}V_{PCC\_h} + Z_{Vhi}\, I_{Ohi}\right). \end{aligned} \tag{4.17}$$

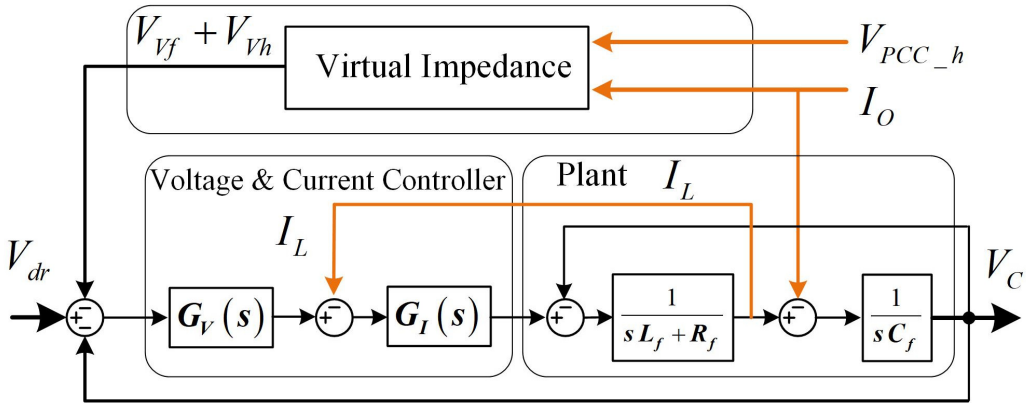

Figure 4.4 Inner control loop block diagram.

4.3 Output Impedance Analysis

By using the proposed harmonic control scheme, the voltage reference in (4.16) is modified to regulate the PCC voltage harmonics and accurately share the power among DG units. To track the voltage reference accurately, the inner control loop should be properly designed and its block diagram is shown in Fig. 4.4. In Fig. 4.4, the DG closed-loop transfer function without considering the virtual impedance is obtained as follows:

$$V_C = G_S(s)V_O^* - Z_O(s)I_O = G_S(s)V_{dr} - Z_O(s)I_O. \tag{4.18}$$

where $G_S(s)$ and $Z_O(s)$ are the control gain and inverter impedance transfer function, respectively. They are given below:

$$G_S(s) = \frac{G_V G_I}{s^2 L_f C_f + s\left(R_f C_f + G_I C_f\right) + G_V G_I + 1}. \tag{4.19}$$

$$Z_O(s) = \frac{\left(sL_f + R_f + G_I\right)}{s^2 L_f C_f + s\left(R_f C_f + G_I C_f\right) + G_V G_I + 1}. \tag{4.20}$$

In (4.19) and (4.20), $G_V(s)$ and $G_I(s)$ are the voltage and current controller transfer functions:

$$G_V(s) = K_{PV} + \frac{2K_{IVf}s}{s^2 + 2\omega_c s + \omega_f^2} + \sum_{h=3,5,7,9} \frac{2K_{IVh}s}{s^2 + 2\omega_c s + \omega_h^2}. \tag{4.21}$$

$$G_I = K_{PI}. \tag{4.22}$$

where K_{PV} and K_{PI} are the proportional gains, and K_{IVf} and K_{IVh} are the resonance gains, respectively.

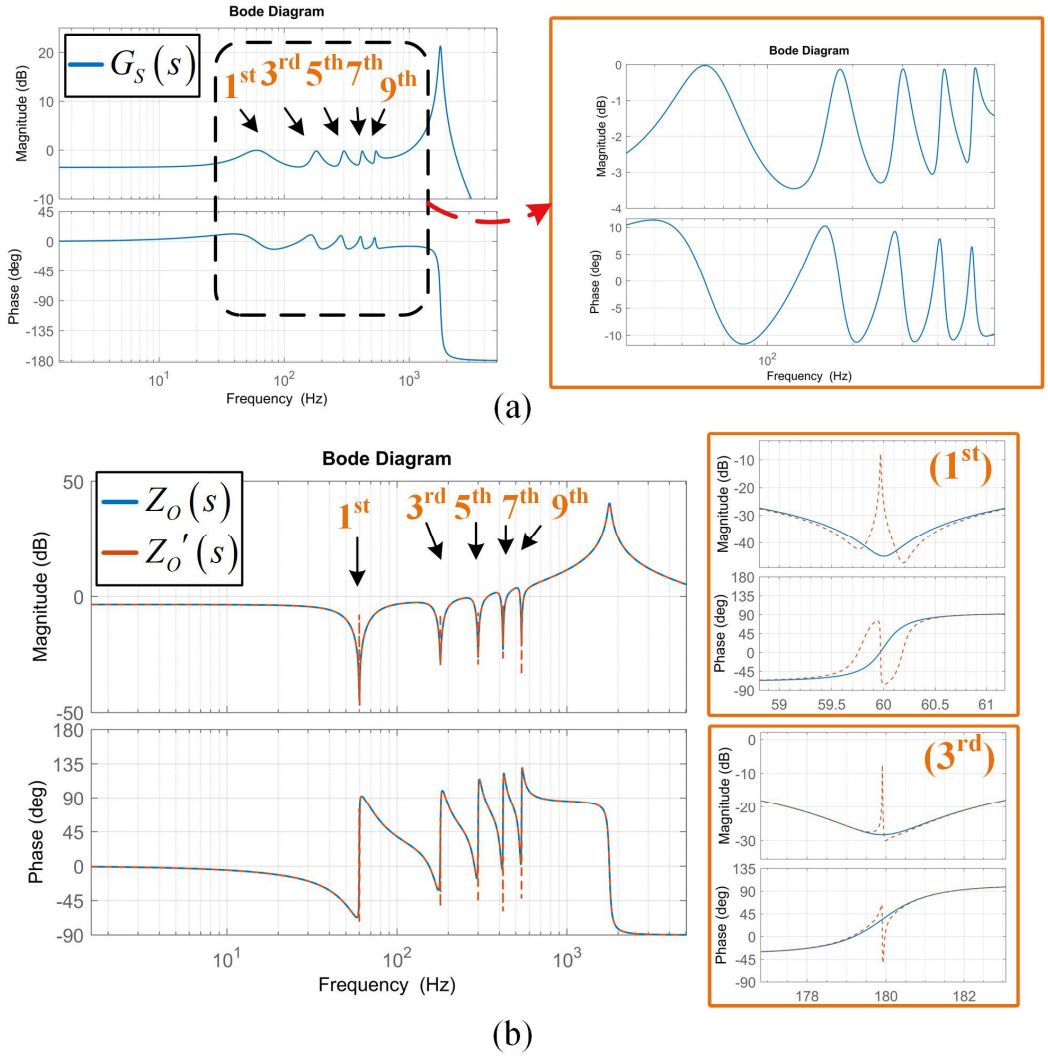

Figure 4.5 Bode diagram of a DG inverter: (a) $G_S(s)$; (b) $Z_O(s)$ and $Z_O^{/}(s)$.

By considering the proposed virtual impedance, the closed-loop transfer function in (4.18) is rewritten as:

$$V_C = G_S(s)\left(V_{dr} - \sum_{h=3,5,7,9} C_h K_h V_{PCC\_h}\right) - Z_O^{/}(s) I_O, \tag{4.23}$$

where $Z_O^{/}(s)$ is the modified output impedance, which is defined as follows:

$$Z_O^{/}(s) = Z_O(s) + G_S(s)\left(Z_{Vf}(s) G_f(s) + \sum_{h=3,5,7,9} C_h Z_{Vh}(s) G_h(s)\right), \tag{4.24}$$

where $G_h(s)$ and $G_f(s)$ are the active bandpass filters (BPFs) to separate the fundamental and harmonic voltage components, respectively. They are obtained as follows:

$$G_f(s) = (\omega_C s) / (s^2 + \omega_C s + \omega_f^2), \tag{4.25}$$

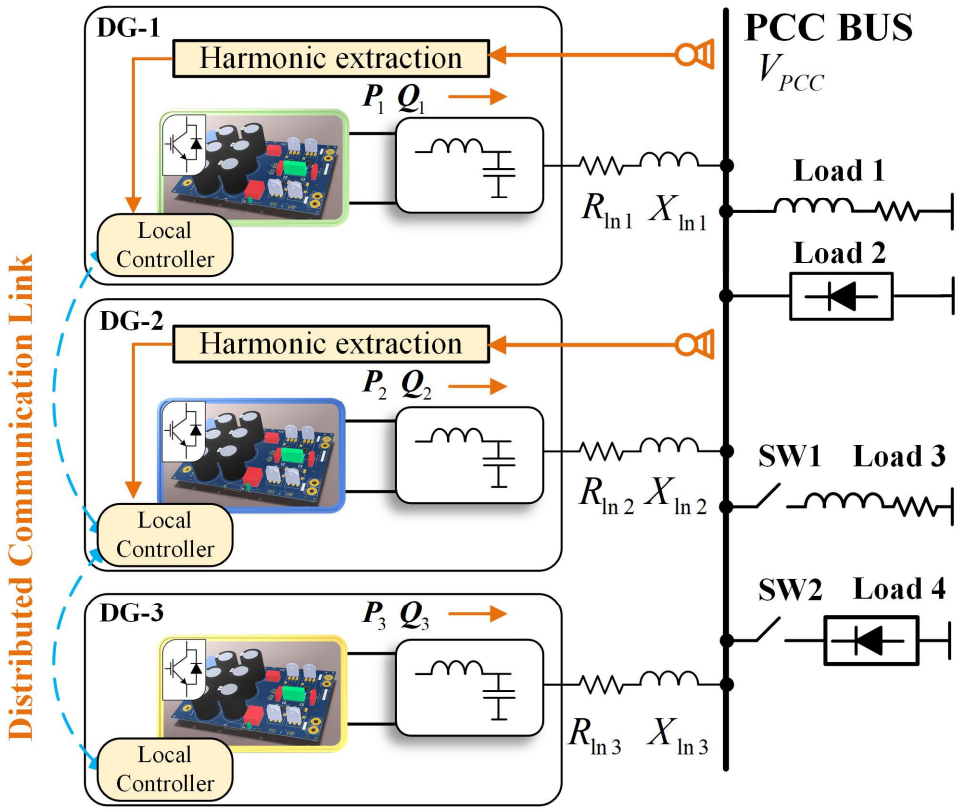

Figure 4.6 Studied microgrid system.

$$G_h(s) = (\omega_C\, s) / \left(s^2 + \omega_C\, s + \omega_h^2\right), \tag{4.26}$$

To evaluate the influence of the proposed virtual impedance on the system, bode diagrams of $G_S(s)$, $Z_O(s)$, and $Z_O^{/}(s)$ are plotted in Fig. 4.5 with the listed parameters in Table 4.1. The magnitude and phase of $G_S(s)$ at the 1st, 3rd, 5th, 7th, and 9th frequencies shown in Fig. 4.5(a) are 1 and 0, respectively. In addition, the magnitude of $Z_O(s)$ at the hth frequency is close to 0, as shown in Fig. 4.5(b). Therefore, the DG output voltage tracks its voltage reference perfectly without a phase delay at both the fundamental and harmonic frequencies.

After properly designing the inner voltage and current controller, the PCC harmonics compensation and harmonic power sharing can be precisely achieved if the DG equivalent impedance is adaptively regulated. By using the proposed control scheme, the fundamental output impedance is modified, as shown in Fig. 4.5(b), with a sufficient gain to compensate for the mismatched line impedance and to properly share the reactive power.

Table 4.1 Microgrid System Parameters

Parameters	Values	Parameters	Values	Parameters	Values
K_{pQ_i}	0.001	V_O	110V	L_f	1.2mH
K_{iQ_i}	0.005 rad/s	$m_i, n_i \mid_{i=1,2,3}$	0.005, 0.002	R_f	0.01Ω
K_{pP_i}	0.001	$HD_{ref\,3,5,7}$	1%,	$HD_{ref\,9}$	0.7%
K_{iP_i}	0.005 rad/s	K_{ph}, K_{ih}	0.1, 2	C_f	20μF
K_{PV}	1.0	K_{pQh}, K_{iQh}	0.01, 0.3	K_{IVh}	30 rad/s
K_{IVf}	180 rad/s	K_{PI}	2	ω_C	2π8 rad/s
$R_{\ln 1}$	0.2Ω	$R_{\ln 2}$	0.3Ω	$R_{\ln 3}$	0.4Ω
$X_{\ln 1}$	0.52Ω	$X_{\ln 2}$	0.805Ω	$X_{\ln 3}$	1.13Ω
P_{Total}	680W	Q_{Total}	370Var	$f_{Switching}$	20KHz
Load 3	10Ω 45mH	G_P, G_Q	0.4, 0.4	$f_{Sampling}$	10KHz
Nonlinear Load 4	120Ω 640uH 150uF	C_H	0.5	f_0	60Hz

From Fig. 4.5(b), it can be seen that the modified output impedance has a finite gain at the dominant harmonic frequencies with the proposed control scheme. Therefore, system damping at the h^{th} frequency is increased, and system stability is attained. Furthermore, the gain and phase of the controller at each harmonic frequency are completely separated. Thus, the harmonic coupling problem is eliminated.

4.4 Closed-Loop Stability Analysis

The system characteristic is examined to validate the system stability with the proposed controller. To simplify the microgrid system, it is assumed that the fundamental power is proportionally shared in the steady-state. Then, the system in Fig. 4.6 can be modeled considering the delay effect in Fig. 4.7. The system transfer function $G_{sys}(s)$ can be obtained by analyzing the block diagram in Fig. 4.7 as follows:

$$G_{sys}(s)=\frac{I_O}{V^*}=\frac{1-D\sum_{h=3,5,7,9} C_h K_h G_h(s)}{DG_f(s)Z_{Vf}+Z_{\ln}+D\sum_{h=3,5,7,9} C_h G_h(s)\left(Z_{Vh}-K_h Z_{\ln}\right)}, \tag{4.27}$$

where D represents the total delay in the harmonic impedance control loop ($T_D = 0.0001s$):

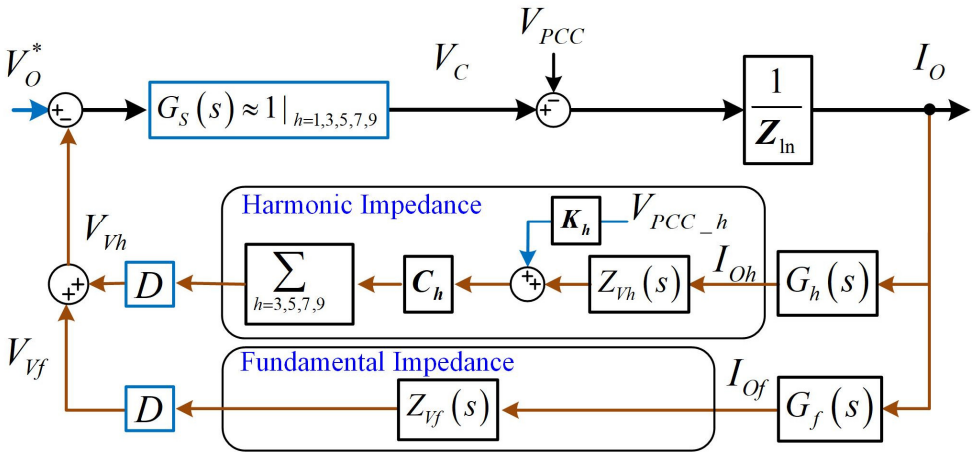

Figure 4.7 Simplified block diagram of the DG control system.

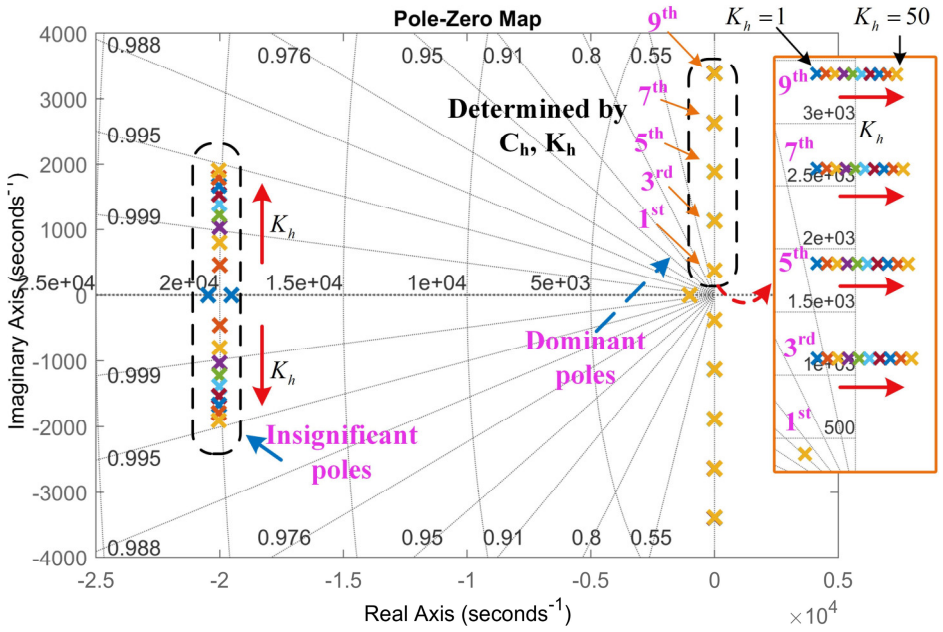

Figure 4.8 Root locus diagram of the system ($C_h = 0.8$, K_h increases from 1 to 50).

$$D = \frac{2 - T_D s}{2 + T_D s}, \tag{4.28}$$

After analyzing the system, the poles of $G_{sys}(s)$ are plotted in Fig. 4.8(b), with K_h increased from 1 to 50 and C_h is set to 0.8. Generally, the control system is stable when all of the poles are located in the left-half plane, as can be seen in Fig. 4.8(b). When K_h increases, the system damping is reduced since the dominant poles move toward the origin coordinates. If K_h is too large ($K_h > 25.5$), the dominant poles are located in the right-half plane. Thus, the system becomes unstable. This system behavior occurs when the absorbed harmonic

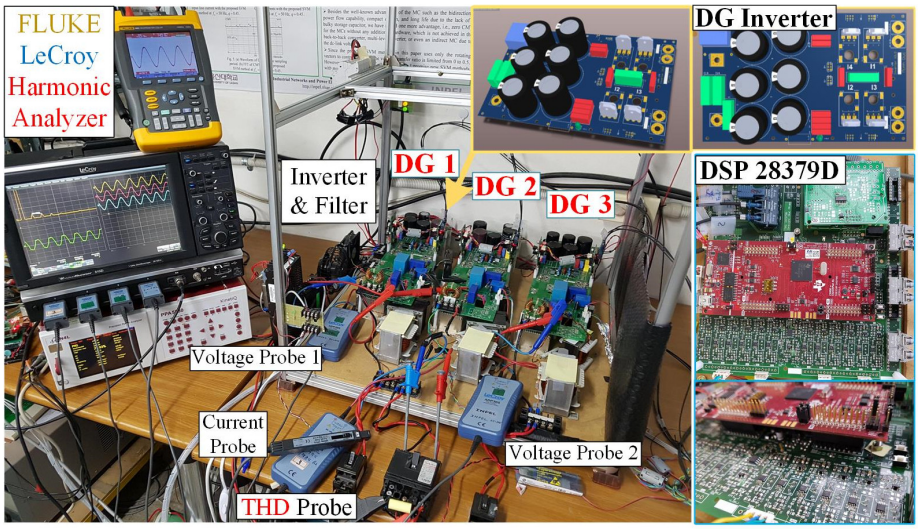

Figure 4.9 Laboratory microgrid system.

current exceeds the DG capability, which implies that the phase margin of the system control loop is reduced to less than 0 degrees. Based on a root locus analysis, the limitation of K_h ($K_h < 25$) is designed to ensure system stability and a fast-transient response. Similarly, a limitation of C_h is designed ($C_h < 2$) to have a high system damping.

4.5 Experimental Results

The AC microgrid system shown in Fig. 4.6 with 3 DG units is set up using the parameters listed in Table 4.1. The DG unit is operated by a DSP (TMS320F28379D) from Texas Instruments, and the 20-ms delay time induced by low-bandwidth contact is generated using a zero-order hold. To obtain real-time monitoring, the fundamental and harmonic powers are exported to an oscilloscope using a DAC module (AD5325BRMZ) and a harmonic analyzer (PPA5530). In the experiment, only DG1 and DG2 are considered to have the capacity to compensate the PCC harmonics voltage. The laboratory microgrid system is shown in Fig. 4.9

The effectiveness of the proposed controller is evaluated by comparing experimental results to those of the conventional method in [53]. The conventional method is well known as the enhanced harmonic virtual impedance, which is regarded as the most advanced control scheme in terms of the PCC harmonic compensation. For a fair comparison, the parameters of the conventional controller are chosen to obtain the same settling time as the proposed

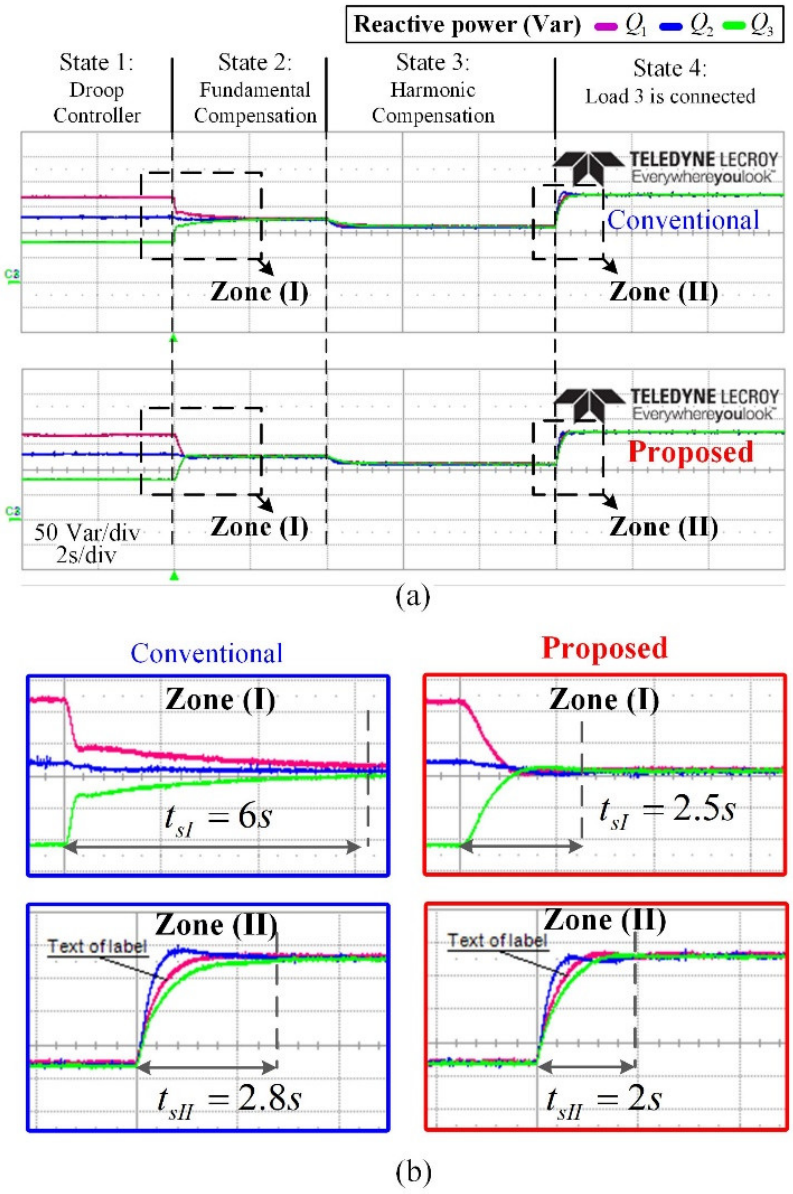

Figure 4.10 Reactive power sharing among distributed generation units: (a) dynamic performance of conventional and proposed controllers; (b) expanded waveforms for zones (I) and (II).

controller. To satisfy the requirements of the IEEE 519-2014 standard [77], HD_{ref} at the 3rd, 5th, and 7th harmonics are set as 1.0%, and HD_{ref} at the 9th is set as 0.7%.

In the experiment, the test conditions are defined as follows.

State 1: The microgrid with load 1 and load 2 adopts the conventional droop controller to autonomously share the load power among the DG units.

State 2: The accurate fundamental power sharing algorithm is adopted to remove the reactive power sharing error.

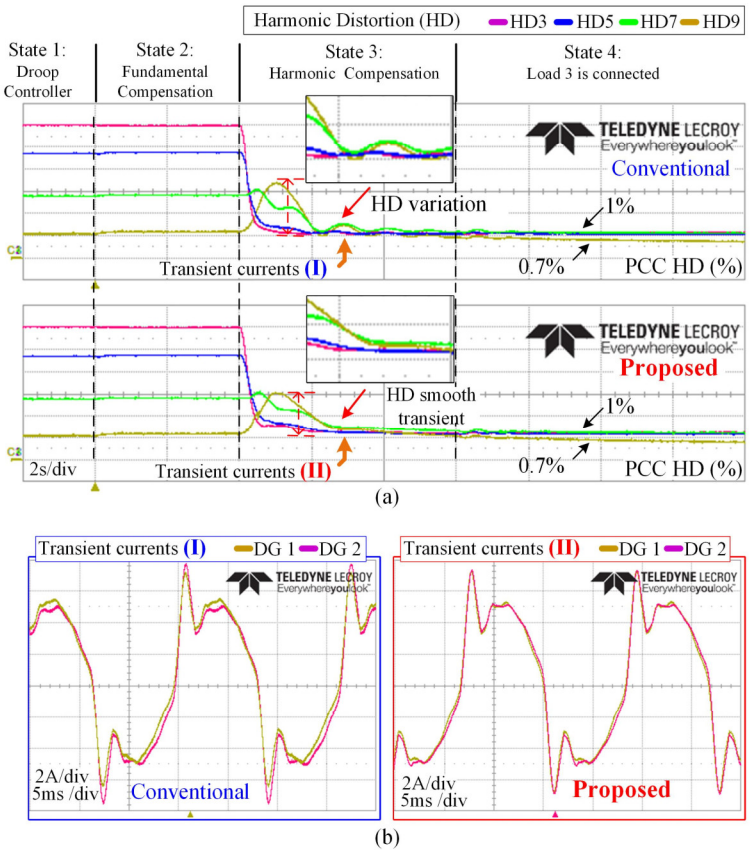

Figure 4.11 PCC power quality: (a) harmonic distortion of the conventional and proposed controllers; (b) transient currents during compensation.

State 3: The harmonic compensation algorithm is applied to the DG units for improving the PCC voltage quality and harmonic power sharing accuracy.

State 4: The additional load 3 is connected to the microgrid system.

According to the test conditions, the predefined states are applied for the experimental verification. Fig. 4.10 shows the efficiency of the conventional and proposed controllers in terms of reactive power sharing. From the expanded waveform of zone (I) in Fig. 4.10(b), it can be seen that the proposed controller considerably reduces the reactive power settling time t_{sI} from 6s to 2.5s when compared to that of the conventional method. When a load is suddenly connected to the microgrid in zone (II), the proposed controller achieves smooth and reduced transient response time t_{sII} from 2.8s to 2s. Therefore, when compared to the conventional control approach, the proposed controller can be seen to have better performance with faster response.

To show the effectiveness of the proposed harmonic control scheme, the harmonic

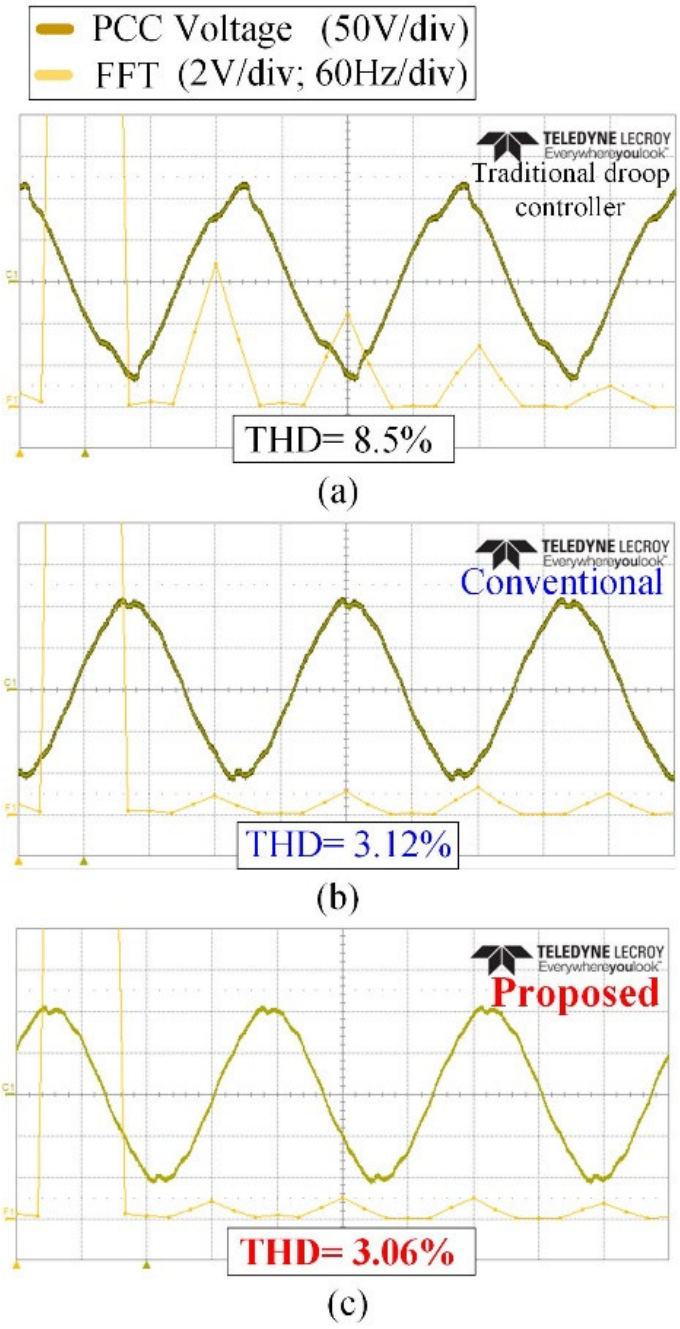

Figure 4.12 THD values of the PCC voltage: (a) before applying the conventional or proposed control methods; (b) after applying the conventional control method; (c) after applying the proposed control method

distortion of the PCC voltage is fully monitored in real-time, as shown in Fig. 4.11(a). In Fig. 4.11(a), the proposed controller shows a smooth transient response, while the conventional controller shows fluctuation. It is important to achieve a smooth transient response because PCC HD oscillation causes harmonic circulating and fluctuating currents among DG units,

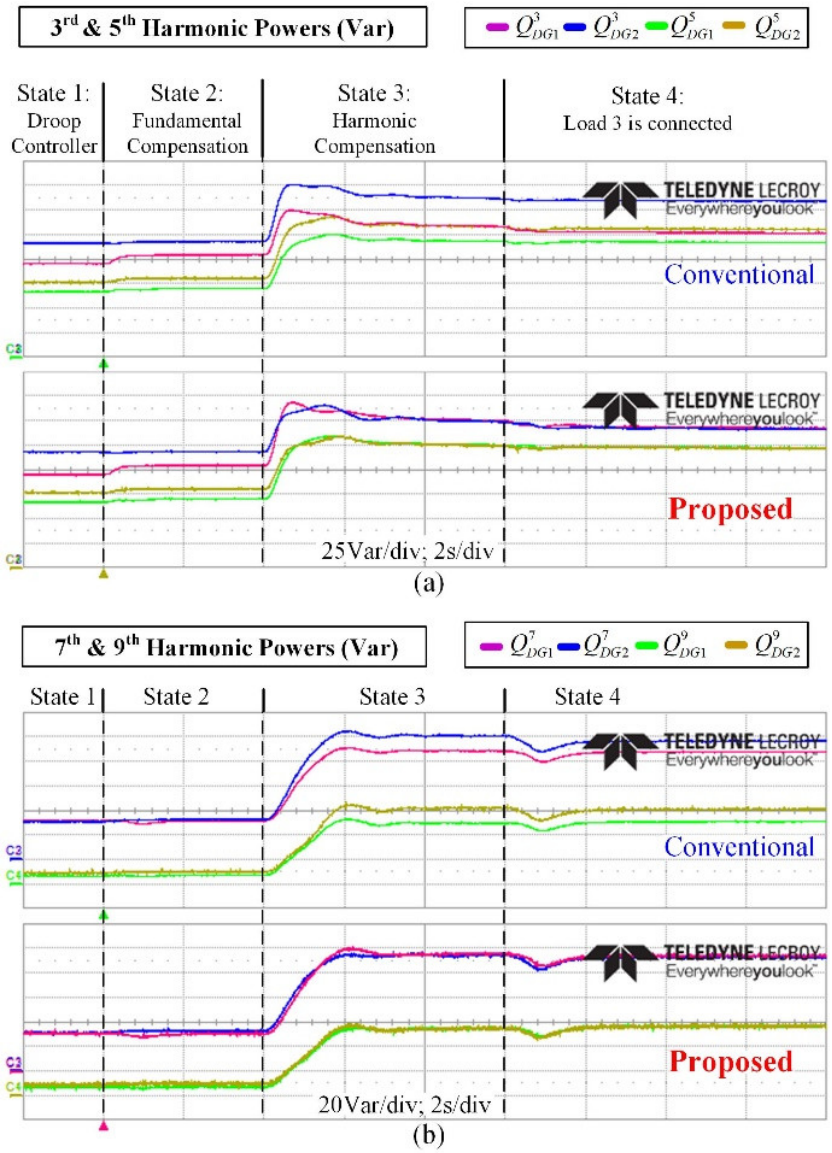

Figure 4.13 Harmonic power sharing performance: (a) 3rd and 5th harmonics; (b) 7th and 9th harmonics.

which reduces the stability and reliability of microgrid systems. When load 3 is connected to the microgrid, the PCC HD remains constant, which demonstrates the assurance of the harmonic compensating performance with the proposed controller, as shown in Fig. 4.11(a).

To show the effectiveness of the proposed controller, DG currents during transients are directly captured using the "Trigger function" in an oscilloscope, and they are shown in Fig. 4.11(b). Since the harmonic power is not equally shared in the conventional controller shown in Fig. 4.11(b), the DG currents have a noticeable harmonic current deviation between DG1 and DG2. Meanwhile, they are minimized with the proposed controller thanks to the equally shared harmonic power.

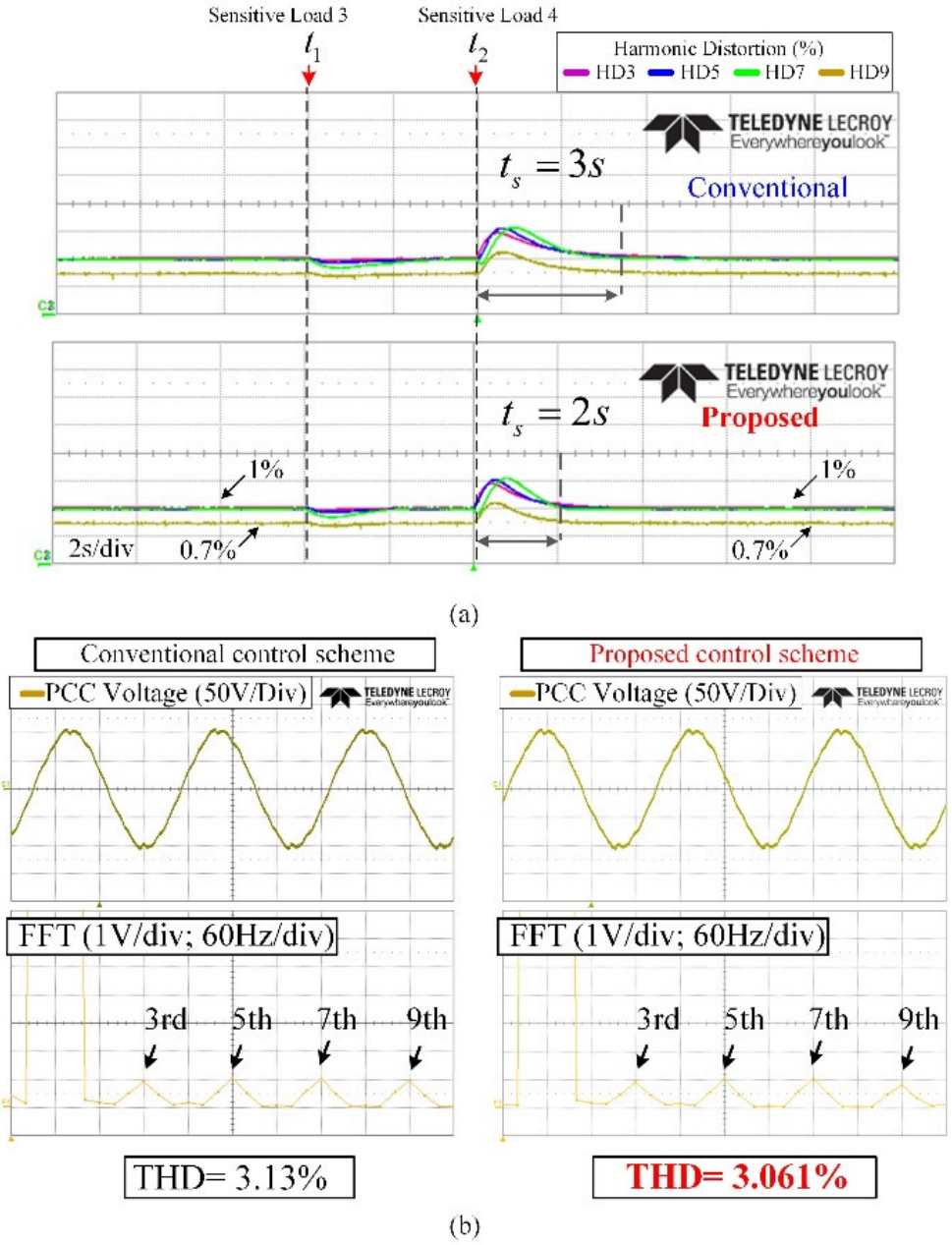

Figure 4.14 Power quality during sensitive load connection: (a) harmonic distortion performance; (b) voltage quality after load connection.

To evaluate the PCC voltage quality, the THD values of the conventional and proposed control methods are measured, and their values are shown in Fig. 4.12(a), Fig. 4.12(b), and Fig. 4.12(c). Before applying the conventional and proposed control methods, as shown in Fig. 4.12(a), the PCC voltage is distorted with a high THD value (THD=8.5%). From Fig. 4.12(b) and Fig. 4.12(c), it can be seen that the PCC voltage quality is improved after compensating the PCC voltage harmonics. It can also be seen that the THD value of the proposed control method is smaller than that of the conventional method (THD=3.06%<3.12%).

Fig. 4.13(a) and Fig. 4.13(b) show the accuracy of the harmonics sharing between the conventional harmonic impedance and proposed harmonic control methods, respectively. From Fig. 4.13(a), it can be seen that the power deviations at the 3rd and 5th harmonics are significant in the conventional method due to the unequal harmonic line impedance. However, in the proposed controller, the 3rd and 5th harmonic powers between DG1 and DG2 reach the desired values within 1s and they remain constant as shown in Fig. 4.13(a) even when load 3 is plugged into the system. In addition, the 7th and 9th harmonic powers are shared accurately among DG units with the proposed control method as shown in Fig. 4.13(b). Hence, the 3rd, 5th, 7th, and 9th harmonic power sharing errors are eliminated with the proposed control method.

To investigate PCC voltage quality during a sensitive load connection, loads 3 and 4 are connected to the PCC bus at t_1 and t_2 when the microgrid is operated in state 3, as shown in Fig. 4.14(a). From Fig. 4.14(a) and Fig. 4.14(b), the harmonic distortion performance of the proposed control method is faster than that of the conventional control method with a remarkable reduction of t_s from 3s to 2s. In addition, the proposed control method has a smaller THD value than that of the conventional method despite the sensitive load connection (3.061%<3.13%). It is obvious from the obtained experimental results that the proposed control method increases the quality of the PCC voltage. It can also be seen that its performance is guaranteed regardless of the sensitive load connection.

4.6 Conclusion of the Chapter

In this chapter, an enhanced compensation strategy is proposed to simultaneously achieve a desirable PCC harmonics compensation (THD<5%) and an accurate distribution of the power in both the fundamental and harmonic components. By adaptively controlling both the fundamental and harmonic equivalent impedance, the mismatched line impedance among DG units and harmonic currents are well compensated. Thus, both fundamental and harmonic power sharing errors are eliminated. In addition, the equivalent harmonic impedance is regulated to achieve a high PCC harmonic voltage quality, which complies with IEEE 519 standards. Furthermore, the proposed control strategy can be applied to a microgrid system without the use of microgrid system parameters. Even if the loads change suddenly, the microgrid system maintains good fundamental and harmonic power sharing performance with

excellent transient behaviors. The effectiveness and reliability of the proposed control method are demonstrated by a number of experimental studies.

Chapter 5

Conclusions and Future Works

5.1 Conclusions

In this thesis, an advanced virtual impedance control scheme has been developed for islanded microgrids to enhance the power sharing accuracy and improve PCC voltage quality. First of all, the thesis examined the inaccurate reactive power sharing, harmonic power sharing, and PCC voltage distortion problems in islanded microgrids. Then, many control schemes have been proposed to improve microgrid control performance. The reliability and effectiveness of the proposed control strategy are validated by simulation and experimental results. The summarized conclusions of the thesis are listed in the following.

In chapter 2, a centralized virtual impedance control scheme has been proposed to realize accurate active and reactive power sharing. Because no knowledge of microgrid configuration is required, the control method is simple and easy to implement to the microgrid system. Furthermore, the microgrid system still has good power sharing performance even if the load changes during the communication interruption. Hence, our control scheme is very useful for the effective operation of DGs in islanded microgrid. However, the communication link between MGCC and each DG units is necessary to implement the control method, so that the proposed control method might not apply to the islanded microgrid system with a high number of DG units. Furthermore, the voltage distortion issue at the PCC bus has not been considered in this chapter.

To attenuate PCC voltage distortion and reactive power sharing error, the harmonic mitigation scheme is presented in chapter 3. In the proposed method, the resistive-capacitive virtual impedances are introduced to the output of converter to regulate active and reactive powers among DG units. In addition, resistive-capacitive virtual impedances have also been

extended to the 3rd, 5th, and 7th harmonic frequencies to compensate for the PCC harmonic voltage. To improve the control feasibility, the control scheme was designed in both a centralized and distributed approach, and it does not require a detailed microgrid structure. Although the control scheme in this chapter can mitigate the PCC voltage harmonic distortion, it cannot share the harmonic power properly among DG units.

To simultaneously compensate the PCC voltage distortion and share the harmonic power, the effective impedance-based harmonics compensation is proposed in chapter 4. By adaptively controlling both the fundamental and harmonic equivalent impedance, the mismatched line impedance among DG units and harmonic currents are well compensated with the proposed control scheme. In addition, a high PCC harmonic voltage quality is guaranteed and complied with IEEE 519 standards.

When the microgrid mainly consists of linear load, the control scheme in chapter 2 is a suitable solution to realize accurate active and reactive power sharing. On the other hand, when nonlinear loads are extensively used, the adaptive impedance scheme in chapter 3 can be adopted to improve the PCC voltage quality without degrading fundamental power sharing performance. In the strict microgrid system where accurate harmonic power sharing is a required function, the control scheme in chapter 4 becomes a cost-effective solution because it only requires a distributed communication link among DG units.

5.2 Future Works

Although various control methods have been proposed to address the power sharing inaccuracy and PCC voltage distortion issues, to further enhance the islanded microgrid operation, some certain areas are needed to be investigated in the future such as:

- The modified nonlinear droop controller for improving the active and reactive power sharing accuracy.
- Model-based predictive control for PCC voltage harmonics compensation.
- Sensor-less synchronization methods for seamlessly connecting a DG unit to the microgrid in both grid-connected and islanded mode.
- Fault protection in islanded microgrids such as overload protection, short-circuit protection, and fault override capability of inverters.

Bibliography

[1] D. E. Olivares *et al.*, "Trends in microgrid control," *IEEE Transactions on Smart Grid*, vol. 5, no. 4, pp. 1905–1919, Jul. 2014

[2] F. Nejabatkhah, Y. W. Li, and H. Tian, "Power Quality Control of Smart Hybrid AC/DC Microgrids: An Overview," *IEEE Access*, vol. 7, pp. 52295–52318, 2019

[3] "IEEE Guide for Conducting Distribution Impact Studies for Distributed Resource Interconnection," *IEEE Std 1547.7-2013*, pp. 1–137, Feb. 2014

[4] F. Katiraei and M. R. Iravani, "Power management strategies for a microgrid with multiple distributed generation units," *IEEE Transactions on Power Systems*, vol. 21, no. 4, pp. 1821–1831, 2006

[5] I. Patrao, E. Figueres, G. Garcerá, and R. González-Medina, "Microgrid architectures for low voltage distributed generation," *Renewable and Sustainable Energy Reviews*, vol. 43. pp. 415–424, 2015.

[6] J. He and Y. W. Li, "Analysis, design, and implementation of virtual impedance for power electronics interfaced distributed generation," *IEEE Transactions on Industry Applications*, vol. 47, no. 6, pp. 2525–2538, 2011

[7] J. M. Carrasco *et al.*, "Power-electronic systems for the grid integration of renewable energy sources: A survey," *IEEE Transactions on Industrial Electronics*, vol. 53, no. 4. pp. 1002–1016, 2006.

[8] Y. Xue, L. Chang, S. B. Kjær, J. Bordonau, and T. Shimizu, "Topologies of single-phase inverters for small distributed power generators: An overview," *IEEE Transactions on Power Electronics*, 2004

[9] A. Camacho, M. Castilla, J. Miret, A. Borrell, and L. G. De Vicuña, "Active and reactive power strategies with peak current limitation for distributed generation

inverters during unbalanced grid faults," *IEEE Transactions on Industrial Electronics*, vol. 62, no. 3, pp. 1515–1525, 2015

[10] M. Montoya, R. Sherick, P. Haralson, R. Neal, and R. Yinger, "Islands in the Storm: Integrating microgrids into the larger grid," *IEEE Power and Energy Magazine*, vol. 11, no. 4, pp. 33–39, 2013

[11] M. A. Zamani, T. S. Sidhu, and A. Yazdani, "Investigations Into the Control and Protection of an Existing Distribution Network to Operate as a Microgrid: A Case Study," *IEEE Transactions on Industrial Electronics*, vol. 61, no. 4, pp. 1904–1915, Apr. 2014

[12] J. Kim, J. M. Guerrero, P. Rodriguez, R. Teodorescu, and K. Nam, "Mode adaptive droop control with virtual output impedances for an inverter-based flexible AC microgrid," *IEEE Transactions on Power Electronics*, vol. 26, no. 3, pp. 689–701, 2011

[13] A. Mehrizi-Sani and R. Iravani, "Potential-function based control of a microgrid in islanded and grid-connected modes," *IEEE Transactions on Power Systems*, vol. 25, no. 4, pp. 1883–1891, 2010

[14] J. He, L. Du, B. Liang, Y. Li, and C. Wang, "A Coupled Virtual Impedance for Parallel AC/DC Converter Based Power Electronics System," *IEEE Transactions on Smart Grid*, vol. 10, no. 3, pp. 3387–3400, 2019

[15] P. Basak, S. Chowdhury, S. Halder Nee Dey, and S. P. Chowdhury, "A literature review on integration of distributed energy resources in the perspective of control, protection and stability of microgrid," *Renewable and Sustainable Energy Reviews*, vol. 16, no. 8. pp. 5545–5556, 2012.

[16] J. A. P. Lopes, C. L. Moreira, and A. G. Madureira, "Defining control strategies for microgrids islanded operation," *IEEE Transactions on Power Systems*, vol. 21, no. 2, pp. 916–924, 2006

[17] T. L. Vandoorn, J. C. Vasquez, J. De Kooning, J. M. Guerrero, and L. Vandevelde, "Microgrids: Hierarchical control and an overview of the control and reserve management strategies," *IEEE Industrial Electronics Magazine*, vol. 7, no. 4, pp. 42–55, 2013

[18] M.-D. Pham and H.-H. Lee, "Improved Reactive Power Sharing and Harmonic Voltage Compensation in Islanded Microgrids Using Resistive-Capacitive Virtual Impedance," *Journal of Power Electronics*, vol. 19, no. 6, pp. 1575–1581, 2019.

[19] J. C. Vasquez, R. A. Mastromauro, J. M. Guerrero, and M. Liserre, "Voltage support provided by a droop-controlled multifunctional inverter," *IEEE Transactions on Industrial Electronics*, 2009

[20] A. Micallef, M. Apap, C. Spiteri-Staines, J. M. Guerrero, and J. C. Vasquez, "Reactive power sharing and voltage harmonic distortion compensation of droop controlled single phase islanded microgrids," *IEEE Transactions on Smart Grid*, vol. 5, no. 3, pp. 1149–1158, 2014

[21] J. He and Y. W. Li, "An enhanced microgrid load demand sharing strategy," *IEEE Transactions on Power Electronics*, vol. 27, no. 9, pp. 3984–3995, Sep. 2012

[22] Y. W. Li, "Control and resonance damping of voltage-source and current-source converters with LC filters," *IEEE Transactions on Industrial Electronics*, vol. 56, no. 5, pp. 1511–1521, 2009

[23] M. D. Pham and H. H. Lee, "Fuzzy PID controller for PCC voltage harmonic compensation in islanded microgrid," in *Lecture Notes in Computer Science (including subseries Lecture Notes in Artificial Intelligence and Lecture Notes in Bioinformatics)*, vol. 10954 LNCS, Springer, Cham, 2018, pp. 231–242.

[24] M. Duc Pham and H. H. Lee, "An Effective PCC Voltage Harmonic Compensation and Harmonic Power Sharing in Islanded Microgrid," in *IECON 2018 - 44th Annual Conference of the IEEE Industrial Electronics Society*, Oct. 2018, pp. 89–94.

[25] M. D. Pham and H. H. Lee, "Resonance Mitigation and Harmonics Compensation in Islanded Microgrids via Virtual Damping Resistance and Virtual Shunt Filter," in *IECON 2019 - 45th Annual Conference of the IEEE Industrial Electronics Society*, 2019, vol. 1, pp. 2475–2480.

[26] H. Han, Y. Liu, Y. Sun, M. Su, and J. M. Guerrero, "An improved droop control strategy for reactive power sharing in islanded microgrid," *IEEE Transactions on Power Electronics*, 2015

[27] Y. Han, H. Li, P. Shen, E. A. A. Coelho, and J. M. Guerrero, "Review of Active and Reactive Power Sharing Strategies in Hierarchical Controlled Microgrids," *IEEE Transactions on Power Electronics*, vol. 32, no. 3, pp. 2427–2451, Mar. 2017

[28] H. Han, X. Hou, J. Yang, J. Wu, M. Su, and J. M. Guerrero, "Review of power sharing control strategies for islanding operation of AC microgrids," *IEEE Transactions on Smart Grid*, vol. 7, no. 1, pp. 200–215, Jan. 2016

[29] W. Yao, M. Chen, J. Matas, J. M. Guerrero, and Z. M. Qian, "Design and analysis of the droop control method for parallel inverters considering the impact of the complex impedance on the power sharing," *IEEE Transactions on Industrial Electronics*, vol. 58, no. 2, pp. 576–588, 2011

[30] C. T. Lee, C. C. Chu, and P. T. Cheng, "A new droop control method for the autonomous operation of distributed energy resource interface converters," *IEEE Transactions on Power Electronics*, vol. 28, no. 4, pp. 1980–1993, Apr. 2013

[31] Q.-C. Zhong, "Robust Droop Controller for Accurate Proportional Load Sharing Among Inverters Operated in Parallel," *IEEE Transactions on Industrial Electronics*, vol. 60, no. 4, pp. 1281–1290, Apr. 2013

[32] J. He, Y. Pan, B. Liang, and C. Wang, "A simple decentralized islanding microgrid power sharing method without using droop control," *IEEE Transactions on Smart Grid*, vol. 9, no. 6, pp. 6128–6139, 2018

[33] J. M. Guerrero, N. Berbel, J. Matas, L. G. De Vicuña, and J. Miret, "Decentralized control for parallel operation of distributed generation inverters in microgrids using resistive output impedance," in *IECON Proceedings (Industrial Electronics Conference)*, 2006, pp. 5149–5154.

[34] J. M. Guerrero, L. García de Vicuña, J. Matas, M. Castilla, and J. Miret, "Output impedance design of parallel-connected UPS inverters with wireless load-sharing control," *IEEE Transactions on Industrial Electronics*, vol. 52, no. 4, pp. 1126–1135, 2005

[35] J. He, Y. W. Li, J. M. Guerrero, F. Blaabjerg, and J. C. Vasquez, "An islanding Microgrid power sharing approach using enhanced virtual impedance control scheme,"

IEEE Transactions on Power Electronics, vol. 28, no. 11, pp. 5272–5282, 2013

[36] Y. Zhu, F. Zhuo, F. Wang, B. Liu, and Y. Zhao, "A Wireless Load Sharing Strategy for Islanded Microgrid Based on Feeder Current Sensing," *IEEE Transactions on Power Electronics*, vol. 30, no. 12, pp. 6706–6719, 2015

[37] H. Han, Y. Liu, Y. Sun, M. Su, and J. M. Guerrero, "An improved droop control strategy for reactive power sharing in islanded microgrid," *IEEE Transactions on Power Electronics*, vol. 30, no. 6, pp. 3133–3141, 2015

[38] L. Lin, H. Ma, and Z. Bai, "An Improved Proportional Load-Sharing Strategy for Meshed Parallel Inverters System with Complex Impedances," *IEEE Transactions on Power Electronics*, vol. 32, no. 9, pp. 7338–7351, 2017

[39] H. Mahmood, D. Michaelson, and J. Jiang, "Accurate reactive power sharing in an islanded microgrid using adaptive virtual impedances," *IEEE Transactions on Power Electronics*, vol. 30, no. 3, pp. 1605–1617, Mar. 2015

[40] F. Zandi, B. Fani, I. Sadeghkhani, and A. Orakzadeh, "Adaptive complex virtual impedance control scheme for accurate reactive power sharing of inverter interfaced autonomous microgrids," *IET Generation, Transmission & Distribution*, vol. 12, no. 22, pp. 6021–6032, 2018

[41] J. He, Y. W. Li, and F. Blaabjerg, "An enhanced islanding microgrid reactive power, imbalance power, and harmonic power sharing scheme," *IEEE Transactions on Power Electronics*, vol. 30, no. 6, pp. 3389–3401, Jun. 2015

[42] Z. Li and X. Jia, "An Improved VSG Control Strategy Based on the Amplitude-frequency Characteristics of Virtual Power," *IEEE Access*, vol. 7, pp. 101096–101105, 2019

[43] H. Cai, X. He, J. Shi, H. Zhao, and P. Zhang, "Power decoupling strategy based on 'virtual negative resistor' for inverters in low-voltage microgrids," *IET Power Electronics*, vol. 9, no. 5, pp. 1037–1044, 2016

[44] Z. Chen, X. Pei, M. Yang, and L. Peng, "An Adaptive Virtual Resistor (AVR) Control Strategy for Low-Voltage Parallel Inverters," *IEEE Transactions on Power Electronics*, vol. 34, no. 1, pp. 863–876, Jan. 2019

[45] Q. Sun, R. Han, H. Zhang, J. Zhou, and J. M. Guerrero, "A Multiagent-Based Consensus Algorithm for Distributed Coordinated Control of Distributed Generators in the Energy Internet," *IEEE Transactions on Smart Grid*, vol. 6, no. 6, pp. 3006–3019, Nov. 2015

[46] H. Zhang, S. Kim, Q. Sun, and J. Zhou, "Distributed Adaptive Virtual Impedance Control for Accurate Reactive Power Sharing Based on Consensus Control in Microgrids," *IEEE Transactions on Smart Grid*, vol. 8, no. 4, pp. 1749–1761, 2017

[47] M. H. Cintuglu, T. Youssef, and O. A. Mohammed, "Development and application of a real-time testbed for multiagent system interoperability: A case study on hierarchical microgrid control," *IEEE Transactions on Smart Grid*, vol. 9, no. 3, pp. 1759–1768, 2018

[48] Y. Zhu, Q. Fan, B. Liu, and T. Wang, "An Enhanced Virtual Impedance Optimization Method for Reactive Power Sharing in Microgrids," *IEEE Transactions on Power Electronics*, vol. 33, no. 12, pp. 10390–10402, Dec. 2018

[49] A. Raghami, G. Ledwich, and Y. Mishra, "Improved Reactive Power Sharing Among Customers' Inverters Using Online Thévenin Estimates," *IEEE Transactions on Power Systems*, vol. 34, no. 6, pp. 4168–4176, 2019

[50] H. Moussa, A. Shahin, J. P. Martin, B. Nahid-Mobarakeh, S. Pierfederici, and N. Moubayed, "Harmonic Power Sharing with Voltage Distortion Compensation of Droop Controlled Islanded Microgrids," *IEEE Transactions on Smart Grid*, vol. 9, no. 5, pp. 5335–5347, 2018

[51] J. Zhou, S. Kim, H. Zhang, Q. Sun, and R. Han, "Consensus-Based Distributed Control for Accurate Reactive, Harmonic, and Imbalance Power Sharing in Microgrids," *IEEE Transactions on Smart Grid*, vol. 9, no. 4, pp. 2453–2467, 2018

[52] X. Wang, F. Blaabjerg, and Z. Chen, "Autonomous control of inverter-interfaced distributed generation units for harmonic current filtering and resonance damping in an islanded microgrid," *IEEE Transactions on Industry Applications*, vol. 50, no. 1, pp. 452–461, 2014

[53] A. Micallef, M. Apap, C. Spiteri-Staines, and J. M. Guerrero, "Mitigation of Harmonics

in Grid-Connected and Islanded Microgrids Via Virtual Admittances and Impedances," *IEEE Transactions on Smart Grid*, vol. 8, no. 2, pp. 651–661, 2017

[54] Y. Han, P. Shen, X. Zhao, and J. M. Guerrero, "An Enhanced Power Sharing Scheme for Voltage Unbalance and Harmonics Compensation in an Islanded AC Microgrid," *IEEE Transactions on Energy Conversion*, vol. 31, no. 3, pp. 1037–1050, Sep. 2016

[55] M. Savaghebi, A. Jalilian, J. C. Vasquez, and J. M. Guerrero, "Secondary control for voltage quality enhancement in microgrids," *IEEE Transactions on Smart Grid*, vol. 3, no. 4, pp. 1893–1902, 2012

[56] L. Meng *et al.*, "Distributed Voltage Unbalance Compensation in Islanded Microgrids by Using a Dynamic Consensus Algorithm," *IEEE Transactions on Power Electronics*, vol. 31, no. 1, pp. 827–838, 2016

[57] "IEEE Recommended Practices and Requirements for Harmonic Control in Electric Power Systems, "IEEE std 519-1992," *IEEE*, 1992

[58] J. He, Y. W. Li, and M. S. Munir, "A flexible harmonic control approach through voltage-controlled DG-grid interfacing converters," *IEEE Transactions on Industrial Electronics*, vol. 59, no. 1, pp. 444–455, 2012

[59] H. Moussa, A. Shahin, J.-P. Martin, B. Nahid-Mobarakeh, S. Pierfederici, and N. Nazih Moubayed, "Harmonic Power Sharing with Voltage Distortion Compensation of Droop controlled Islanded microgrids," *IEEE Transactions on Smart Grid*, pp. 1–1, 2017

[60] M. D. Pham and H. H. Lee, "Impedance-based harmonics compensation with accurate harmonic power sharing in distorted microgrids," *Journal of Power Electronics*, 2020

[61] J. He, Y. W. Li, D. Bosnjak, and B. Harris, "Investigation and active damping of multiple resonances in a parallel-inverter-based microgrid," *IEEE Transactions on Power Electronics*, vol. 28, no. 1, pp. 234–246, 2013

[62] A. Kahrobaeian and Y. A.-R. Ibrahim Mohamed, "Networked-Based Hybrid Distributed Power Sharing and Control for Islanded Microgrid Systems," *IEEE Transactions on Power Electronics*, vol. 30, no. 2, pp. 603–617, Feb. 2015

[63] X. Lu, J. M. Guerrero, K. Sun, and J. C. Vasquez, "An improved droop control method

for dc microgrids based on low bandwidth communication with dc bus voltage restoration and enhanced current sharing accuracy," *IEEE Transactions on Power Electronics*, vol. 29, no. 4, pp. 1800–1812, 2014

[64] E. A. A. Coelho, P. C. Cortizo, and P. F. D. Garcia, "Small-signal stability for parallel-connected inverters in stand-alone AC supply systems," *IEEE Transactions on Industry Applications*, vol. 38, no. 2, pp. 533–542, 2002

[65] X. Wang, Y. W. Li, F. Blaabjerg, and P. C. Loh, "Virtual-Impedance-Based Control for Voltage-Source and Current-Source Converters," *IEEE Transactions on Power Electronics*, vol. 30, no. 12, pp. 7019–7037, Dec. 2015

[66] J. Liu, Y. Miura, H. Bevrani, and T. Ise, "Enhanced Virtual Synchronous Generator Control for Parallel Inverters in Microgrids," *IEEE Transactions on Smart Grid*, vol. 8, no. 5, pp. 2268–2277, Sep. 2017

[67] J. Svensson, M. Bongiorno, and A. Sannino, "Practical implementation of delayed signal cancellation method for phase-sequence separation," *IEEE Transactions on Power Delivery*, vol. 22, no. 1, pp. 18–26, 2007

[68] H. Fujita and H. Akagi, "A Practical Approach to Harmonic Compensation in Power Systems Series Connection of Passive and Active Filters," *IEEE Transactions on Industry Applications*, vol. 27, no. 6, pp. 1020–1025, Nov. 1991

[69] W. Wu *et al.*, "A robust passive damping method for LLCL-filter-based grid-tied inverters to minimize the effect of grid harmonic voltages," *IEEE Transactions on Power Electronics*, vol. 29, no. 7, pp. 3279–3289, Jul. 2014

[70] F. Xiao, L. Dong, L. Li, and X. Liao, "A Frequency-Fixed SOGI-Based PLL for Single-Phase Grid-Connected Converters," *IEEE Transactions on Power Electronics*, vol. 32, no. 3, pp. 1713–1719, 2017

[71] L. Asiminoael, F. Blaabjerg, and S. Hansen, "Detection is key - Harmonic detection methods for active power filter applications," *IEEE Industry Applications Magazine*, vol. 13, no. 4, pp. 22–33, 2007

[72] N. Pogaku, M. Prodanovic, and T. C. Green, "Modeling, Analysis and Testing of Autonomous Operation of an Inverter-Based Microgrid," *IEEE Transactions on Power*

Electronics, vol. 22, no. 2, pp. 613–625, Mar. 2007

[73] E. A. A. Coelho *et al.*, "Small-Signal Analysis of the Microgrid Secondary Control Considering a Communication Time Delay," *IEEE Transactions on Industrial Electronics*, vol. 63, no. 10, pp. 6257–6269, Oct. 2016

[74] M.-D. Pham and H.-H. Lee, "Effective Coordinated Virtual Impedance Control for Accurate Power Sharing in Islanded Microgrid," *IEEE Transactions on Industrial Electronics*, vol. 68, no. 3, pp. 2279–2288, Mar. 2021

[75] D. Arricibita, P. Sanchis, R. Gonzalez, and L. Marroyo, "Impedance Emulation for Voltage Harmonic Compensation in PWM Stand-Alone Inverters," *IEEE Transactions on Energy Conversion*, vol. 32, no. 4, pp. 1335–1344, 2017

[76] IEEE Std. 1459 - 2010, *IEEE Std 1459-2010*, vol. 40, no. October. 2010.

[77] "IEEE 519-2014 Recommended Practice and Requirements for Harmonic Control in Electric Power Systems," *IEEE Std 519-2014 (Revision of IEEE Std 519-1992)*. pp. 1–29, 2014.

Publications

Journal Papers

[J1] **M.-D. Pham** and H.-H. Lee, "Effective Coordinated Virtual Impedance Control for Accurate Power Sharing in Islanded Microgrid," IEEE Transactions on Industrial Electronics, vol. 68, no. 3, pp. 2279–2288, Mar. 2021.

[J2] **M.-D. Pham** and H.-H. Lee, "Improved Reactive Power Sharing and Harmonic Voltage Compensation in Islanded Microgrids Using Resistive-Capacitive Virtual Impedance," Journal of Power Electronics, vol. 19, no. 6, pp. 1575–1581, 2019.

[J3] **M.-D. Pham** and H.-H. Lee, "Coordinated virtual resistance and capacitance control scheme for accurate reactive power sharing and selective harmonic compensation in islanded microgrid," IET Generation, Transmission and Distribution, vol. 14, no. 22, pp. 5104–5113, 2020.

[J4] **M. D. Pham** and H. H. Lee, "Impedance-based harmonics compensation with accurate harmonic power sharing in distorted microgrids," Journal of Power Electronics, 2020.

[J5] **M.-D. Pham** and H.-H. Lee, "Accurate power sharing and harmonic mitigation scheme for parallel operation of single-phase voltage source inverters," Journal of Power Electronics, vol. 21, no. 1, pp. 164–172, 2021.

[J6] **M.-D. Pham**, V.-T. Hoang, and H.-H. Lee, "Cost-effective synchronization strategy for distributed generators in islanded microgrids," Journal of Power Electronics, 2021.

[J7] **M.-D. Pham**, and H.-H. Lee, "Consensus-Based Distributed Control Scheme for PCC Voltage Harmonic Mitigation and Enhanced Power Sharing in Islanded Microgrids," IET Generation, Transmission and Distribution, Early Accepted.

Conference Papers

[C1] **M.-D. Pham** and H.-H. Lee, "Enhanced Reactive Power Sharing and Voltage Restoration in Islanded Microgrid," in Proceedings of the KIPE Conference, 2016, pp. 47–48.

[C2] **M.-D. Pham** and H.-H. Lee, "Fuzzy PID Controller for Reactive Power Accuracy and Circulating Current Suppression in Islanded Microgrid," in Intelligent Computing Methodologies, 2017, pp. 241–252.

[C3] **M. D. Pham** and H. H. Lee, "Adaptive control of DC-DC converter based on hybrid fuzzy PID controller," in Lecture Notes in Computer Science, 2017, pp. 253–263.

[C4] **M.-D. Pham** and H.-H. Lee, "An Enhanced Reactive Power Sharing and Secondary Voltage Restoration Control in Islanded Microgrid," in International Conference on Mobile and Wireless Technology, 2017, pp. 519–527.

[C5] **M. D. Pham** and H. H. Lee, "Fuzzy PID controller for PCC voltage harmonic compensation in islanded microgrid," in Lecture Notes in Computer Science (including subseries Lecture Notes in Artificial Intelligence and Lecture Notes in Bioinformatics), vol. 10954 LNCS, Springer, Cham, 2018, pp. 231–242.

[C6] **M. Duc Pham** and H. H. Lee, "An Effective PCC Voltage Harmonic Compensation and Harmonic Power Sharing in Islanded Microgrid," in IECON 2018 - 44th Annual Conference of the IEEE Industrial Electronics Society, Oct. 2018, pp. 89–94.

[C7] **M.-D. Pham** and H.-H. Lee, "An Enhanced PCC Harmonic Voltage Mitigation and Reactive Power Sharing in Islanded Microgrid," in Proceedings of the KIPE Conference, 2018, pp. 138–140.

[C8] **M. D. Pham** and H. H. Lee, "Resonance Mitigation and Harmonics Compensation in Islanded Microgrids via Virtual Damping Resistance and Virtual Shunt Filter," in IECON 2019 - 45th Annual Conference of the IEEE Industrial Electronics Society, 2019, vol. 1, pp. 2475–2480.

[C9] **M. D. Pham** and H.-H. Lee, "Accurate Reactive Power Sharing and Harmonic Mitigation in Islanded Microgrids Using Adaptive Virtual Capacitance," in 2020 15th IEEE Conference on Industrial Electronics and Applications (ICIEA), Nov. 2020, pp. 687–692.

[C10] **M. D. Pham** and H. H. Lee, "Adaptive Virtual Impedance Control Method for Accurate Reactive Power Sharing and Circulating Current Suppression in Islanded Microgrid," in 2019 IEEE Student Conference on Electric Machines and Systems (SCEMS 2019), Nov. 2019, pp. 1–5.

[C11] **M. D. Pham** and H. H. Lee, "A Centralized Shifted Voltage Control Method for Accurate Power Sharing in DC Islanded Microgrids", in 19th International Conference on Renewable Energies and Power Quality (ICREPQ'21)